THERMAL MODELING OF LASER DRILLING AND CUTTING OF ENGINEERING MATERIALS

By

RAVINDRA H. PATIL

Bachelor of Engineering

Government College of Engineering

University of Pune

Pune, India

1997

Submitted to the Faculty of the
Graduate College of the
Oklahoma State University
in partial fulfillment of
the requirements for
the Degree of
MASTER OF SCIENCE
July, 2005

THERMAL MODELING OF LASER DRILLING AND

CUTTING OF ENGINEERING MATERIALS

Thesis Approved:

Dr. Ranga Komanduri

Thesis Advisor

Dr. Hongbing Lu

Dr. Samit Roy

Dr. A. Gordon Emslie

Dean of the Graduate College

.

SUMMARY

Lasers are used to drill small holes of high aspect ratio in difficult-to-drill materials. In this investigation, thermal aspects of laser drilling and cutting process are modeled using the Jaeger's heat source method. The laser beam is considered as a circular moving plane disc heat source. The resulting equation is a general solution, in that it can be used for transient as well as quasi-steady state conditions. It can be used with different laser beam distributions, such as normal, bimodal, and uniform. Simpson 1/3 rd numerical integration method is used to solve the heat source equation and programmed using Visual Basic.NET.

Temperature rise at any time and at any location in the workpiece drilled or cut is determined using the laser beam parameters and the thermal properties of workmaterials, such as AISI-1036 steel, and CP-titanium. Fusion and evaporation temperatures of the workmaterials are used to calculate the amount of material removed by each laser pulse for a given laser beam parameters. The effect of latent heat of fusion and evaporation are considered. Effect of different laser beam parameters, such as energy density, beam radius, and pulse duration on the profile of laser drilled hole and cut materials are investigated. Mass and energy balance were done for the laser machining process. Using this method, the number of laser pulses required to drill a hole of required depth and diameter can be calculated. Heat affected zone (HAZ) calculations were also performed for different materials.

ACKNOWLEDGEMENTS

I would like to thank Dr. Ranga Komanduri for his encouragement and advice through out my master study. I would also like to thank Dr. S. Roy, and Dr. H. B. Lu for kindly serving on the committee. I would like to thank Dr. Z. B. Hou for many useful discussions.

I am grateful to my parents, brothers, and sisters for their support, guidance, and encouragement. I would like to thank my friends Jayprakash, Bruno, and Sara Elizabeth for their encouragement.

I would also like to thank Rutuparna, Milind, Sony, Madhan, Ganesh, Amol, Bala, Abdul, Shiva, Tejas, and Rohit for their kind help. Thanks are also due to all my colleagues in the manufacturing research group for their help and friendship.

Finally, I would like to thank the School of Mechanical and Aerospace Engineering for providing the opportunity to pursue my M.S. at Oklahoma State University.

TABLE OF CONTENTS

LIST OF TABLES

LIST OF FIGURES

NOMENCLATURE

θ_m	Temperature rise ^{0}C at M(x, y, z)
c	Specific heat of conducting medium
p	Power of the laser beam, J/s
a	Thermal diffusivity, mm^2/s
r_0	Radius of the laser beam, mm
r	$\sqrt{x^2 + y^2}$, mm
λ	Thermal conductivity, J/mm s ^{0}C = $a \cdot c \cdot \rho$
gg	Boundary coefficient with its value between +1 and -1, when gg = +1, it is the adiabatic boundary, when gg < +1 it is convective cooling boundary
I_0	Modified Bessel functions of the first kind and order zero
$P' = \frac{r * r_i}{2a\tau}$	Where r_i is from 0 to r_0

when,

$P' \geq 0 \;\&\; P' \leq 0.3$, $I_0(P') \approx 1$

$0.3 < P' < 1.6$, $I_0(P') \approx 0.935 * e^{(0.35P')}$

$1.6 \leq P' \leq 3$, $I_0(P') \approx 0.529 * e^{(0.735P')}$

$P' > 3.0$, $I_0(P') \approx \frac{1}{\sqrt{2\pi p'}} e^{P'}$

E	Young's modulus, N/mm^2
α	Coefficient of linear thermal expansion, /^{0}C
ε_r	Strain in r direction
ε_θ	Strain in θ direction
ε_z	Strain in z direction
σ_r	r -component of stress, N/mm^2
σ_θ	θ -component of stress, N/mm^2
σ_z	z -component of stress, N/mm^2
ρ	Density of material, kg/mm^3
$\theta(R,\tau)$	The temperature rise, ^{0}C due to point heat source at time, τ
Q_{pt}	Heat liberated instantaneously by a point heat source, J
q_{rg}	Heat liberation rate of a ring segment of radius r_i, J/s
Q_{rg}	Heat liberated by the ring source instantaneously at time $\tau = 0$, J
Q_{disc}	Heat liberated by the disc heat source, J/cm^2
τ_i	Instantaneous time, s
t	Pulse on-time, s
τ =	$t - \tau_i$, s

CHAPTER 1

INTRODUCTION

Lasers are used in the fabrication industry for a wide variety of applications. They have found application in areas where conventional processing is not able to perform the work satisfactorily because of thermal damage, distortion, need for vacuum or in-accessibility of the workpiece. It is very important to investigate the complex phenomena involved in laser machining in order to control and optimize the overall quality of the laser machined finished products.

In this chapter (Chapter 1), an overview of laser machining is presented. Different types of laser machining as well as their advantages and disadvantages are given. Characteristics of the laser beam are also covered in this chapter. Chapter 2 gives the background and literature review of thermal modeling of laser machining processes. The methods of energy balance and effect of laser machining on the workpiece properties are also given in Chapter 2. Problem statement is defined in Chapter 3. An approach for theoretical analysis is presented in Chapter 4. Equations for the point heat source, ring heat source, and finally moving circular disc heat source are utilized in modeling the laser machining process.

Chapter 5 provides the methodology for modeling different types of laser drilling and cutting/grooving processes. The computational investigations of laser machining process are discussed in this chapter, which is composed of analytical method for

solving the temperature rise equations of a moving circular disc heat source, development of a computer interface for computing the temperature profiles. The energy balance for laser drilling and cutting/grooving process and the profile of laser drilled hole or cut/groove are given in this chapter. Individual laser parameters are investigated for their effects on laser drilling and cutting/grooving processes, and optimization of the process is proposed in Chapter 6. In addition, comparison of the analytical results obtained in this investigation with the numerical and experimental results from the literature review are performed and discussed in this chapter. Chapter 7 gives conclusions and future work. This is followed by references and appendices.

1.1 Laser

Much of the summary on laser and its application to manufacturing processes is abstracted from the book, Laser machining-theory and practice by G. Chryssolouris [1]. Laser, an acronym for light amplification by stimulated emission of radiation, is essentially a coherent, convergent, and monochromatic beam of electromagnetic radiation with wavelength ranging from ultra-violet to infrared [1]. Laser can deliver very low (~mW) to extremely high (1–100 KW) focused power with a precise spot size and interaction time (10^{-3} to 10^{-15} s) on to any kind of substrate through any medium. Laser is distinguished from other electromagnetic radiation mainly in terms of its coherence, spectral purity, and ability to propagate in a straight line. As a result, laser has wide applications from very mundane (bar code scanner) to most sophisticated (3-dimensional holography), mere commercial (audio recording) to purely scientific (spectroscopy), routine (printer) to futuristic (optical computer), and life saving (surgery) to life threatening (weapons/guide) [3].

The unique properties of laser light can be quantified by examining the optical properties, such as monochromaticity, coherence, diffraction, and radiance. Diffraction is the phenomenon by which light bends around sharp edged objects. Typically laser beam divergence angles ranges from 0.2 milliradiance for He-Ne lasers to 10 milliradians for ND: YAG lasers. This property of laser light produces a directional energy source which can focus a large amount of luminous energy on a small area. In machining application, this directional characteristic allows precise control of the laser beam direction relative to workpiece position. For focusing laser light, the diffraction effect is related to the ratio between focal length and aperture or beam diameter. The radiance of the light source is the amount of the power per unit area emitted by the light source for a given solid angle. The solid angle can be thought of as the cone through which the light passes. Lasers have high output powers for small areas which they use to emit the beam. In addition, the beams possess low divergence, which causes them to be transmitted over a small solid angle. Thus, laser light sources possess extremely high radiance. While monochromaticity, high coherence, and low diffraction individually are not critical factors for laser machining, the combination of these characteristic make the laser beam a powerful tool for machining. High power and energy density can be achieved on the surface of workpiece, which leads to rapid phase change of the material and to subsequent material removal [1].

Lasers can be categorized accordingly to their lasing media, as gas, liquid, or solid. Also, all lasers operate in two temporal modes: continuous wave (CW) and pulsed mode. In the CW mode, the laser beam is emitted without interruption. In the pulsed mode, the laser beam is emitted periodically [1].

Solid state lasers use ions suspended in a crystalline matrix to produce laser light. The two main classes of dopants or ions in the lasing medium are chromium (Cr^{3+}) for ruby lasers and Neodinium (Nd^{3+}) for ND: YAG and ND: glass lasers. Ruby lasers generally are not used for drilling because of low energy efficiency and low achievable power. ND: glass lasers are used in the application which requires low pulse repetition rates and high pulse energies. The pulse operation of neodymium lasers make them desirable for hole piercing and deep keyhole welding application [1].

The five major characteristics of the laser beam which are critical in determining the type of laser to use for a particular application are beam power, wavelength, temporal mode, spatial mode, and focal spot size. Other practical and economic considerations include output stability of power and TEM mode, the physical size of the unit, projected lifetime of the laser, gas or flash lamp consumption, availability of the service and parts, the power requirements, and the efficiency of the laser [1].

Laser power is the most basic characteristic of a laser. The required laser system should have appropriate power to machine a given material. Highest continuous wave laser power is obtained from CO_2 lasers while Nd: YAG lasers provide the highest peak power for pulsed operation. The amount of the laser power required is determined by examining the optical and thermal properties of the workpiece material or a group of materials to be machined. The abosorptivity of the material surface has the largest influence on the laser power requirements. The material absorptivity determines the fraction of the impinging radiation energy that is actually absorbed by the material. The remainder of the beam energy is reflected back into the environment. Thus, the laser power must be adjusted so that the required amount of power for achieving the desired

material removal at the desired processing rate is absorbed by the surface, instead of only impinging on the surface. The absorptive value depends on the wavelength of the beam impinging on the surface, surface roughness, temperature, phase of the material, and use of surface coatings. Estimation of power requirements can be performed by using models of the specific laser machining process to relate the material properties, operating parameters, such as laser power and process rate, and material removal characteristic, such as depth of cut, hole depth, and the shape of the cut [1].

Wavelength is the characteristic spatial length associated with one cycle of vibration for a photon in the laser beam. The optical resonator of the laser must be properly designed to produce the correct wavelength. The absorptivity of materials can be highly dependent on the wavelength of incident light, and thus certain lasers will be more suitable for the processing of different classes of materials, e.g. some metals such as aluminum and copper show low absorptivity at a wavelength of 10.6 μm, which is the characteristic wavelength for CO_2 lasers. Therefore, in order to machine these materials effectively, either a high power laser or one with a different wavelength must be used. Materials can be machined more effectively by using Nd: YAG laser with 1.06 μm wavelength, whereby the copper and aluminum absorptivity values are much higher. Resonator design is crucial to the production of proper wavelength of light [1].

Laser can operate in a continuous wave (CW) mode or a pulsed beam mode as shown in Figure 1.1.

In the CW mode, the laser beam is emitted without interruption. In the pulsed beam mode, the laser beam is emitted periodically. Pumped energy is stored until a

threshold energy is reached, and then the stored energy is discharged rapidly into the laser cavity.

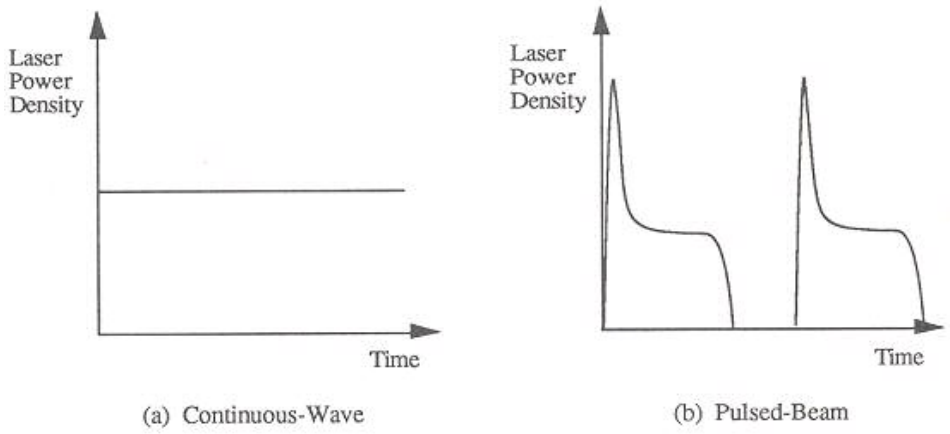

Fig. 1.1 Laser beam temporal modes [1]

Through this process, short duration pulses with high energy densities can be generated from lower level of continuous power. CW operation offers the advantage of smooth surface after machining. Pulsed beam operation allows deeper drilling or cutting depth to be achieved compared to a continuous beam operating at a given beam power, but pulsed operation may result in larger surface irregularities in the machined parts due to a periodic beam output. Typically, solid lasers operate best in pulsed mode and at relatively lower power in continuous mode. Gas laser typically operate in a continuous mode with limited pulse capability. The selection of a laser and an operating mode will depend on the desired machining operation. Pulsed operation is usually best for deep penetration process. The concentration of energy in each pulse leads to a small percentage of energy lost though conduction in to the workpiece or dissipation to the environment. Pulsing is used to minimize the heat affected zone in materials that are sensitive to elevated temperatures, such as polymers. Continuous power operation is used when high average power is required, which is important for achieving high

material removal rate. When laser and material coupling is good, continuous power operation will not suffer from large losses. Continuous wave operation provides smooth cutting surface, while pulsing can create a wavy surface due to its periodic nature [1].

The beam profile can be characterized by its Transverse Electromagnetic Mode (TEM). TEM modes are normally written in the form of $TEM_{nm.}$ The subscripts n and m denote the number of nodes in directions orthogonal to the beam propagation, such as TEM_{00} or $TEM_{01.}$ TEM_{00} has a Gaussian spatial distribution and is usually considered the best mode for laser beam machining because the phase front is uniform and there is a smooth drop off of irradiance from the beam center. This minimizes diffraction effects during focusing and allows the generation of small spot sizes [1].

In material processing, irradiance (power per unit area) of the laser beam at the material surface is of prime importance. Irradiance great enough to melt or vaporize any material can be generated by focusing a laser beam. The maximum irradiance is obtained at the focal point of the lens, where the beam is at its smallest diameter. The location of this smallest diameter is called the focal spot. Irradiance values of billions of watts per square centimeter can be obtained at the focal spot. The imperfection of the optical components and diffraction effects limits the size of the obtainable focal spots.

1.2 Laser machining

Manufacturers need the ability to produce small or micro circular holes, in the range of hundreds to few thousands, in a single workpiece at very shallow angles to the surface. Such requirements and the limitation of the conventional drilling process, have contributed to the search for non-traditional processes for hole making. Several non-traditional processes used in hole making are EDM (Electrical Discharge Machining),

ECM (Electrochemical Machining), LBM (Laser-Beam Machining), EBM (Electron-Beam Machining), PCM (Photochemical Machining), and USM (Ultrasonic Machining) [2].

Principle lasers used for material removal purposes are the Nd-YAG (Neodymium-Yttrium Aluminum Garnet), the ruby, and the carbon dioxide (CO_2). For pulsed operation, a power supply produces short, intense burst of electricity into the flash lamps, which concentrates their light flux on the lasing material. The resulting energy from the excited atoms is released at a characteristic, constant frequency. The monochromatic light is amplified during successive reflections from the mirrors. The thoroughly collimated light exits through the partially reflecting mirrors to the lens which focuses it just below the surface of the workpiece. The small beam divergence, high peak power, and single frequency provide excellent, small diameter spots of light with energy densities up to 3×10^{10} W/in^2, which can sublimate almost any material. Cutting requires energy densities of 10^7 to10^9 W/in^2, at which most material can not conduct energy into the body of the workpiece fast enough to prevent melting and vaporization.

Workpiece surface reflectivity, absorption coefficient, thermal conductivity, specific heat, thermal diffusivity, heat of fusion, and heat of vaporization are important factors in laser work. Sharp, short, Gaussian-mode repetitive pulses are best for cutting because they have high energy densities. Laser beam machining is not a mass material removal process. It is a fast, easily controlled process with a non-contact, non-wearing tool [1].

In general, laser machining can be divided into one, two and three dimensional process. Since the laser beam is a directional heat source, it can be viewed as a one-dimensional line source with a line thickness equal to the beam diameter. In case of a

one dimensional process (drilling), the laser beam is stationary relative to the workpiece. The erosion front, located at the bottom of the drilled hole, propagates in the direction of the line source in order to remove the material. In case of two-dimensional process (cutting), the laser beam is in relative motion with respect to the workpiece. Material removal occurs by moving the line source in a direction perpendicular to the line direction and forms a two-dimensional surface. The erosion front is located at the leading edge of the line source. For three-dimensional machining, two or more laser beams are used and each beam forms a surface through relative motion with workpiece. The erosion front for each surface is found at the leading edge of each laser beam. When the surfaces intersect, the three-dimensional volume bounded by the surfaces is removed [1].

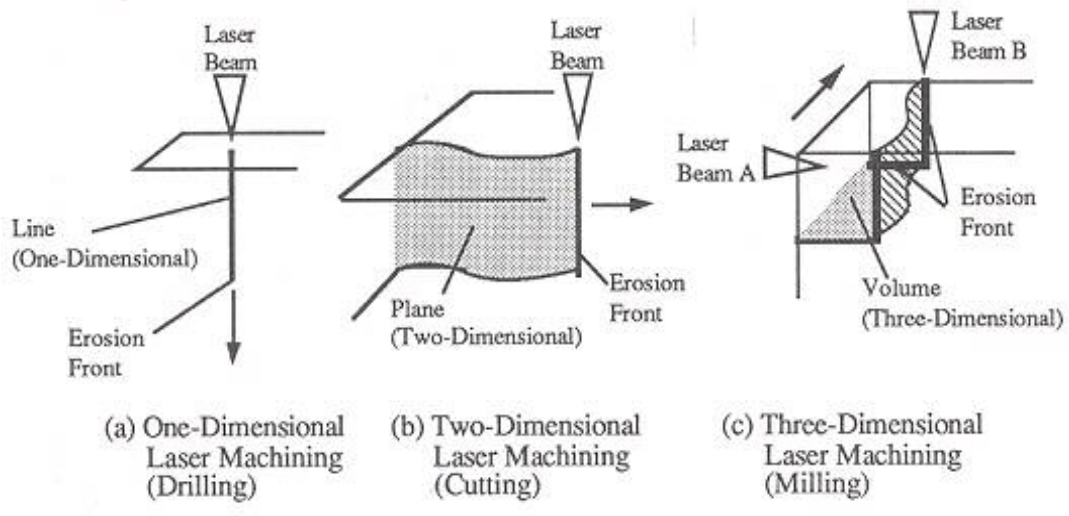

Fig. 1.2 Schematic of one, two, and three-dimensional laser machining [1]

1.2.1 Advantages of laser machining

Several situations favor the application of non-traditional processes to hole making: workpiece material that is difficult to machine by conventional mechanical drilling, shallow entry angle, noncircular shapes, small or microhole size, large depth to

diameter ratio, large number of holes per workpiece or assembly, burr less machining, need for special surface-integrity characteristics, such as freedom from distortion or residual stresses, and contoured holes [2].

Advantages of the laser beam machining are: ease of automation for complex hole patterns, absence of tool wear and breakage, ability to drill at shallow angles, rapid drilling rates. Instant availability of a wide range of hole sizes, ability to drill any materials, capability to drill at inaccessible locations, capability to drill very small holes with very large depth to diameter ratios, operability in an environment including air, inert gas, vacuum, certain liquids make laser machining popular. The laser beam can be projected through a transparent window, and finally because of the extreme intensity can be used with materials sensitive to heat shock, such as ceramics. Most of the current laser beams machining applications are in small-hole drilling, such as fuel filters, carburetors nozzles, hypodermic needles, holes for lock-nut safety wires, and for jet-engine-blade cooling holes [2].

Laser machining is a thermal process. The effectiveness of laser machining depends upon the thermal and optical properties rather than mechanical properties of the material to be machined. Therefore, materials which exhibit a high degree of brittleness or hardness and have favorable thermal properties, chiefly diffusivity and conductivity are well suited for laser machining [2].

Laser machining is a non-contact process. Since energy transfer between the laser and the material occurs through irradiation, no cutting forces are generated by the laser and so consequently no mechanically induced material damage, no tool wear, and

no machine vibration. Also, the material removal rate for laser machining is not limited by constraints, such as maximum tool force, built-up edge formation, or tool chatter [2].

Laser machining eliminates the replacement costs associated with tool wear and breakage. Machine downtime for tool replacement and recalibration are eliminated. Unlike other non-traditional machining processes, laser machining does not require vacuum or any other special environments to operate.

Laser machining is a flexible process. When combined with a multi-axis workpiece positioning system or robot, the laser beam can be used for drilling, cutting, grooving, welding, and heat treating processes on a single machine. The laser machining can result in higher precision and smaller kerf widths and smaller hole diameters than comparable mechanical process [2].

Laser drilling offers an alternative to mechanical drilling, punching, broaching, and wire EDM. It is especially adaptable for small holes with large depth-to-diameter ratios. With laser drilling, a wide range of hole diameters are obtainable. Material, such as steel, nickel alloys, aluminum, copper, brass, borosilicate glass, quartz, ceramic, plastic and rubber are all drilled successfully using a laser. The laser is so fast and so repeatable that it is particularly ideal for high production volumes associated with fully automated or semi-automated tooling applications.

The nature of the laser beam used in laser drilling allows holes to be drilled in the hardest of materials, from aerospace alloys, diamond, and ceramics. Through the use of laser drilling, holes can be created even in coated materials. The main applications are in aerospace where cooling holes needs to be drilled. The programmable nature of

lasers allows for very high speed drilling applications where many thousands of holes are required in short cycle times [2].

1.2.2 Disadvantages of laser machining

Since laser machining is primarily a thermal process, there are certain disadvantages associated with the process. In most laser machining techniques, the removal of material occurs by melting or vaporization of the entire volume to be removed. Since this phase change of the material occurs on an atom by atom basis, laser machining requires significantly higher energy inputs and processing times than equivalent mechanical process. During laser machining, high power densities are introduced on the surface of the workpiece in order to raise the temperature of the volume to be removed to the melting and evaporation point. In metals, the conduction heat resulting from the high energy density on the workpiece creates a heat-affected zone (HAZ) near the vicinity of erosion front. In plastic and polymer-matrix composites, material decomposition may occur as a result of high temperatures, which cause the breakdown of the polymer into charred residues and gaseous products. High expenditure is required to install laser machining system and also skilled operators are required to operate and maintain the system. Safety measures have to be taken prior to and during the use of the laser machining system [2].

Holes with stepped diameters cannot be drilled using a laser. Due to instabilities in the laser drilling process, depth control in the blind hole drilling is difficult. For deep holes, the effects of beam divergence may become unacceptable. This problem can be compensated for by using a longer focal length lens or by continuously moving the focal point from the workpiece surface to a point at the workpiece interior [1].

1.3 Laser drilling [1]

Laser drilling involves a stationary laser beam which uses its high power density to melt or vaporize material from the workpiece. In principle, laser drilling is governed by an energy balance between the irradiating energy from the laser beam and the conduction heat into the workpiece, the energy losses to the environment, and the energy required for phase change in the workpiece. The incident beam energy has a spatial intensity distribution which in laser drilling is usually a Gaussian distribution produced by a laser operating in the TEM_{00} mode. The focused beam radius is usually specified as the distance between the beam center and a point where the intensity is reduced from its maximum value at the beam center by a factor of e^{-2} (e = 2.7182); the average diameter of the drilled hole may be less than the beam diameter due to various heat loss effects. As shown in Figure 1.3, d is the diameter of the laser beam. These heat losses are primarily due to conduction into the interior of the workpiece and losses to the environment which divert the beam energy away from the actual hole drilling process.

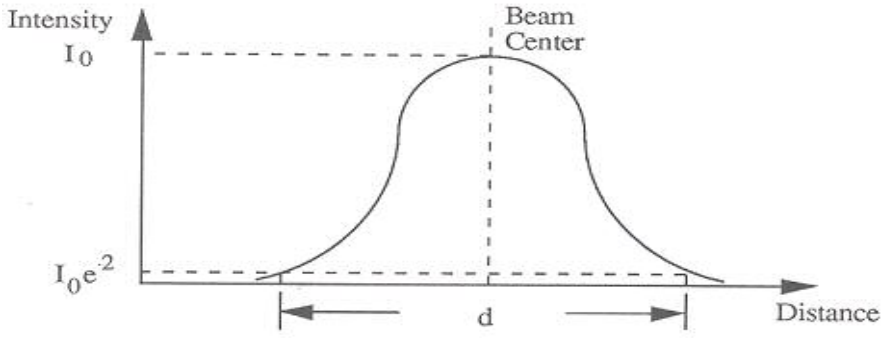

Fig. 1.3 Spatial intensity distribution for TEM_{00} laser beam [1]

Energy losses occur due to a number of physical phenomena during laser machining: If the material removal process involves melting, the molten material may

accumulate along the side and bottom of the hole, causing laser beam energy loss in two ways. First, energy may be expended to superheat the accumulated molten material in the hole above the melting point. In percussion drilling, another heat loss is the molten material may resolidify between successive pulses. Therefore, a portion of the beam energy during each pulse is expended to remelt the resolidified material. Plasma formation may occur with materials, such as ceramics are vaporized. An opaque cloud of vaporized material often forms above the beam-material interaction zone. This cloud absorbs some of the incoming laser beam energy and increases its temperature until plasma is formed. However, in some cases, the heated plasma acts as a secondary heat source which improves the drilling process. Dimensional accuracy can be affected because the directionality of the plasma is difficult to control. Use of an inert assist gas can help in reducing the effect of plasma formation by removing vaporized debris from the path of the laser beam.

The absorption of the laser beam energy depends on the wavelength of the laser radiation and the spectral absorptivity characteristics of the material processed. Metals such as aluminum and copper have high reflectivity for CO_2 laser radiation (10.6 μm wavelength); so for these materials, Nd: YAG laser is more effective. In the case of metals and ceramics, the presence of molten layer changes the absorptivity value and absorptivity of a surface also depends on its orientation with respect to beam direction. Absorption of beam energy is shown to reach a maximum value for angles of incident above $80^{0.}$ The beam energy not absorbed by the workpiece is reflected in a different direction from the incoming energy. For deep holes, multiple beam reflections may

occur along the wall of the hole, thus decreasing the availability of the beam energy for material removal.

The use of a gas jet during laser drilling can aid in cooling the erosion front through convective heat transfer. When a high pressure gas jet is used along with a laser beam, a supersonic gas flow is formed and the thermal dissipation to the jet becomes significant. With an increase in the thermal dissipation, more beam energy is required to maintain melting /vaporization temperature at the erosion front [1].

There are several variations in laser drilling. The material removal rate for drilling of metals can be substantially increased by introducing a reactive gas to enhance the laser cutting process. In this case, chemical reactions between the workpiece material and the gas become an important secondary material removal mechanism. However, chemical reactions tend to propagate in all directions and dimensional control of the reaction process becomes difficult. Large diameter holes (diameters above 1.3 mm) can be produced by a trepanning method, in which the beam is scanned in a circular trajectory to obtain final geometry. The trepanning method is a circular through cutting technique, with the machining speed determined by the scanning velocity of the beam.

1.4 Laser cutting [1]

In laser through-cutting process, a kerf is created through relative motion between the laser beam and the workpiece. The physical mechanisms for material removal and energy losses are shown in Figure 1.4 which are similar to those for drilling.

The incoming laser beam energy is balanced by the conduction heat, energy for melting or vaporization of the material and heat losses to the environment. However,

due to relative beam/workpiece movement, the erosion front formed in front of the laser beam and the temperature fields in the workpiece are stationary with respect to the coordinate system moving with the laser beam. Therefore, laser cutting can be considered as a steady state thermal process. Since the workpiece thickness is equal to the depth of cut, conduction heat occurs in the plane of the workpiece. The temperature inside the workpiece is dependent on the distance to the erosion front and independent of time.

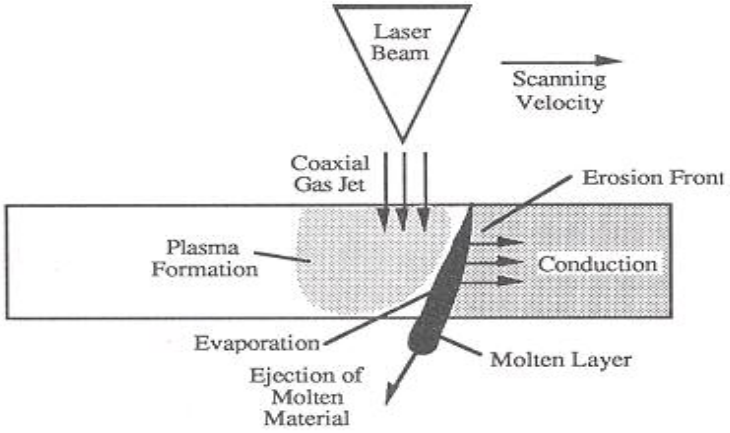

Fig. 1.4 Schematic of laser through-cutting [1]

When the material is removed through melting, a molten layer forms at the erosion front. The accumulated molten material can be expelled out from the bottom of the kerf with the aid of an axial gas jet. Laser cutting produces kerf widths which are narrower than those achievable with mechanical cutting. When coupled with a multi-axis position control system for the workpiece, shapes can also be cut from the curved workpiece. For cutting fibrous material, such as wood, paper or composites, the laser beam vaporizes the volume of the material removed, thereby eliminating the residue and debris which remain after mechanical cutting.

Laser cutting effectiveness reduces as the workpiece thickness increases. Laser cutting produces a tapered kerf shape, compared to the straight vertical kerf walls achievable by conventional methods. The kerf taper is a result of divergence of the laser beam and becomes more pronounced as the workpiece thickness increases. The kerf taper can be reduced by adjusting the focal point of the laser beam to the interior of the workpiece instead of on the workpiece surface [2].

In many instances, the ability of laser to cut can be further improved by focusing the assist gas. The assist gas serves two purposes: to help in combustion, and to blow the debris or molten metal away from the kerf.

1.5 Laser grooving [1]

In the laser grooving process, a groove is produced by scanning a laser beam over the workpiece surface. Unlike through-cutting, the laser beam does not penetrate through the entire workpiece thickness.

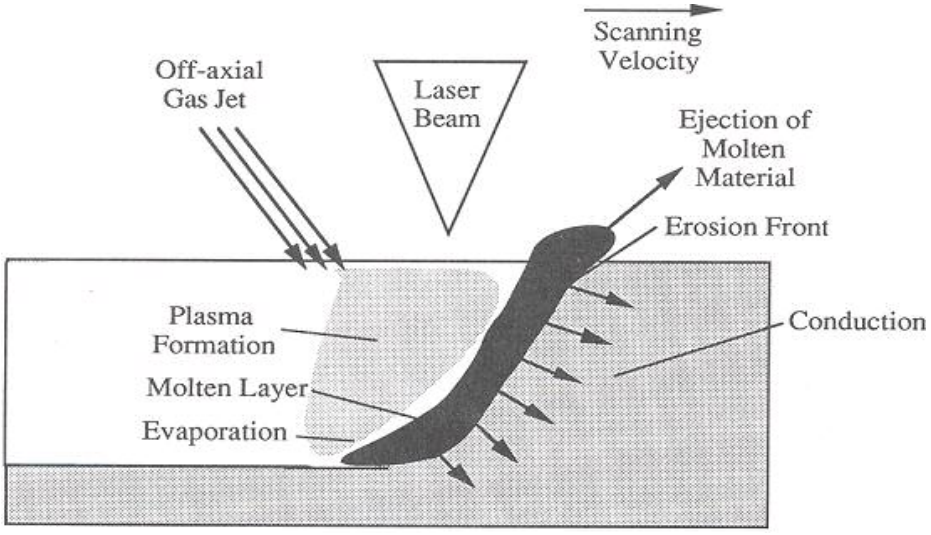

Fig. 1.5 Schematic of laser grooving [1]

The physical mechanisms of laser grooving are similar to those of laser drilling and cutting process. Similar to laser grooving process, laser scribing creates a blind

groove on the surface of a workpiece. However, in laser scribing the ratio of groove depth to groove width is close to one, and groove depths are typically very small.

When applied to metals and ceramics, these process results in, molten material accumulation at the erosion front. However, unlike in laser cutting, a coaxial gas jet is not effective for ejecting molten material due to the presence of groove bottom. The groove depth can fluctuate due to disturbances caused by laser beam changes, mechanical vibration, material impurities, and gas jet fluctuations. Unevenness in groove depth can decrease surface quality and mechanical strength of the finished part.

1.6 Laser machining effects on the material

Laser processing is more sensitive to material quality than are other processes. The surface finish can dramatically affect the quality of cutting. In most cases, steel must be clean, pickled, and oil-free. Impurities on low-grade steel are highly reactive to the thermal process, especially when oxygen is used as a processing gas. Hot rolled steel presents serious quality problems in cutting because of the surface scale. The surface tends to melt in with the metal, creating an undesirable finish. If the material surface is not smooth, the assist gas and laser focus can be altered, affecting the quality of the cut [34].

Laser cutting can leave a recast layer on the surface. Because lasers melt and burn some of the metal, remelted materials are deposited on the side of the cut edges and on the bottom of the cut. This layer of deposited materials is highly stressed and may crack, especially if it is an oxide. Although these cracks are small, they can propagate into the material, creating larger cracks. This is especially true of inside corners with small radii, where stresses are higher [34].

During laser cutting of steels, a huge amount of energy is conducted into the workpiece resulting in changes in the material properties and the microstructure of the steel. This activity results in a narrow zone exactly adjacent to the laser cut that experiences changes in material properties. Typically, the changes occur either as grain refinement, or as precipitation of carbides (which are harmful for corrosion resistance properties of steel) and other impurities such as sulfides and phosphides. The entire region which differs from the base material in properties can be defined as the heat affected zone or HAZ. A heat affected zone (HAZ) is produced during laser cutting. A HAZ forms in metals when the temperature rises above the critical transformation point temperature. In laser cutting, this is localized near the cutting zone. In carbon steel, the higher the hardenability, the greater the HAZ. For example, laser processing produces a HAZ of about 0.18 mm on 7 mm thick, 4140 steel. Since the HAZ is brittle, this area has a lower tolerance for cracking during bending or stress. In most cases, the HAZ can be eliminated by post-heat treating the part, but there is a risk of distortion [34].

HAZ cracks are a particular problem for the more crack sensitive alloys such as the 6000-alloys. The cracks are caused by low melting point phases present at the grain boundaries. Due to the thermal cycle of welding, the temperature may be so high that these phases melt. During the cooling phase the unmelted material shrinks, resulting in residual tensile stresses. A material deficiency at the grain boundary may then result in voids or intergranular, crack like defects. The presence of small HAZ cracks does not necessarily affect the mechanical strength of a weld; however, it may reduce the fatigue lifetime and the fracture toughness. It is difficult to know how to avoid HAZ cracks. Some factors may, however, affect the tendency to HAZ cracking. The welding process

or welding parameters may also affect the tendency. High heat input will increase the HAZ size and also increase the size of the zone prone to give HAZ cracks [34].

Laser cutting creates more stresses in material than do other methods such as water-jet cutting. In most cases, laser processing produces little distortion in material, but this depends on the laser's parameters, the material thickness, and its composition. Distortion is more likely to occur when a laser is applied to thin materials with wall thicknesses of 0.001 to 0.005 inches or shim-stock material. Thinner materials are more easily distorted because a recast layer forms on the edge, and the resolidification of the molten material can more easily warp thinner material [33].

Distortion from laser processing is a result of the sudden rise in temperature of the material near the cutting zone. Distortion is also created by the rapid solidification of the cutting zone. In addition, distortion also can be attributed to the rapid solidification of material remaining on the sides of the cut. Adding a water quenching system to the laser cutting nozzle can reduce heat-induced stress. This process works well when cutting tubes with diameters less than 1/4 inch and usually prevents slag from forming on the opposing walls [33].

CHAPTER 2

LITERATURE REVIEW

Lasers have found a wide range of applications. Therefore, it is very important to study the mechanism of material removal and main factors controlling the laser processes. They may include both theoretical and experimental studies. Thus, to take advantages of laser processing and to achieve appropriate laser machining results, numerous investigations have been conducted to develop a thorough understanding of the physical processes involved. Traditional research efforts on laser material processing include: (1) theoretical studies, which are based on mathematical equations governing the fundamental physical phenomena, such as heat transfer, phase transformation, fluid motion, plasma formation, thermo-mechanical stress/strain, (2) methods of energy and mass balance of laser machining processes, (3) experimental studies, which were carried out to validate the results of the theoretical studies, and (4) effect of laser machining on the workpiece properties. These studies are discussed in this chapter.

2.1 Thermal modeling of laser drilling processes

Adams *et al.* [3] discussed the complex laser drilling process. Laser beam machining is a high speed ablation process. The high intensity obtained by focusing the pulsed energy emitted by a ruby laser has offered great potential as a tool for nearly forceless machining. With most substances, almost all of the material removed by the

laser beam leaves in the liquid state. Only a small fraction is vaporized, and the high rate of vaporization exerts forces which expels the liquid metals. All features of laser beam machining improve with increased laser intensity. The higher the intensity, the less heat is resonant in the uncut material, an important consideration for the materials which are sensitive to heat shock. Higher intensity provides more efficient process in terms of volume of material removal per unit of energy. Heat affected zone in the laser machining process can be reduced using a higher laser beam intensity [3].

The radiant energy delivered to a surface by a focused laser beam is consumed in four ways: 1. Part of the energy (a large part in the case of highly reflective metal surface) is reflected and lost, 2. most of the energy which is not reflected is used for melting, 3. a relatively small part of the energy is used to evaporate liquid metal, and 4. a very small part of the energy is conducted into the un-melted base material. Relative magnitude of these four avenues of heat consumption depends upon the thermal and optical properties of the material being worked, and the intensity and pulse duration of the laser beam. The evaporation of a very small part of the liquid metal takes place so rapidly under the high intensities of a focused laser beam that a substantial impulse is transmitted to the liquid. Most of the material leaves the surface being worked in the liquid state and at relatively high velocity. Not all the energy which leaves the laser-head reaches the material surface; some of the energy is absorbed enroute. Part of the material being expelled from the surface stays in the path of the beam in the form of small droplets and continues to absorb energy [3].

As energy of uniform high intensity is delivered to a worksurface, there is an initial transient period, after which steady-state ablation is established; it will continue as

long as the energy continues to be supplied at a uniform intensity. This steady-state ablation is characterized by a constant rate of material removal and by the establishment of a steady temperature distribution in the solid immediately in advance of the ablating surface. This steady temperature distribution is given by

$$\frac{T - T_o}{T_m - T_o} = e^{-\frac{Vx}{\alpha}} \tag{2.1}$$

with the boundary conditions as $T = T_o$ when x is very large, and $T = T_m$ when $x = 0$.

where, T is a temperature at distance x below the ablating surface, T_0 is initial temperature of the material being worked, T_m is melting point of the material being worked, V is steady ablation velocity, α is thermal diffusivity of the material i.e. $\alpha = K/(\rho C_\rho)$; K, ρ, C_ρ are thermal conductivity, density, and specific heat respectively of the workpiece. x is measured from the moving ablating surface boundary.

The depth at which heat penetrates beyond the ablating surface, also called heat affected zone (HAZ), is given by

$$X_c = \alpha/V \tag{2.2}$$

The characteristic depth X_c is the depth during steady state ablation which has experienced a temperature rise from T_0 to T_m.

During the initial transient period when ablation is just beginning, part of the heat delivered to the workpiece surface is used to establish temperature distribution within the solid. Once steady conditions are obtained, the heat contained in the solid does not increase any further, and the value of this steady heat content is given by

$$(Q/A)_0 = \frac{K(T_m - T_o)}{V} \tag{2.3}$$

where $(Q/A)_0$ is the heat per unit area contained in the solid beneath the ablating surface. After the heat contained in the solid has reached its steady values, all of the heat arriving at the material surface is used for melting and vaporization of the metal. The governing relationship is given by

$$f = V\rho H \tag{2.4}$$

where, f is the heat flow rate per unit area, H is the heat required for melting and vaporization, the heat per unit weight of material required to elevate the temperature of the solid from its initial value to the melting point, plus the heat of fusion, plus the additional heat supplied to boil a small fraction of the metal which has been melted.

After steady ablation is realized, the relationship between the intensity, exposure time, thickness of the material which has been removed, and the thermal properties of the material is given by [3]

$$f\theta = \frac{K(T_m - T_o)\rho H}{f} + \rho H d \tag{2.5}$$

$$d = \frac{f\theta}{\rho H} - \frac{K(T_m - T_o)}{f} \tag{2.6}$$

where θ is the exposure time Therefore, $f\theta$ is the total heat which has been supplied per unit area from the beginning of the ablation process and d is the thickness of the material which has been removed during the exposure time.

Adams *et al.* [3] mentioned that it is advantageous to use as high laser intensity and as short a pulse time as possible. The high intensities minimizes the extend of heat affected zone and the resident heat in the material after ablation.

Paek *et al.* [4] developed a model that uses a continuous, distributed, and moving heat source to describe the temperature profile, shape of the drilled hole, and

thermal stress propagation for laser drilled holes in high purity fired alumina ceramic substrate material. The temperature profile and the tangential stress distribution of the laser formed hole are calculated to indicate the magnitude of those factors that can influence the potential fracture of the alumina material. These factors are of interest in establishing optimum laser drilling parameters. In this, experimental results of the CO_2 and ruby laser drilled holes are compared with theoretical analysis. The focused laser beam is used for hole drilling of an isotropic material. It is important to determine the range of the laser drilling parameters, since thermal stresses produced due to laser drilling process can fracture the material. Two mathematical models are developed with semi-infinite and finite bodies as shown in Figure 2.1 [4],

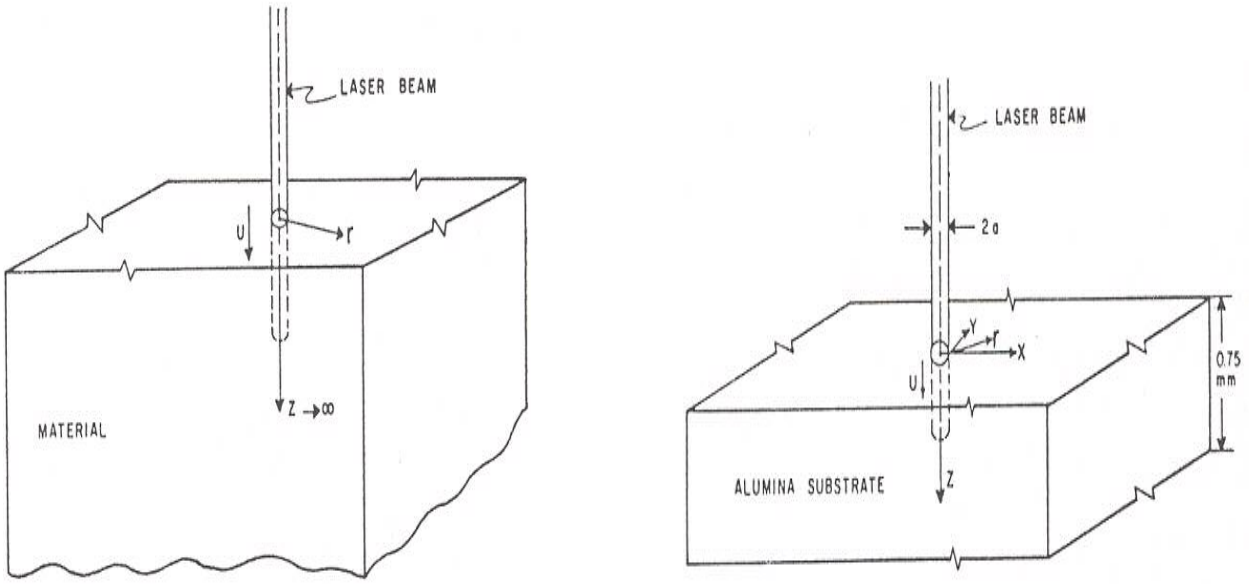

Fig. 2.1 Physical model and its coordinate system for semi-infinite and finite case with the corresponding boundary conditions [4]

In this model, thermal and mechanical properties are assumed constant through out the drilling process, reflective losses and heat losses through the bounding surfaces are neglected. The velocity of vaporization for the moving source equation is calculated

from the experimental study. The penetration depth was measured experimentally and differentiated with respect to time to obtain the laser drilling velocity. Mechanism of the drilling process involves initial absorption of energy into the surface, which greatly increases the vibratory and electronic energy content of the molecular structure beyond their equilibrium values, subsurface (50 to 500 Å) vaporization of localized areas, explosive expansion of these areas with subsequent removal of particulate matter, rapid rise of temperature with heating to melting and vaporization of adjacent areas within the focused beam spot, and repetition of the above steps several times for the duration of the laser pulse [4].

Material in and near the surface is explosively removed as the leading portion of the laser pulse is absorbed by the ceramic, providing enough energy to break the molecular and atomic bonds of the alumina structure. Large groups or clusters of the molecules and particles are expelled from the surface in all three states of matter as well as the plasma state. Radiation from the latter part of the laser pulse is absorbed by the remaining material, which rapidly begins to melt. The bulk of this molten mass is then evaporated by sudden increase in absorption energy, together with an accelerated rise in temperature. The temperature rise distribution due to a continuous disc heat source of a laser beam moving in the z-direction is given by [4],

$$T(r,z,t)=\int_0^a\int_0^t \frac{q(r',t')r'}{4\sqrt{\pi}\left[K(t-t')\right]^{3/2}}\left[\exp\left\{-\frac{r^2+r'^2+\left[z-f(t')\right]^2}{4K(t-t')}\right\}\right] I_0\left(\frac{rr'}{2K(t-t')}\right)dt'\,dr' \qquad (2.7)$$

The method of image heat source [29] is used to meet the boundary conditions expressed in Figure 2.1. For the first case, the source is located at z' = f (t') along the z-

direction and its image at z' = -f (t'), which moves in an opposite direction to the source and the corresponding solution is given as [4],

$$T(r,z,t)=\int_0^a\int_0^t \frac{P(r',t')}{4\rho C_p\sqrt{\pi}\left[K(t-t')\right]^{3/2}}.\exp\left\{-\frac{r^2+r'^2}{4K(t-t')}\right\}.I_0\left(\frac{rr'}{2K(t-t')}\right)r' \\ \left[\exp\left\{-\frac{\left[z-f(t')\right]^2}{4K(t-t')}\right\}+\exp\left\{-\frac{\left[z+f(t')\right]^2}{4K(t-t')}\right\}\right]dt'\,dr' \tag{2.8}$$

where P (r', t') is the laser intensity in J/cm^2 s.

For the second case, the image technique is applied so that the solution may be obtained by arranging multiple reflections of the bounding planes. The solution is given by [4],

$$T(r,z,t)=\int_0^a\int_0^t \frac{P(r',t')}{2\rho C_p K(t-t')d}.e^{\left\{-\frac{r^2+r'^2}{4K(t-t')}\right\}}.I_0\left(\frac{rr'}{2K(t-t')}\right). \\ \left[1+\sum_{n=1}^{\infty}\cos\frac{n\pi\left[z+f(t')\right]}{d}e^{\left\{-\frac{Kn^2\pi^2(t-t')}{d^2}\right\}}+\sum_{n=1}^{\infty}\cos\frac{n\pi\left[z-f(t')\right]}{d}e^{\left\{-\frac{Kn^2\pi^2(t-t')}{d^2}\right\}}\right]r'\,dt'\,dr' \tag{2.9}$$

where d is the thickness of substrate, K is the thermal diffusivity, k is thermal conductivity, P(r',t') is the laser intensity, Q is the strength of instantaneous point heat source, q(r',t') is the strength of continuous ring source, R is the distance between point (x,y,z) and heat source location, r, θ are for polar coordinate, and t, t' are for time, The term f(t') is the location of the moving source at time t = t', which is measured experimentally as the penetration depth obtained in alumina by the ruby laser. These solutions are final expressions to predict the temperature distributions in the material occurring during laser drilling process and satisfy the boundary conditions. The results for the temperature distribution are given in Figures 2.2 and 2.3.

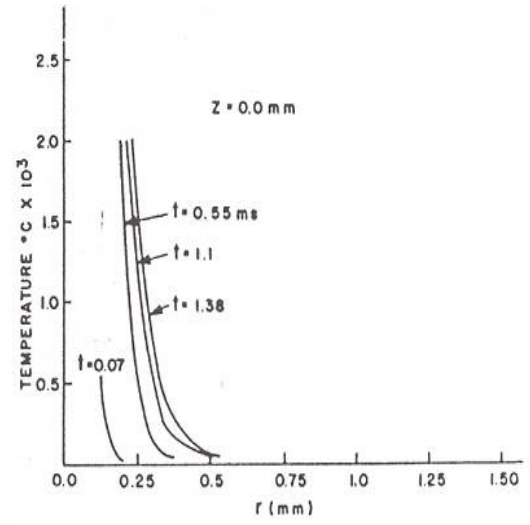

Fig. 2.2 Calculated temperature profile on the surface of Al_2O_3 [4]

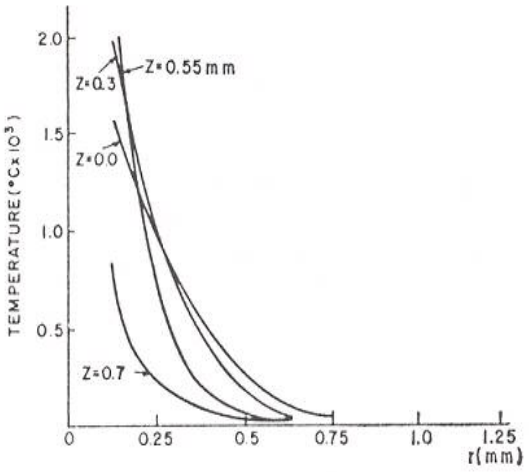

Fig. 2.3 Calculated temperature profile at various depths in Al_2O_3 [4]

In case of large temperature gradient, high stresses, which may exceed the fracture limit of the material, can develop. The stress-strain relation, in terms of the cylindrical co-ordinate system are given as [4],

$$\varepsilon_r = \frac{1}{E}\left[\sigma_r - \nu(\sigma_\theta + \sigma_z)\right] + \alpha T \tag{2.10}$$

$$\varepsilon_\theta = \frac{1}{E}\left[\sigma_\theta - \nu(\sigma_r + \sigma_z)\right] + \alpha T \tag{2.11}$$

$$\varepsilon_z = \frac{1}{E}\left[\sigma_z - \nu(\sigma_z + \sigma_\theta)\right] + \alpha T \tag{2.12}$$

Plane strain case which gives higher values of stresses than the plane stress case is used. The three-components of the thermal stresses in the cylindrical co-ordinate system are given by [4],

$$\sigma_r = \left(\frac{\alpha E}{1-\nu}\right)\frac{1}{r^2}\left[-\int_g^r Trdr\right] \tag{2.13}$$

$$\sigma_\theta = \left(\frac{\alpha E}{1-\nu}\right)\frac{1}{r^2}\left[\int_g^r Trdr - Tr^2\right] \tag{2.14}$$

$$\sigma_z = -\left(\frac{\alpha E}{1-\nu}\right)T \tag{2.15}$$

where $g = b(z)$, radius of the drilled hole as a function of z.

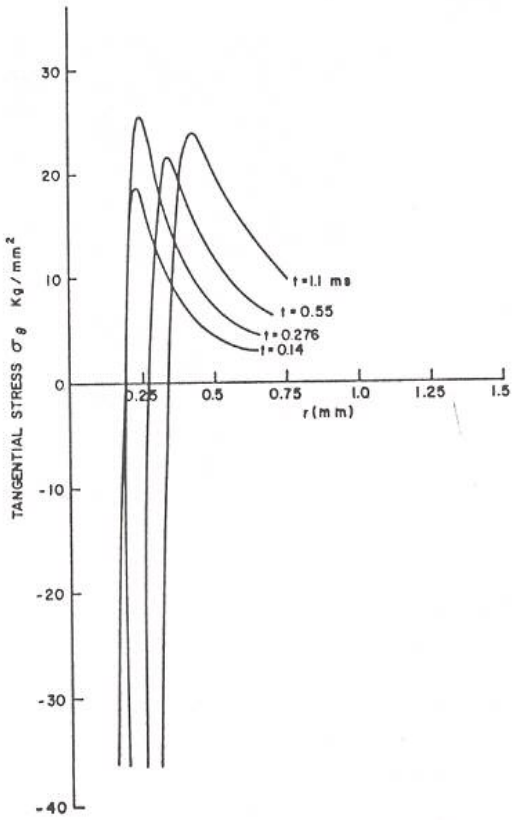

Fig. 2.4 Calculated tangential stress distribution in the r-direction on the surface of Al_2O_3 (z = 0 mm) [4]

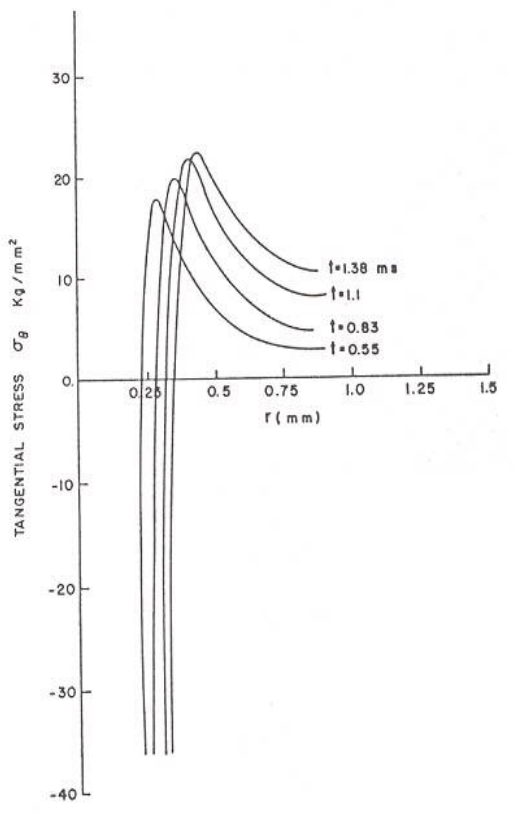

Fig. 2.5 Calculated tangential stress distribution in the r-direction in Al_2O_3 at depth z = 0.25 mm [4]

Of the three components of stress, the tangential stress component σ_θ is more significant with respect to potential fracture of the material. The distribution of the tangential stress and its propagation is obtained from the above equation and is shown in Figures 2.4 and 2.5.

Paek *et al.* [4] also predicted the profile of the laser drilled hole using the isotherm at the vaporization temperature.

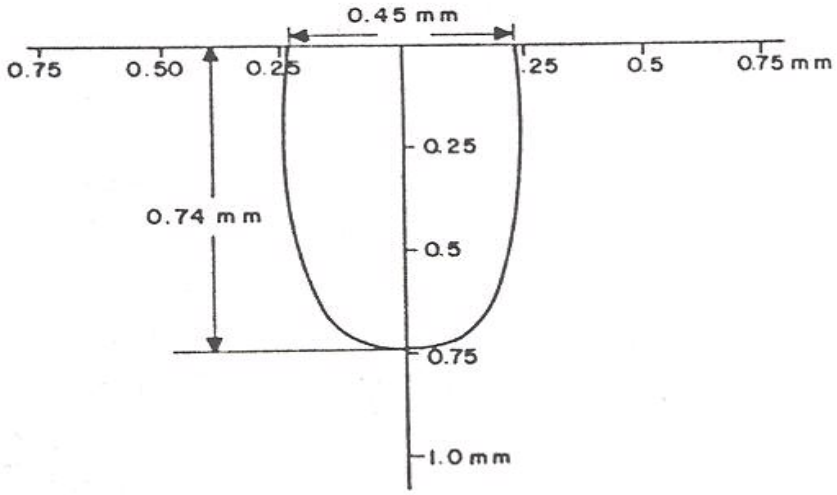

Fig. 2.6 Predicted shape of drilled hole in Al_2O_3 for ruby radiation [4]

Thermal stress analysis is summarized in Figure 2.7, which gives the maximum tangential stress (solid line) and its radial location (dotted line) measured from the center of the focused beam spot for any time during the laser pulse.

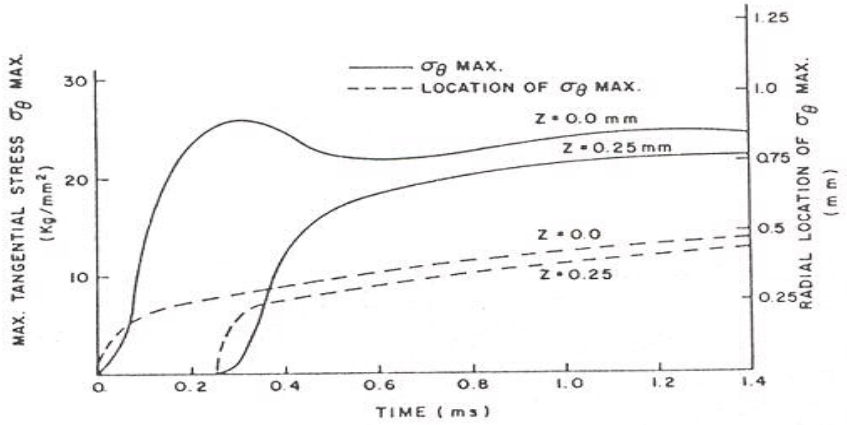

Fig. 2.7 Maximum tangential stress and its radial location for given time (ruby laser) [4]

It can be seen from Figure 2.7 that stress decreases as it propagates into the material (in a radial direction) as time goes by after about 0.3 ms. The net effect of the

propagation of these stress waves in the material is to reduce its strength [4]. According to Paek *et al.* [4], the shorter pulse length generally gives lower stresses. Longer pulses will generate higher stresses because heat will penetrate or diffuse further into the material. Since the magnitude of the stress is governed essentially by the temperature profile, it is necessary for laser hole drilling to maintain sufficiently high beam intensity for a minimum time to remove a given mass of material. It is observed that residual stresses are retained after each laser pulse. For multiple-pulse hole drilling, these residual stresses can accumulate to a fracture level depending upon the magnitude of the residual stress and the number of pulses used.

The quantitative connection between the absorbed laser energy and the extracted material volume is studied by Allmen [5]. From direct measurement of metal drilling efficiency of an Nd-YAG laser over a broad intensity region, the optimal results can be expected only in a quite narrow intensity region e.g. for metals, the range is from 5 to 50 MW/cm^2. For lower intensities heat conduction and reflection losses are dominant. For higher intensities, effect such as beam defocusing in the vapor cloud and air-breakdown severely degrade the drilling efficiency and the reproducibility of the drilling process. In this analysis, heat conduction and vapor absorption losses are neglected and thermal properties of the material are assumed constant. For expulsion of metal in liquid form, a mechanism involving radial liquid movement caused by the evaporation pressure is considered. It is observed from the experimental study that the expulsed liquid material must come from the bottom of the holes and not from the walls.

The expulsed liquid jet forms the envelope of a cone. From the regular and nearly polished surface of the drilled holes, it appears that laminar flows of the liquid

instead of a series of explosions occur. It is observed that the absorbing layer, after a certain warm-up time, moves at a constant velocity into the material, provided the laser intensity remains constant. The condition for such a behavior is equilibrium between the absorbed intensity Φ and the energy flux carried away with the expulsion material (consist of a vapor and a liquid part). The global energy balance is given by [5],

$$\Phi = j_v L_v + J_l L_l \tag{2.16}$$

and the drilling velocity is given by [5],

$$u = \left(\frac{1}{\rho}\right)\left(j_v + j_l\right) \tag{2.17}$$

where, ρ is the density of the material, j is the expulsion rate (g/cm^2 s), and L is the specific absorbed energy of the expulsed material with subscripts v and l for vapor and liquid components, respectively.

From the one dimensional heat conduction theory about a system with a constantly moving heat source, the equilibrium temperature distribution in a medium with density ρ, and specific heat $C_{p,}$ and thermal diffusivity K is given by [5],

$$T(u,\zeta) = \frac{\phi'}{\rho C_p u}\exp\left(-\frac{\zeta u}{K}\right) \tag{2.18}$$

where u is the velocity, Φ' is the power density of the source, and ζ is the moving coordinate in the direction of the velocity u.

Equation 2.18 does not include any phase transition and gives only an estimate for the actual temperature distribution and also does not consider the heat conduction losses. The power density Φ' of the moving heat source is the difference between the absorbed laser intensity and the power density carried away from the absorbing layer by the evaporation material [5].

$$\phi^{'} = \phi - j_d L_e \tag{2.19}$$

where L_e is the heat of evaporation. In front of the evaporating surface, a liquid layer is formed by heat conduction. The pressure of the evaporating surface acting on this layer causes the liquid to move in a radial direction out of the pressure zone. A condition for the liquid expulsion mechanism to start is given by the surface tension of the liquid metal, which must be overcome by the tangential pressure force. At lower intensities, the drilling mechanism is normal. At higher laser beam intensities, the splashes of resolidified material are deposited around the edges of the holes. Therefore, in order to obtain clean holes, it is necessary to operate at slightly higher intensities, where the kinetic energy of the expulsed liquid is high enough to prevent liquid deposit.

Yilbas [6] investigated the effect of plasma absorption of the laser beam energy. Laser produced plasma consists of vapor and liquid phases. Ejected liquid particles sizes vary from a few micrometers to 250 μm. These particles contribute to the absorption of incident laser light. They also cause the burst of vapor. However, in the vapor zone, charged and neutral particles also contribute to the absorption of the laser incident beam. An electron absorbs a photon as it moves from one free state to a more energetic one in the ion field. This is known as inverse Bremsstrahlung or free-free absorption. Plasma zone can be divided in three parts as shown in Figure 2.8.

In the flare zone, the interaction is complicated and the mechanism is highly dependent upon the laser output power, focus position, and material. The interface zone is closely related to the flare zone and it is observed that absorption of the incident beam is relatively higher in this zone. However, heating of the target by flares is also important, for they act like a heat source for the target influencing the hole formation.

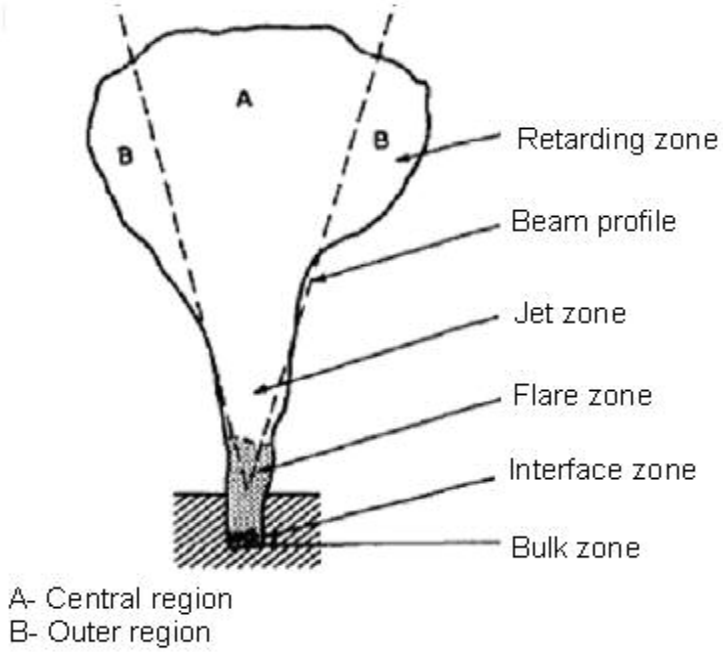

Fig 2.8 Diagram showing the planes in the plasma plume [6]

The absorption and heating in the flares have an inverse coupling effect on the resultant hole geometry. It is observed that due to absorption and subsequent expansion of the flares, the transmittance (I/I_o) changes with time, where I is the beam intensity after passing through a certain distance in the plasma, I_o is the intensity of the incident beam.

In the jet zone, relatively low values of transmittance are found compared with the values in the flare zone. The plasma pressure in the jet zone is very small due to very high velocities of the particles and the low density of the plasma [6].

The retarding zone has a larger radial size than the other zones as shown in Figure 2.8. The focus size of the incident beam is larger and produces a lower plasma density in the central region than in the outer region. The plasma is not disturbed by the incident laser beam and becomes cooler resulting in lower particle velocities and thus

transmittance is very low in this zone. Thus, the jet and retarding zones have less effect on the resultant hole geometry [6].

Yilbas *et al.* [7] proposed that due to the transient nature of the plasma, variation in electron density and temperature occurs with heating pulse. The overall absorption coefficient is higher at the central core of the plasma, and as the distance from the irradiated spot increases, this coefficient decreases. Higher electron density and lower temperature results in higher overall absorption coefficients. It is observed that almost 13 % of the incident power intensity is absorbed by the plasma at a plane 2.6 mm away from the irradiated spot.

Allmen *et al.* [8] proposed that metal surface shows a strong decrease of reflectivity with high intensity laser pulse. It is observed that above certain threshold intensity, most of the laser power was absorbed in the condensed target material. Initially during the laser pulse, reflected signal remains practically constant at a level corresponding to the reflectivity of the cold surface. When the critical surface temperature is reached, fast decrease of the reflected signal is observed and constant low reflectivity during the end of the laser pulse is seen. Experimental data indicates that the effect of enhanced absorptivity is started with an absorption wave emanating from the center of the illuminated area, shortly after the expulsion of liquid metal has started (around the evaporation temperature). This reflectivity drop is due to the ionization of the vapor (plasma). Plasma in close contact with the metal surface can account for enhanced bulk absorption. The absorbed heat seems to be transferred from the plasma to the condensed surface mainly by conduction process. In this last regime

of the laser pulse, 80% absorption of laser power in the condensed material is observed.

Sankaranarayanan *et al*. [9] studied the energy losses in the metal plasma during laser drilling. A plume consisting of vapor and ionized particles from the workpiece is commonly formed during various types of laser material processing. The process parameters, such as the laser power, spot diameter, scanning speed, material properties, and shielding gas affect the properties of the vapor–plasma plume.

The laser energy can be partitioned between the plasma and the workpiece in three ways: (i) the plasma absorbs most of the laser energy and less energy reaches the workpiece; this is encountered at higher irradiances (ii) the laser energy is equally distributed between the plasma and the workpiece, thus raising their temperatures (iii) more laser energy is deposited on the workpiece and the plasma absorbs less energy. Thermodynamically, three mechanisms are expected to affect the plasma conditions as a result of the absorption of laser energy by the plasma. These mechanisms are: (i) increase in the internal energy of the plasma, such as the plasma temperature, (ii) plasma volume expansion work, such as an increase in the plasma height and radius, and (iii) energy loss from the plasma to the surroundings and the substrate.

The laser–plasma interaction is modeled by considering various aspects of heat transfer, including melting, vaporization, metal vapor ionization, and plasma absorption. Threshold irradiance for improved process efficiency is found to exist. At power densities above 4.4×10^8 W/cm^2, less than 20% of the incident laser energy reaches the target. The drilling process becomes inefficient at power densities above 10^8 W/cm^2 because more of the laser energy is absorbed by the plasma and less energy is

available for the drilling process at such power densities. When the incident laser irradiance is less than this threshold value more of the laser energy reaches the workpiece. When the incident laser irradiance is higher than this threshold value, less of the laser energy reaches the workpiece.

Duley *et al*. [10] investigated the kinetic effects in drilling with the CO_2 laser. The time evolution of the holes drilled in fused quartz with a CW, CO_2 laser has been studied. It is shown that drilling proceeds by a complex balance between absorption and channeling of incident radiation. During drilling, the tip of the hole is often far removed from the optical axis and appears to propagate along a helical path on moving into material. Initially, rapid vaporization occurs with the hole profile being determined mainly by the radial dependence of the laser intensity. As the hole depth increases, the sides of the hole become steeper, so that reflection dominates absorption and channeling becomes important. The angle of the sides at every point adjusts itself so that a critical absorbed intensity is maintained at all points removed from the tip of the hole. This critical intensity is required to maintain a thin liquid layer over the entire surface of the hole. Vaporization occurs at the tip of hole until the depth has increased to a point where the total intensity (channeled plus incident) drops to a critical value, where only melting is possible. When a liquid phase is present, the tip of hole oscillates to minimize the surface tension of the liquid surface and to maximize the power absorption. Further increase in depth is due to propagation of a fusion front. Also striations in the hole are due to momentary filling in of the hole by liquid running in off the walls of the hole. Momentary decreases in the depth occur when melted material fills in the end of the hole.

Dabby *et al.* [11] analyzed high-intensity laser-induced vaporization and explosion of solid material. Material removal from the front surface of a solid by a high-intensity laser beam is analytically treated. This model allows for transmission of laser energy past the front surface and for transient phenomena. It is found that for certain laser and material parameters subsurface temperatures will exceed the surface temperature. Vaporization of the front surface occurs removing energy from the region near the front surface. This cooling mechanism causes the maximum temperature to lie below the surface. If sufficient heat generation within the solid occurs because of optical absorption, the removal of energy by vaporization of the front surface may not be rapid enough to prevent the inner portion of the material from reaching temperatures that are substantially higher than the surface vaporization temperature. If the temperature reached is high enough to cause vaporization of the material at depths below the surface, tremendous pressures arising from the vaporized materials will develop, that would explosively remove the intervening material. Material removed based upon this explosive technique is more efficient than conventional means of laser drilling that depend upon the vaporization of all material removed. It is also observed that material removal will continue even after the laser pulse ends.

Hamilton *at al.* [12] investigated experimentally the drilling effects on metals with CO_2 laser with pulse duration in the 15 to 50 μs region. The drilling efficiency, which is measured as depth drilled per unit of energy, is a function of the peak and average power density of the laser pulse and decreases with increasing power density over the pulse range studied. Linear relationship has been found between the hole depth and the number of laser pulses. According to the experimental results, in the case of short

pulses (4 μs), much of the incident energy does not reach the target because of the absorption wave decoupling effects. However, the photographic study suggests that decoupling is much less severe in the case of longer pulses (20 μs).

Yoshioka *et al.* [13] described a procedure for the numerical prediction of the hole shape drilled by high-power density beams by determining the fundamental drilling characteristics of metals and comparing the calculated results with the experimental results. This procedure is based on appropriate zoning of the region to be drilled and on the assumption that as metal is melted it is forced out of the hole by forces exerted by vaporizing metal. Data were obtained for mild steel, copper, aluminum, and molybdenum.

Material is removed in both vaporized and molten states. The quantity removed by vaporization, however, is negligible compared with that by melting. Therefore, for the present calculations, material removal is assumed to occur only in the molten state. The exact laser beam radius could not be obtained by experiment because the laser beam used was a multi-mode pulsed ruby laser. Therefore in this investigation, in the calculation, the beam radius was assumed to be the radius at which the calculated hole radius agreed with the experimental radius [13].

During drilling by multiple pulses there is normally a fixed time interval between pulses. Because of heat diffusion during this time, molten metal removal does not begin immediately at the start of the next pulse. The lag time, defined as the time required to initiate molten metal removal from the hole at the beginning of each pulse, can be predicted by the proposed method. When a hole is drilled by multiple pulses, the lag

time increases as the hole becomes deeper. When this lag time becomes equal to the pulse duration, drilling cannot proceed further as shown in Figure 2.9.

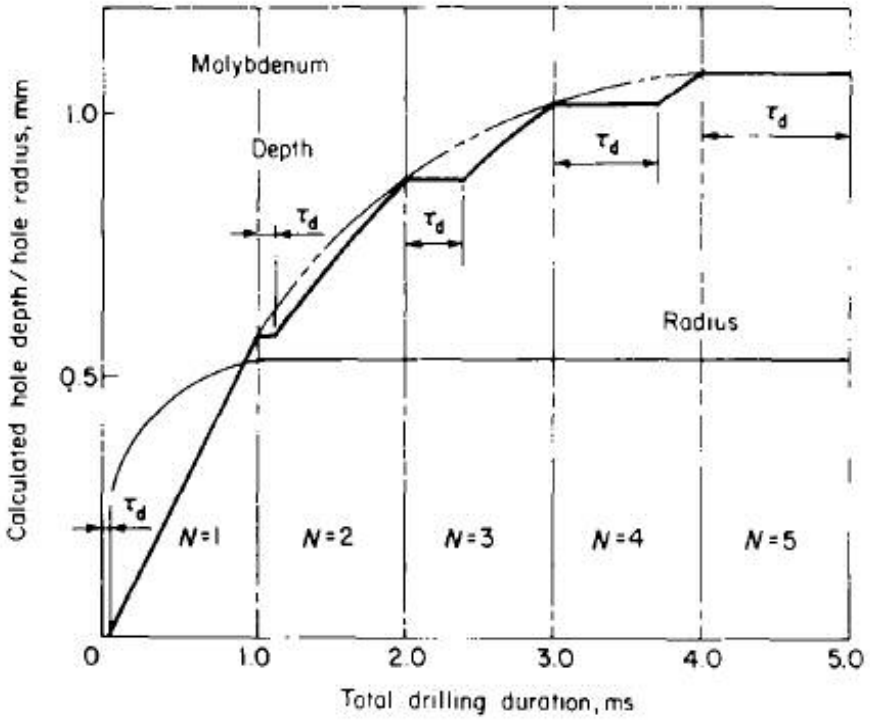

Fig. 2.9 Relationship between total drilling duration and calculated hole depth and hole radius experimentally [13]

The depth increases as the number of pulses increases; however, the rate of increase gradually becomes smaller. The hole diameter becomes larger with increase of the pulse duration; therefore, a small diameter hole is produced by multiple pulses of short duration. Within the first pulse, the hole diameter increases as the bombarding time increases as shown in Figure 2.9. After this pulse, however, hole diameter remains constant. The temperature rise of the hole edge on the target surface cannot exceed the temperature raised by the first pulse. Thus, the hole diameter is determined by the pulse duration and not by the number of pulses.

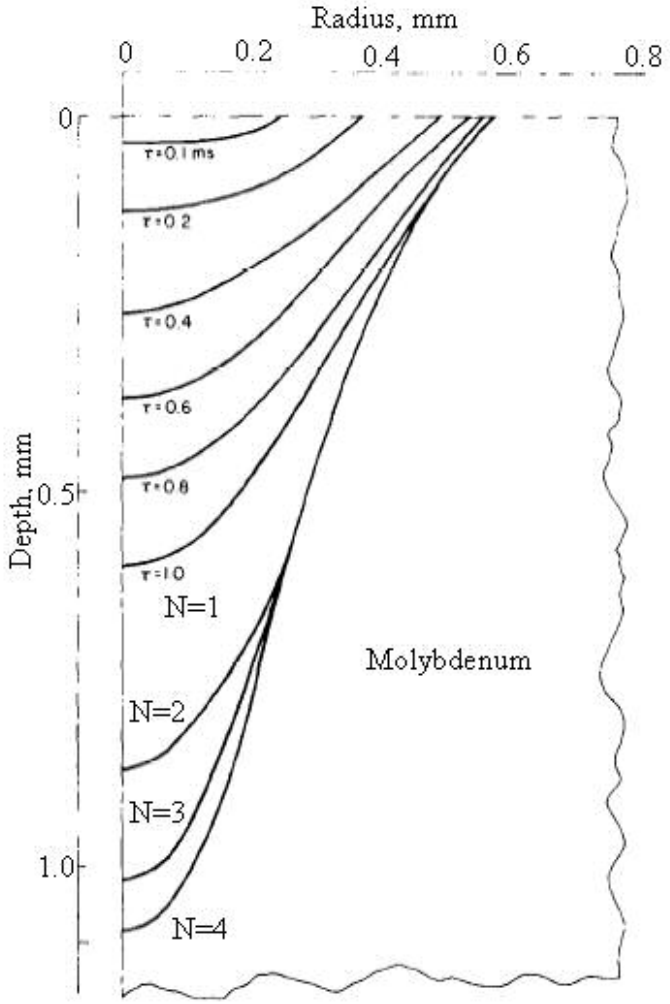

Fig. 2.10 Variation of hole shape with pulse duration and number of pulses [13]

Cross-sections of the hole for single pulses of 0.1, 0.2, 0.4, 0.6, 0.8, and 1.0 ms, and multiple pulses of 1 ms are shown in Figure 2.10. At the initial stage of drilling, the hole shape resembles a frustum of a cone but it becomes a true cone as drilling proceeds. In multiple pulse drilling, only the depth increases but the diameter does not increase.

Yilbas [14] studied the influence of the main process variables on hole quality. Hole quality is judged by the internal form, taper and related geometrical features, and

the extent of heat-affected material. Schematic of the salient geometric features of the laser-drilled holes is shown in Figure 2.10.

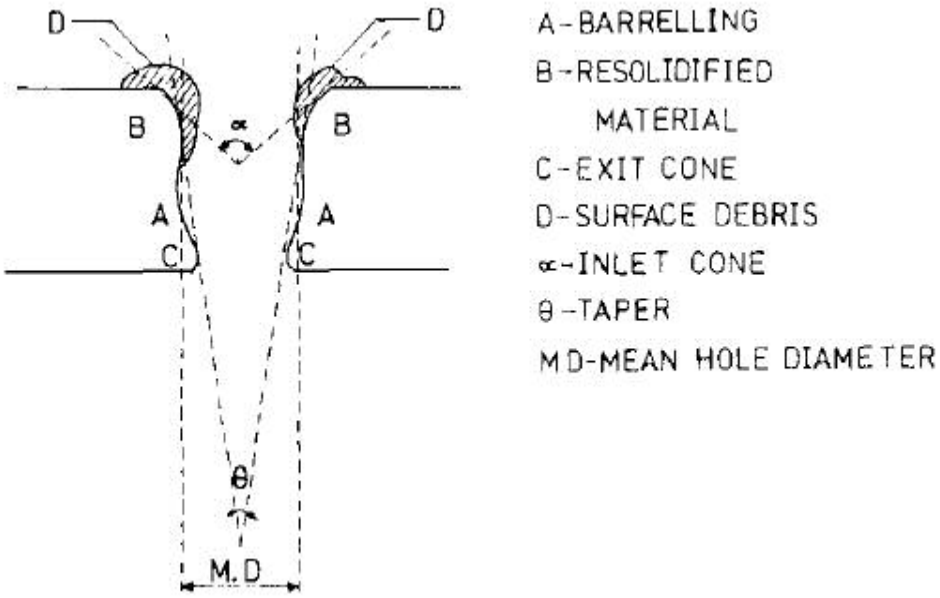

Fig. 2.11 Salient geometrical features of laser-drilled holes [14]

Barreling is the effect of energy trapped inside the workpiece to form a cavity. The formation of the barrel can guide the ejected material as it passes through the hole, forcing the molten material around the hole to come away from the sides. Resolidified material indicates the amount of material that had vaporized or melted during drilling, but had not escaped from the hole and so had resolidified on the internal surface [15]. Taper is the measure of overall taper of the hole sides, but does not include inlet and exit cones. The surface debris is an indication of the amount of resolidified materials appearing on the surface of the hole. The inlet and the exit cones are the measure between the entrance and minimum hole diameters and the measure between the minimum and exit hole diameter, respectively, and usually the inlet cone has a bigger value than the exit cone [15].

An increase in pulse energy increases the mean hole diameter. The effect of laser beam energy is very significant on all features of hole geometry. The effect of the focal position is very significant on surface debris, inlet cone, and barreling and exit cone. The amount of taper increases as thickness increases. The effect of drilling-medium pressure is very significant on all features of hole geometry except the inlet cone. Effect of energy and pressure is thickness dependent. From the dimensional analysis, it is observed that surface debris, inlet cone, mean hole diameter, and overall quality are affected by energy for all of the workpieces. The effects of the focal position appear in the inlet cone, exit cone and overall quality, in such a way that at lowered beam waist the hole quality improves. The inlet cones, barreling and overall quality are affected by thickness. At lower thickness of workpiece, the overall quality increases. The effects of pressure are found to be significant on surface debris, barreling, exit cone, mean hole diameter and overall quality. At low levels of pressure, the overall quality improves as per the analysis by Yilbas [14].

Chan *et al.* [16] developed a one dimensional steady-state model describing the damage by material removal by vaporization and liquid expulsion due to laser-material interactions. When vaporization occurs, there exists a discontinuity across the Knudsen layer of a few molecular mean free paths. This discontinuity is modeled by a Mott-Smith-type solution. The vaporization process creates a recoil pressure that pushes the vapor away from the target and expels the liquid phases. Closed-form analytical solutions are obtained for three different materials- aluminum, a superalloy, and titanium. The absorbed laser energy is partitioned into (1) lost into the substrate, (2) latent heat of fusion and vaporization, and (3) creating recoil pressure to push the vapor

away and expel the liquid. It is observed that the surface temperature increases with increase in absorbed power. The liquid-layer thickness decreases as the absorbed power increases. At higher power, the vaporizing temperature is high so that the recoil pressure is also high and as a result the liquid layer becomes thinner [16].

The total material removal rate is equal to the sum of vaporization and liquid expulsion rates. For all the material under study, the vaporization rate increases with power. However, the liquid-expulsion rate behaves differently for different materials. At lower power, the vaporizing temperature is low and the expulsion rate is low because of low recoil pressure. At higher laser beam power, the vaporizing temperature is high. However, the thickness of liquid layer is small so that the liquid-expulsion rate becomes small. At low powers, there is more liquid expulsion than vaporization. At higher power, vaporization is the dominant form of material removal [16].

Yilbas [17] investigated the drilling speed during laser drilling of metals. A statistical analysis for the effect of thickness of the workpiece, type of the material, power intensity, the focal length, and position of focal plane of the lens on the results for drilling speed for titanium, nickel, EN58B, and tantalum is determined. It is observed that titanium drills fastest, followed by nickel, then EN58B, with tantalum as slowest. This is because titanium has low thermal diffusivity and high absorption coefficient resulting in relatively higher temperature gradients than other materials under study.

Consequently, titanium evaporates early, giving rise to high recoil pressure occurring in the evaporating region of the workpiece. This enhances the cratering and increases mass removal from the crater. This is valid for all parameters, although situation changes some what with thickness of the workpiece. For thick workpieces, the

drag forces due to recoil pressure on the liquid layer in the crater are sufficient to drive liquid material along the hole walls to be ejected as particles are swept onto the surface surrounding the damage crater. The situation for the thin targets is different because the target is penetrated before bulk of the molten material is removed from the crater [17].

Consequently, when high pressures within the crater are relieved and drag forces reduced by target penetration, the liquid residue attached to the hole walls drawn back into the crater by surface forces to resolidify, thereby blocking the hole and hence reduces the drilling speed. Drilling speed decreases as the workpiece is moved further from the focus. Drilling speed which is the representation of the depth of the drilled hole decrease with increase in pulse length [17].

Kar *et al.* [18] proposed a simple two-dimensional axi-symmetric model for laser-induced material removal by considering multiple reflections of the laser beam inside the cavity and shear stress-induced liquid metal flow into account. The vaporization of the liquid metal and the melting of the solid substrate at the liquid-vapor and the solid-liquid interfaces, respectively, are modeled by applying the Stefan condition at various points on the interfaces. The effects of various process parameters, such as the laser power, laser beam radius, and the laser pulse on-time on the cavity depth, the recast layer thickness, and the cavity tapering are examined.

The conclusions of this investigation [18] are summarized as follows: (a) the laser-induced cavity depth increases as the laser intensity increases. Multiple reflections lead to the formation of deeper cavities than when multiple reflections are absent. (b) The recast layer thickness decreases as the laser intensity increases. Multiple reflections generate thinner recast layer than when reflections are not taken into

account. (c) The cylindricity of the laser-induced cavity increases as the laser intensity increases. The cavity is more cylindrical in the presence of multiple reflections than in the absence of any reflections. (d) The effects of the liquid metal flow, which is caused by the shear stress at the liquid-vapor interface, on the cavity parameters such as the cavity depth, and the recast layer thickness are found to be insignificant. The rate of material removal due to vaporization is found to be several orders of magnitude higher than that due to the liquid metal flow. (e) The cavity depth varies linearly with the gross laser intensity when reflections of the laser beam inside the laser-induced cavity are not taken into account. However, this variation is found to be nonlinear when multiple reflections are considered in the mathematical model.

Yilbas *et al.* [19] considered the efficiency of laser drilling of stainless steel and developed a laser heat-transfer mechanism taking into account the phase-changes. They computed the efficiency for holes drilled in stainless steel workpieces of 0.5 and 1 mm thicknesses. Drilling efficiency is defined as [19],

H = [energy required to form a hole (Q_{req})] / [energy input (Q_{input})] (2.20)

$$\eta = m_{hole}\left(\int_{T_0}^{T_m} C_p dT + \int_{T_m}^{T_v} C_p dT + L_m + L_v\right)/\left(E_{laser\ output\ energy}\right) \quad (2.21)$$

where m_{hole} is the mass of the material filling the hole ($\pi D^2 Z/4$) , Cp is the specific heat of the workpiece, T_o is the room temperature, T_m is the melting temperature, T_v is the evaporation temperature, L_m is the latent heat of melting, and L_v is the latent heat of evaporation. Efficiency varies with power intensity and pressure of the ambient gas used for drilling. However, for thin samples, the efficiency is not significantly affected by the power intensity because the cavity produced in the workpiece during laser

interaction is reduced which produces less recoil pressure. Therefore, the mass removal rate becomes independent of the power received by the workpiece, i.e. the mean hole diameter is relatively less affected by the laser power received at the surface. For a 0.5 mm thick workpiece, the efficiency is reduced considerably and the maximum value is 14%.

Modest [20] proposed a three-dimensional, transient model for laser machining of ablating/decomposing materials. A three-dimensional heat conduction model has developed to predict the transient temperature distribution inside a thick solid that is irradiated by a moving laser source, and the changing shape of a groove carved into it by the evaporation of material. The laser may operate in CW or pulse mode with arbitrary temporal as well as spatial intensity distribution. The governing equations are solved using a finite difference method on an algebraically-generated boundary-fitted coordinate system. The accuracy of the present transient model was verified by comparison with previous three-dimensional codes that were limited to quasi-steady CW operation. Groove shapes and temperature distributions, as well as their transient development, for various machining conditions are presented, demonstrating the differences in the ablation process between CW, pulsed, and Q-switched (or other pulses of extremely short duration) laser operations.

A three dimensional, fully transient conduction model was developed that is capable of predicting the shape of a developing hole or groove that is formed by ablation of material, caused by a stationary or moving laser. The model allows the treatment of variable thermo physical and radiative material properties, as well as laser intensities of arbitrary spatial and temporal shape. Sample calculations were carried out

to study qualitative differences in material removal when CW, normally-pulsed (pulse length ~ 100 μs), and short-pulsed (pulse length ~100 ns) lasers are employed. The results show that during short-pulsed laser ablation, conduction losses are essentially negligible, resulting in substantially larger removal rates than for CW operation for identical conditions, and an extremely thin (small fraction of a single beam radius) heat-affected layer. Ablation with normally pulsed lasers, on the other hand, results in removal rates which approach those of a Q-switched laser, but the thickness of the heat-affected layer is much larger approaching that of the CW laser. The calculations further indicate that, during short-pulsed laser ablation, the material cools off rapidly after the end of the pulse, returning to ambient conditions well before the beginning of the subsequent pulse.

Ganesh *et al.* [21] developed a direct computer simulation technique to analyze quantitatively the influence of the fluid flow and heat transfer in the transient development of a laser drilled hole in a turbine airfoil material, where the material removal is effected by vaporization and melt ejection. The coupled conduction heat transfer in the solid and the advection-diffusion heat transfer in the liquid metal, the fluid dynamics of melt expulsion and the tracking of solid–liquid and liquid–vapor interfaces have been mathematically modeled for the 2D axi-symmetric case. The donor–acceptor cell method, involving the volume of fluid approach is used to solve the complex problem and a versatile numerical code has been developed. It takes into account all thermo-physical properties including latent heat of vaporization, gravity, and surface tension driving forces. The novelty of this model is to treat the melted pool surface as a deformable free surface. The impressed pressure and temperature on the melt surface

is provided by a one dimensional gas dynamics model whose vaporization kinetics is also discussed. The model is used to simulate drilling for a number of spatially and temporally varying laser intensity profiles. It is found that resolidification of melt (recast formation) occurred throughout the pulse interval and had significant effect on the developing hole geometry, while the effect of vaporization material removal on the hole geometry is found to be small. Comparison of the simulated results indicates the material removed per joule of energy absorbed appears to be inversely proportional to the square root of the peak beam intensity and the drilling rate appears to be proportional to the square root of the surface pressure.

2.2 Energy balance for laser machining processes

Semak *et al.* [22] carried out a theoretical analysis of energy balance in the laser–metal interaction zone. The heat transfer due to recoil-pressure-induced melt flow is taken into consideration. It is shown that, for the absorbed laser intensities typical in welding and cutting, the recoil pressure induces high-velocity melt-flow ejection from the interaction zone. This melt flow carries away from the interaction zone a significant portion of the absorbed laser intensity (about 70 to 90% at low laser intensities); thus, convection-related terms can be ignored neither in calculations of the energy balance in the interaction zone nor in calculations of the thermal field in the vicinity of the weld pool or cutting front.

It is observed that the recoil pressure can play a significant role in the ejection of melt from the interaction zone even for low melt surface temperatures close to the melting point. The velocity of the keyhole-wall front or cutting front is determined by the

absorbed laser intensity and can be either lower or higher than the beam's translation velocity [22].

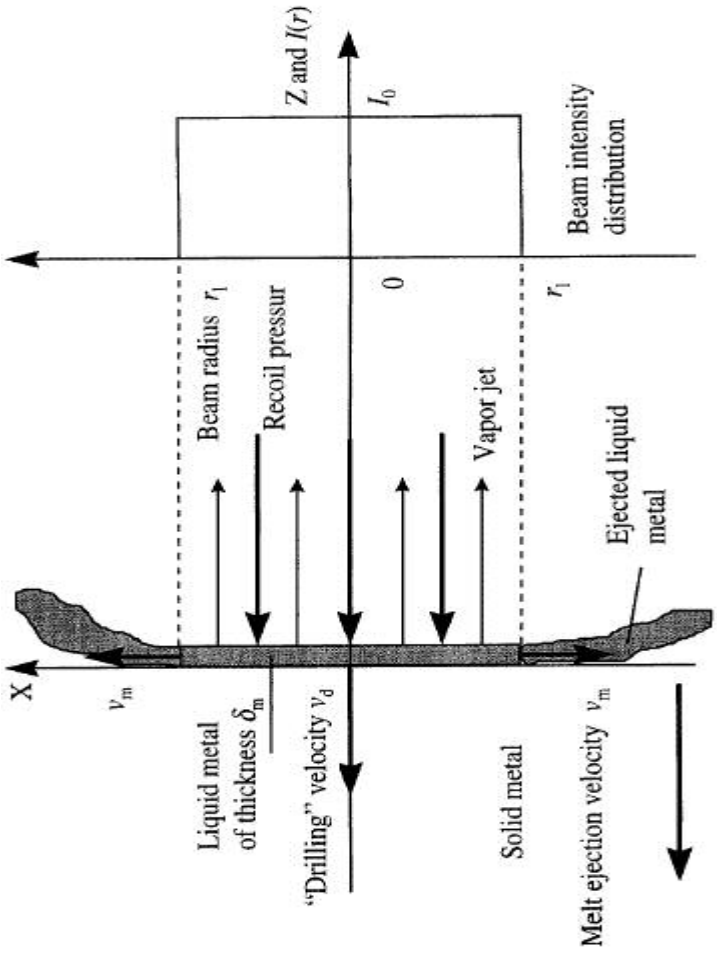

Fig. 2.12 The physical model of melt removal from the interaction zone, the cross section in the X – Z plane is shown [22]

A thermal model of the melting and vaporization phenomena in the laser drilling process has been developed by energy balance analysis at the solid-liquid and liquid-vapor interfaces by Zhange *et al.*[66]. The dependence of saturation temperature on the back pressure was accounted for by the Clausius/Clapeyron equation. The conduction heat loss to the workpiece is also included in the model and is solved using an integral approximate method. The predicted material removal rate qualitatively agreed very well

with the experiment data. The amount of heat lost through conduction is found to be very small and its effect on the vaporization is not significant. However, the location of melting front is significantly affected by conduction heat loss especially for lower laser intensity and longer pulse. The existence of sub-cooling in the solid is helpful in reducing the thickness of recast layer.

2.3 Laser Cutting

Kaplan [23] proposed an analytical model of metal cutting with a laser beam. The process of cutting metals with a laser beam is described by a mathematical model comprising a set of balance equations for mass, momentum, and energy. Numerical evaluations of the analytical model provide explanations of the process behavior both for inert and for oxygen gas cutting. It is observed that the kerf width decreases with increasing speed due to heat conduction, whereas cutting front angle and absorption together with thickness, speed, and temperature of the melt film all increase. For thicker metals and low speeds, the speed limit is reached when the laser beam is geometrically completely consumed, whereas for thinner metals, the higher speed can increase the heat flux threshold above the laser intensity thus permitting the cut front ignition. For higher speeds, the evaporation temperature is reached and can lead to a broadening of the kerf width. Using a higher gas pressure, increases the diffusion limited oxidation rate and provides higher cutting velocities, while the fraction of oxidized metal decreases substantially with increasing speed.

Mathematical modeling of the cut kerf geometry for laser fusion cutting of thick metals is carried out by Duan *et al.* [24]. This investigation presents a mathematical model for CO_2 laser fusion cutting to calculate the three-dimensional stationary

geometric shape of the cutting front for thick metals. This model considers the effect of multiple reflections on the cutting front geometry as well as all relevant parameters of the laser beam. The effects of multiple reflections are functions of the inclined angle of the cutting front and the cutting depth. The effects of various laser processing parameters, multiple reflections, and inert gas pressure on the geometric shape of the cutting front have been analyzed systematically and in detail. Most mathematical models of laser fusion cutting do not consider the effect of multiple reflections within the cut kerf. The main reason may be that the thickness of the materials being processed in these models is limited to less than 3 mm and then the effect of multiple reflections on the absorptivity is very small and can be neglected without causing much error. However, with an increase in material thickness and a cutting speed close to the maximum value, the effect of multiple reflections on the absorptivity becomes stronger at the lower position of the cutting front because the inclined angle of the cutting front increases, as shown in Figure 2.13.

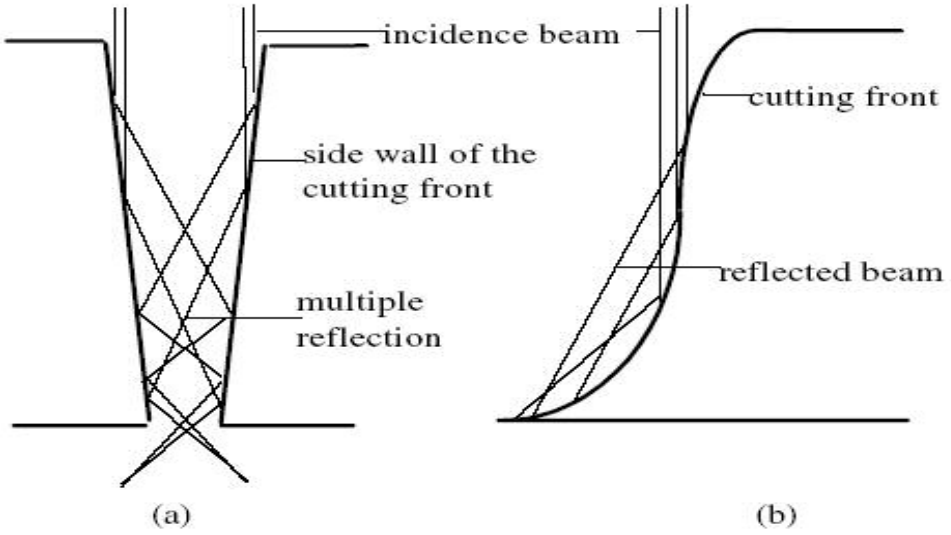

Fig 2.13 Multiple reflections of laser beam in both the cutting front and the side walls of the cutting front: (a) front view and (b) side view [24]

In this case, the effect of neglecting multiple reflections will result in a large error in the calculation of the cut depth or cutting speed. The absorption coefficient for multiple reflections in the keyhole was estimated by Kaplan [23].

$$\alpha_{mr} = 1 - [\rho_{Fr}(\pi / 2)]^{(\pi/(4\bar{\theta}_w)-1)} \quad (2.22)$$

where α_{mr} is the absorption coefficient of multiple reflections, ρ_{Fr} is the Fresnel reflection coefficient that is, in general, angle-dependent and $\bar{\theta}_w$ is the mean wall angle. The absorption of multiple reflections in the laser fusion cutting process is obviously less than that in keyhole process because the laser beam is only absorbed by the cutting front. Therefore, the absorption coefficient for multiple reflections in cutting, α_{mrc} in laser fusion cutting is taken approximately as one-third of the value of the keyhole value according to the geometric shape of the cutting front, i.e. $\alpha_{mrc} = \alpha_{mr}/3$.

For lower thickness (< 3 mm) of the workpiece, the effect of multiple reflection is neglected. The theoretical results show that multiple reflections are a function of the cutting depth and angle of inclination of the cutting front and that they become more significant with an increase in material thickness and cutting speed. The geometric shape of the cutting front is strongly dependent on the cutting speed, laser power and focal position but only slightly on the assisted inert gas pressure. With an increase in the cutting speed, the inclined angle of the cutting front increases and the cut-through depth decreases. With an increase in the laser power, the cutting front becomes steeper and the cut-through depth increases. There is an optimal range of focus position for a group of cutting parameters. Any large deviation will reduce the cut-through depth, increase the inclined angle of the cutting front, and also deteriorate the cut quality. The inert assisted gas jet has little influence on the geometric shape of the cutting front. This

model can be used to predict the cutting thickness for a given group of cutting parameters or the optimal process parameters for a given material thickness, estimate the cut edge quality, and provide a more precise boundary condition for the calculation of gas flow field distribution inside the cut kerf [23].

Prusa *et al.* [25] estimated heat conduction losses in laser machining process. In order for the models to closely represent the physics of the process, the heat lost by conduction during cutting has to be incorporated. This investigation outlines the details of a mathematical model used for estimation of heat conduction losses in laser cutting by employing integral methods to solve the three-dimensional, heat conduction equation. The energy balance equation is given by,

$$Q_{Laser} + Q_{oxidation} = \dot{m}(c\Delta T + h_f) + Q_{conduction} \tag{2.23}$$

where h_f is the latent heat of fusion. Latent heat due to evaporation is neglected in this analysis. Energy is lost from the cutting zone by conduction, convection, and radiation. The major source of heat loss in laser cutting is conduction, while the contributions of convection and radiation are so small that they can be neglected without loss of accuracy. Simple, yet accurate, correlations are presented for the conduction heat loss rate, as well as for characteristic thicknesses of the heat affected zone (HAZ). These variables are functions only of Peclet number (Pe), which may be thought of as a dimensionless cutting speed. The correlations are then used to predict the cutting speed in laser cutting, and the temperature field in the HAZ. The predictions show an excellent match with experimental results. Cutting speed is predicted using an energy balance at the cutting front. An implicit, nonlinear equation for Pe as a function of Stefan number (Ste) and dimensionless heat of combustion is obtained. Stefan number gives the ratio

of sensible heat to latent heat in the workpiece. Detailed analysis of beam absorptivity, coupled with the dimensionless cutting speed results suggest that dimensional cutting speed may be correlated as a unique function of the ratio of incoming laser power to workpiece thickness. At lower cutting speed, the conduction losses increases; however, at the higher cutting speed opposite trend occurs [25].

2.4 Thermal and mechanical effects on materials induced by laser machining

Luft *et al.* [26] studied thermal and mechanical effects on materials induced by pulsed laser drilling. The microscopic studies showed that for percussion drilling in the high fluence range characterized by high ablation rates of a few micrometers per pulse, the use of shorter pulses (50 ns) did not lead to any appreciable reduction in the melt component, material re-deposition or thermal load on the wall of the hole. In addition, the increasing mechanical loads on the material due to higher pressure in the drilled channel become a limiting factor for the precision of the processing.

It is also known, however, that the use of laser pulses of high intensity (10^{10} W/cm^2) increases the mechanical load placed on the material because of the high ablation and plasma pressures. It is, therefore, important when using short laser pulses for precision micro machining not only to adhere closely to pre-defined geometric contours, but also to have an understanding and control over laser-induced changes in the structure and properties of the material. The aim of using short-pulse lasers for micromachining is to minimize the thermal and mechanical effects upon the material. It is necessary to use special techniques to prepare and study the material to enable the laser-induced structural changes to be demonstrated and to establish the ranges on which the thermal and/or mechanical effects occur [26].

Plastic deformation of the target may result upon laser drilling either directly due to laser-induced pressure surges or indirectly as a consequence of thermally- induced compressive and tensile stresses. Monocrystalline molybdenum and silicon were selected as the test materials because of their sensitivity to these processes. It is observed that melt-free processing is not possible with laser pulses of high fluence. The increase of peak power density above five orders of magnitude through the use of shorter pulses of the same fluence does not result in a corresponding change in the ablation rate. However, it does change the melt expulsion mechanism from flow of liquid towards atomization and makes the re-deposition of material in the drill channel more difficult. The width of the heat affected zone observed on the wall of a hole is not determined by the duration of the pulses. Heat affected zones, in the size range of 5 μm to 10 μm, are seen for deep holes of similar geometry with both ns and fs pulses. Using ns pulses with a high rate of material ablation per pulse, a smaller heat affected zone was established at the bottom of the hole than on the side wall of the hole [26].

The heating of the material in the region surrounding the processed site firstly results in thermally-induced structural changes (e.g. polygonization, re-crystallization). Secondly, the high temperature gradients which result upon localized heating lead to stresses which can cause plastic deformation of the material (by creating dislocations) and permanent (tensile) residual stresses with possible crack formation. The mechanical influence on the material as a result of the pressure surges arising during laser drilling cannot be neglected. Ductile materials react with deformation (bulging upon drilling through the material) whereas brittle materials react with fracture. The requirements for precision, reproducibility, speed, and freedom from damage cannot all

be satisfied at the same time. The laser system deployed and the parameters have to be carefully matched to the processing task. A processing mode which meets all requirements is difficult to determine [26].

Araujo *et al.* [55] studied the effect of laser machining of an aluminum alloy. Laser machining is an attractive alternative to traditional machining of Al-2024 because critical operation parameters in aeronautic industry, such as processing time, versatility, contamination and finish can be improved. The main disadvantage of laser machining is the high temperatures reached by the workmaterial during laser processing. A heat affected zone (HAZ) extension lower than 5 μm is observed. The microstructural analysis shows that this HAZ suffers a heating between 548 and 596 ^{o}C where a liquid phase is present. The high N_2 gas pressure used for the laser cutting induces roughness on this viscous material during laser processing. To improve this feature, the use of other laser wavelengths and/or power is proposed.

Laser processing of structure sensitive hypereutectic ductile iron, a cast alloy employed for dynamically loaded automotive components, was experimentally investigated over a wide range of laser process parameters by Gadag *et al.* [56]. Laser parameters are power (0.5 to 2.5 kW) and scan rate (7.5 to 25 mm/s) leading to solid state transformation, all the way through to melting followed by rapid quenching. Superfine dendritic (at 105 °C/s) or feathery (at l04 °C/s) ledeburite of 0.2 to 0.25 μm lamellar space, γ - austenite and carbide in the laser melted and martensite in the transformed zone or heat-affected zone were observed, depending on the laser process parameters.

Depths of geometric profiles of laser transformed or melt zone structures, parameters, such as dendrile arm spacing, volume fraction of carbide, and surface hardness bear a direct relationship with the energy intensity (10 to100 J/mm^3). There is a minimum energy intensity threshold for solid state transformation hardening (0.2 J/mm^3) and similarly for the initiation of superficial melting (9 J/mm^3) and full melting (15 J/mm^3) in the case of ductile iron. Simulation, modeling, and thermal analysis of laser processing as a three-dimensional quasi-steady moving heat source problem by a finite difference method, considering temperature dependent energy absorptivity of the material to laser radiation, thermal and physical properties and freezing under non-equilibrium conditions enabled determination of the thermal history of the laser treated zone. This includes assessment of the peak temperature attained at the surface, temperature gradients, the freezing time and rates as well as the geometric profile of the melted, transformed or heat-affected zone [55].

CHAPTER 3

PROBLEM STATEMENT

Based on the review of literature, it is apparent that study of the laser machining processes in detail is essential in order to improve quality and efficiency of the laser machining process. Study of laser machining involves both heat transfer and fluid dynamics. It is very important to develop a thermal model which can predict the geometry of the laser drilled hole and the kerf width for a given laser beam parameters. Thermal model of the laser machining facilitates with the optimization the laser beam parameters for maximum productivity for laser machining process. Earlier models are based on numerous assumptions which did not represent the laser machining process accurately. So, it is necessary to consider critical parameters representing the laser machining process so that the thermal model represents the actual laser machining process.

An attempt has been made to develop a thermal model of laser drilling and cutting/grooving using Jaeger's moving circular disc heat source equation. Laser machining involves supply of intense energy locally to the workmaterial. At the surface of the workmaterial, intense laser energy is transformed into heat, which is available for processing. Process model is developed to gain detailed physical insights into the process behavior, e.g. to analyze the dependency of the process outputs on the

operating parameters (laser power, laser beam diameter, pulse duration, and traverse velocity).

Laser drilling, cutting, and grooving models are developed depending on the motion of the circular disc heat source which gives the profile of the laser drilled hole and kerf width of laser cutting and grooving processes. Using this model, one can control the taper of the laser drilled hole and minimize the kerf width in laser cutting. The effects of coefficient of absorption of the laser intensity at the surface of the workpiece and the absorption of the laser beam energy due to plasma generation are included in the model. The workpiece boundary effects are incorporated into the thermal model. The effect of thickness is also incorporated in the model. Thermal model also takes care of the effect of location of starting point of laser cutting/grooving of the workpiece e.g. cutting or grooving from the edge or from the central location of the workpiece. Heat and mass balances for laser drilling, cutting, and grooving processes are also carried out. Latent heat of fusion and evaporation are determined and used in the calculation of energy balance of the thermal processes. Heat consumed to raise the temperature of the workpiece and heat losses due to conduction are also determined. Consequences of laser machining, such as heat affected zone are also determined.

CHAPTER 4

APPROACH

4.1 INTRODUCTION

The fundamental method of solving temperature field problems is to solve partial differential equations for heat conduction based on Fourier's law of conduction, considering initial as well as boundary conditions. However, sometime the heat conduction problems in the field of manufacturing and tribology are rather complicated and are difficult to solve directly from basic partial differential equation. The heat source method is recognized as a very powerful tool for solving these complex problems with the help of stationary or moving heat sources of various shapes, sizes and heat intensity distribution for transient or quasi-steady conditions.

For laser machining, the heat source is represented as a circular disc heat source. Equation for the solution of the instantaneous point heat source in an infinite conduction body is given by [39], [29],

$$\theta(R,\tau) = \frac{Q_{pt}}{c\rho(4\pi a\tau)^{3/2}} e^{-R^2/4a\tau} \tag{4.1}$$

Equation 4.1 can be derived from Fourier's law of heat conduction in solids. Equation for the solution for an instantaneous circular ring heat source in an infinite medium is given by [39], [29],

$$\theta = \frac{Q_{rg}}{c\rho(4\pi a\tau)^{3/2}} \cdot e^{-\frac{r_0^2+r^2+z^2}{4a\tau}} \cdot I_0\left(\frac{r^* r_0}{2a\tau}\right) \quad (4.2)$$

For ease of programming and to increase the speed of computation, the special function $I_0(p')$ can be approximated by a simple function without significant loss of accuracy (<5%).

The solution for instantaneous point heat source problems will be considered as the bases for heat source method. Instantaneous point heat source equation is used to derive the instantaneous ring heat source equation. Instantaneous ring heat source equation is used to derive the moving circular disc heat source to model the laser machining processes analytically. In laser drilling process, the moving circular disc heat source moves in Z-direction perpendicular to the workpiece surface with certain velocity. In case of laser cutting and grooving process, the moving circular disc heat source moves in X-direction parallel to the direction of surface of the workpiece with certain velocity.

4.2 Heat transfer modeling for laser drilling process

Laser beam is a circular disc heat source with a radius equals to the radius of the laser beam. Laser drilling process can be modeled analytically using a circular disc heat source moving along the Z-direction with a velocity v. Heat liberation intensity is uniformly distributed over the entire heat source surface, so the heat liberation rate per unit area, q is given as [39], [29],

$$q = \frac{p}{\pi^* r_0^2} \text{ J/(s cm}^2\text{)} \quad (4.3)$$

where p is the rate of heat liberation per unit time or the power of the laser beam (J/s). The disc heat source can be considered as a combination of a series of concentrical ring segments of width dr_i and radius r_i (ri = 0 to r_0) as shown in Figure 4.1.

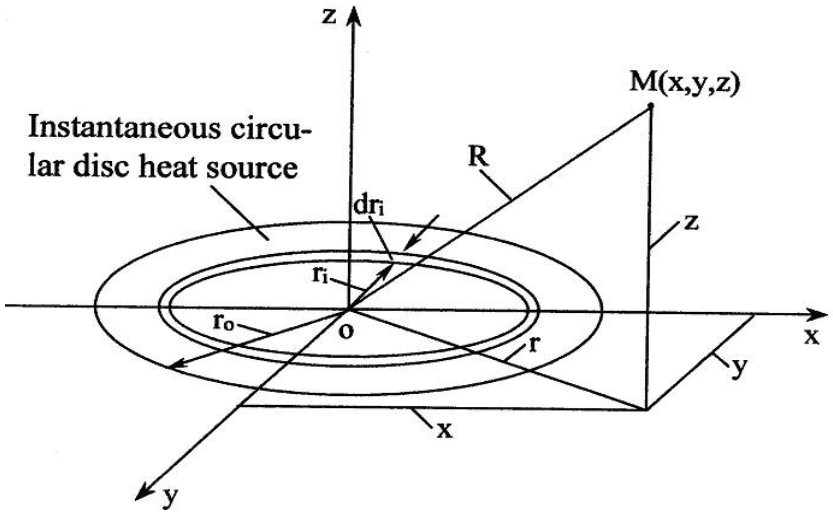

Fig. 4.1 Instantaneous circular disc heat source [29]

The heat liberation rate of the ring segment q_{rg} with radius r_i is given as,

$$q_{rg} = q * 2\pi * r_i * dr_i = {P * 2\pi * r_i * dr_i}\Big/{\pi * r_0^{\,2}} \tag{4.4}$$

In case of laser machining, the heat transfer is transient. Thus, the circular disc heat source equation is derived from the solution of an instantaneous ring heat source (Equation 4.2). The solution of an instantaneous ring heat source of radius $r_{i\,is}$ given by [39], [29],

$$\theta_M = \frac{Q_{rg}}{c\rho(4\pi a\tau)^{3/2}} \cdot e^{-\frac{r_i^2+r^2+z^2}{4a\tau}} \cdot I_0\left(\frac{r * r_i}{2a\tau}\right) \tag{4.5}$$

where θ_M is the temperature rise, ^{0}C at any point M(x, y, z).

Solution for a moving ring heat source moving along Z-axis with velocity v is derived as discussed in this section. Consider a small time interval $d\tau_i$, the total amount

of heat liberated in this time interval can be regarded as liberated instantaneously and is given as [39], [29],

$$Q_{rg} = q_{rg} d\tau_i = \frac{P * 2 * r_i * dr_i * d\tau_i}{r_0^{\,2}} \tag{4.6}$$

Substituting Q_{rg} in Equation 4.5, the temperature rise at any point M at the observation time, t caused by this instantaneous ring heat source is given by [39], [29],

$$d\theta'_M = \frac{P * 2 * r_i * dr_i * d\tau_i}{r_0^{\,2} * c\rho(4\pi a\tau)^{3/2}} \cdot e^{-\frac{ri^2+r^2+z^2}{4a\tau}} \cdot I_0\left(\frac{r * r_i}{2a\tau}\right) \tag{4.7}$$

Expression for the temperature rise at point M, at the observation time, t caused by the moving instantaneous ring heat source is given by [39], [29],

$$d\theta'_M = \frac{P * 2 * r_i * dr_i * d\tau_i}{r_0^{\,2} * c\rho(4\pi a\tau)^{3/2}} \cdot e^{-\frac{ri^2+r^2+(z-v*\tau_i)^2}{4a\tau}} \cdot I_0\left(\frac{r * r_i}{2a\tau}\right) \tag{4.8}$$

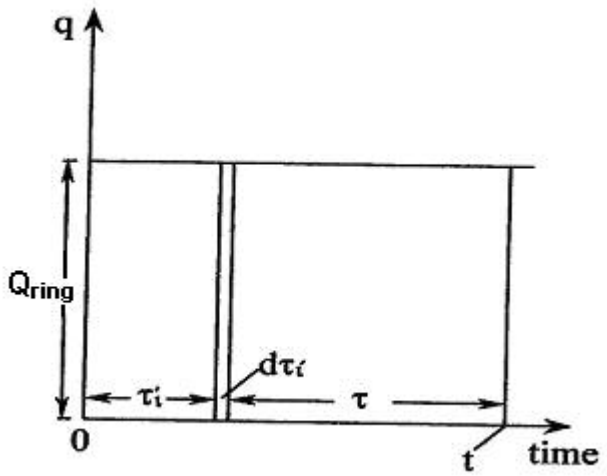

Fig. 4.2 Heat liberation rate q_{rg} with time t [29]

The total temperature rise at point M at time, t caused by this moving ring segment from $\tau_i = 0$ to $\tau_i = t$ is given as [39], [29],

$$d\theta_M = \frac{P*2*r_i*dr_i}{r_0^{\,2}*c\rho(4\pi a)^{3/2}} \int_{\tau_i=0}^{\tau_i=t} \frac{d\tau_i}{\tau^{3/2}} \cdot e^{-\frac{ri^2+r^2+(z-v*\tau_i)^2}{4a\tau}} \cdot I_0\left(\frac{r*r_i}{2a\tau}\right) \tag{4.9}$$

From the Figure 4.2,

$$\tau_i = t - \tau, \qquad d\tau_i = -d\tau$$

when $\tau_i = 0, \tau = t$; when $\tau_i = t, \tau = 0$, then Equation 4.9 becomes,

$$d\theta_M = \frac{P*2*r_i*dr_i}{r_0^{\,2}*c\rho(4\pi a)^{3/2}} \int_{\tau=0}^{\tau=t} \frac{d\tau}{\tau^{3/2}} \cdot e^{-\frac{ri^2+r^2+(z-v*t+v*\tau)^2}{4a\tau}} \cdot I_0\left(\frac{r*r_i}{2a\tau}\right) \tag{4.10}$$

Temperature rise caused by the whole moving disc heat source is given by [39], [29],

$$\theta_M = \frac{2*P}{c\rho*(4\pi a)^{3/2}*r_0^{\,2}} \int_{r_i=0}^{r_i=r_0} r_i \cdot \left[\int_{\tau=0}^{\tau=t} \frac{d\tau}{\tau^{3/2}} \cdot e^{-\frac{ri^2+r^2+(z-v*t+v*\tau)^2}{4a\tau}} \cdot I_0\left(\frac{r*r_i}{2a\tau}\right) \right] dr_i \tag{4.11}$$

Equation 4.11 is used to model the laser drilling process. It is modified for laser cutting and grooving by moving the laser beam heat source in the X - direction instead of in Z- direction for laser drilling process (see Chapter 5 for details).

4.3 Image heat source method

Temperature rise equation (Equation 4.11) is based on the heat conduction in an infinite large conducting medium. In practice, the thermal problems in various manufacturing process such as laser machining are generally experienced in a finite medium with boundaries. Boundary condition can be adiabatic or it may be contacting with a heat sink of another conducting medium or a convective fluid. Different boundary conditions lead to different effects on the temperature rise around the heat source. The image heat source method is used to transform the finite conducting medium problem into an infinite conducting medium. Heat source method is easier to use and provides a

basis for physical understanding of the process. Consider the case of a circular disc heat source S (x_i, z_i) located as shown in Figure 4.3 in a semi-infinite conduction medium with one adiabatic plane boundary and heat liberation intensity Q_{disc} J/cm^2. At the boundary surface ox, there should be no heat flux flowing out or in across it. Assume there is no such boundary (means the medium is infinitely large) instead consider another circular disc heat source S' (x_{ii}, z_{ii}) (image heat source) located symmetrically to the original primary heat source S (x_i, z_i) with respect to the ox surface in the infinite medium as shown in Figure 4.3 with the same amount of heat liberation as the original one [29].

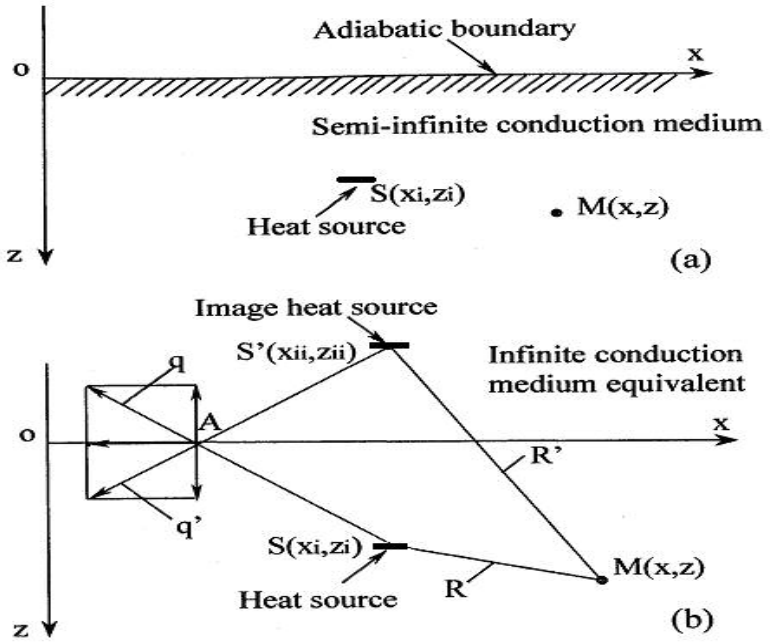

Fig. 4.3 Image heat source method of transforming (a) semi-infinite conduction medium problem into (b) infinite conduction medium problem [29]

The heat flux q and q' should be symmetric with respect to the surface ox and of the same magnitude. Thus, their vertical components are of same magnitude but in the

opposite direction and hence they cancel each other. This means that under the effect of two heat sources at any point on the surface ox there is no heat flux flowing across it as if it is an adiabatic surface. However, the problem is considered as two circular disc heat sources working simultaneously in an infinite medium. This imaginary case is equivalent to the original problem, namely, circular disc heat source working on a finite medium with an adiabatic boundary. Therefore, temperature rise at any point in the workpiece in the finite medium with an adiabatic boundary at any time can be calculated considering the combined effect of primary and the imaginary heat source S and S' working simultaneously in an infinite medium [29].

If the heat source is located at the boundary, the primary heat source and its image heat source are located at same location, so the temperature rise will be twice of the temperature rise due to the primary heat source. However, if the distance between the primary and its image heat source is very large, effect of boundary condition is neglected and temperature rise due to imaginary heat source is zero. Shorter the distance the more is the effect of boundary on temperature rise [29].

CHAPTER 5

METHODOLOGY FOR ANALYSIS

Different types of laser beam distribution, such as normal, bimodal, and uniform distribution can be used in the analysis. Adiabatic boundary conditions with certain value for gg are considered at the top boundary surface of the workpiece, and image heat source (as discussed in chapter 4) are used. Equation 4.11 is used to model the laser drilling, cutting, and grooving processes by moving the laser beam heat source in the Z- and X- directions, respectively.

5.1 Thermal model of laser drilling

In the laser drilling operation, the laser beam is incident on the workpiece surface with the axis of the beam perpendicular to the workpiece surface. Localized heating takes place causing melting and evaporation of the material depending on the thermal properties of the workpiece. In this, the erosion front moves in the Z-direction creating the profile of the laser drilled hole. The laser beam is treated as a circular disc heat source with certain radius. The laser drilling process can be simulated moving this circular disc heat source in the negative Z-direction.

Workpiece is considered as a rectangular block with infinite length and width. However, depending on the thickness, two thermal laser drilling models are developed. For the case of thick workpiece laser drilling model, the workpiece has infinite thickness and thus the effect of only top boundary is considered in the model. For the case of thin

workpiece laser drilling model, the workpiece has finite thickness and thus the effect of top as well as bottom boundaries are considered in the model.

5.1.1 Laser drilling model for thick workpiece

For the case of thick workpiece laser drilling model, the workpiece thickness is assumed infinite. So, we need to consider the effect of top boundary condition only. In thick workpiece laser drilling model as shown in Figure 5.1, S_0 and S_{10} are the primary and image heat sources with respect to boundary 1-1. At the beginning of the laser pulse, the laser beam is at the surface of the workpiece. After some time the laser beam passes a distance $v\tau_i$ in the Z-direction inside the workpiece with a velocity, v. The image of primary heat source also moves in the Z-direction away from the workpiece as shown in Figure 5.1.

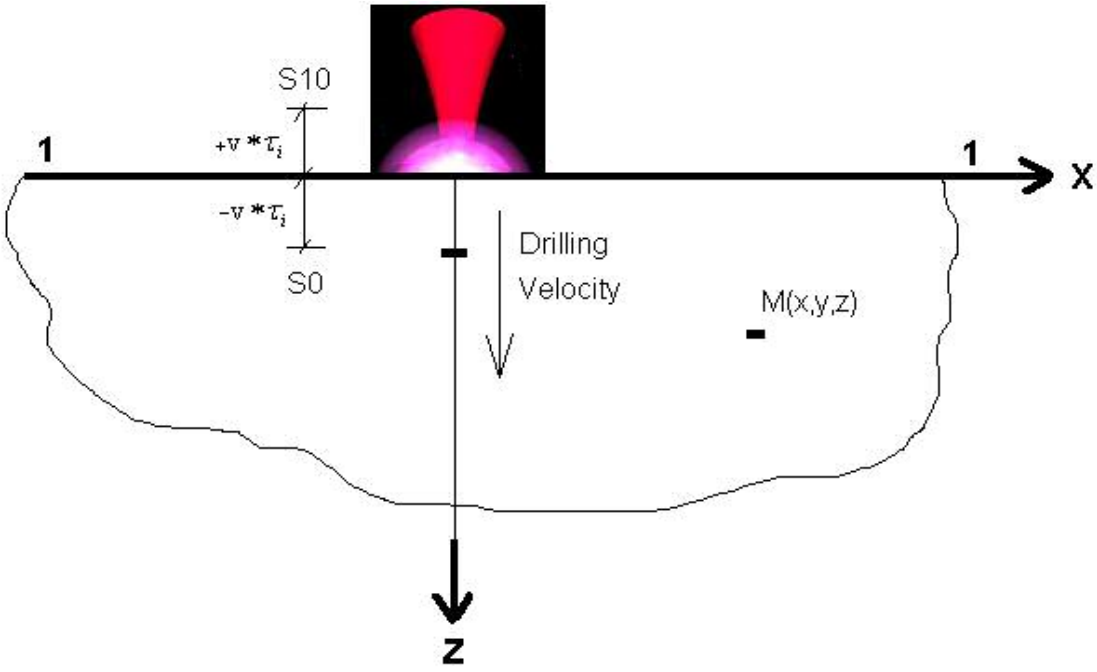

1-1	Boundary of workpiece
S0	Primary heat source
S10	Image of primary heat source w.r.t. 1-1 boundary

Fig. 5.1 Laser drilling - Thick workpiece

The total temperature rise at point M(x,y,z) at time t caused by this moving circular disc heat source using image heat source technique as described in chapter 4 is given by [29],

$$\theta_m = \theta_0 + gg \cdot \theta_{10} \tag{5.1}$$

$$\theta_m = A\left(\frac{2P*a}{\lambda(4\pi a)^{3/2} r_o{}^2}\right)\int_{r_i=0}^{r_i=r_o} B*r_i \left[\int_{\tau=0}^{\tau=t}\left(\frac{1}{\tau^{3/2}}\right)\left[\begin{matrix} e^{\left(-\frac{r_i^2+r^2+(z-vt+v\tau)^2}{4a\tau}\right)} + \\ gg*e^{\left(-\frac{r_i^2+r^2+(z+vt-v\tau)^2}{4a\tau}\right)}\end{matrix}\right] I_o\left(\frac{rr_i}{2a\tau}\right) d\tau\right] dr_i$$

..... (5.2)

Table 5.1 Laser beam distribution [29]

Laser Beam Distribution	A	B
Normal	9	$e^{-\left(\frac{3r_i}{r_o}\right)^2}$
Bimodal	4.3677	$e^{-\left(3.947\frac{r_i}{r_o}-0.947\right)^2} + e^{-\left(3.947\frac{r_i}{r_o}+0.947\right)^2}$
Uniform	1	1

In Equation 5.2, r = $\sqrt{x^2+y^2}$, r_o is the radius of the laser beam, and t is the on-time of the laser pulse. gg is a coefficient representing the effect of condition of the top boundary of the workpiece. Its value is in between +1 and -1. When gg = 1, it is the adiabatic boundary. When gg <1, it is the convective boundary with some cooling effect. Stronger the cooling, the smaller is the value of gg. Table 5.1 gives the values for the coefficients A and B in Equation 5.2 for different laser beam distributions, such as normal, bimodal, and uniform.

5.1.2 Laser drilling model of thin workpiece

In thin workpiece laser drilling, the workpiece has finite thickness. So, we need to consider the effect of top and bottom surface boundaries. As shown in Figure 5.2, in thin workpiece laser drilling model, S_0 is the primary heat source; S_{10}, S_{120}, S_{1210}, and S_{12120} are image heat sources with respect to boundary 1-1, and S_{20}, S_{210}, and S_{2120} are image heat sources with respect to boundary 2-2.

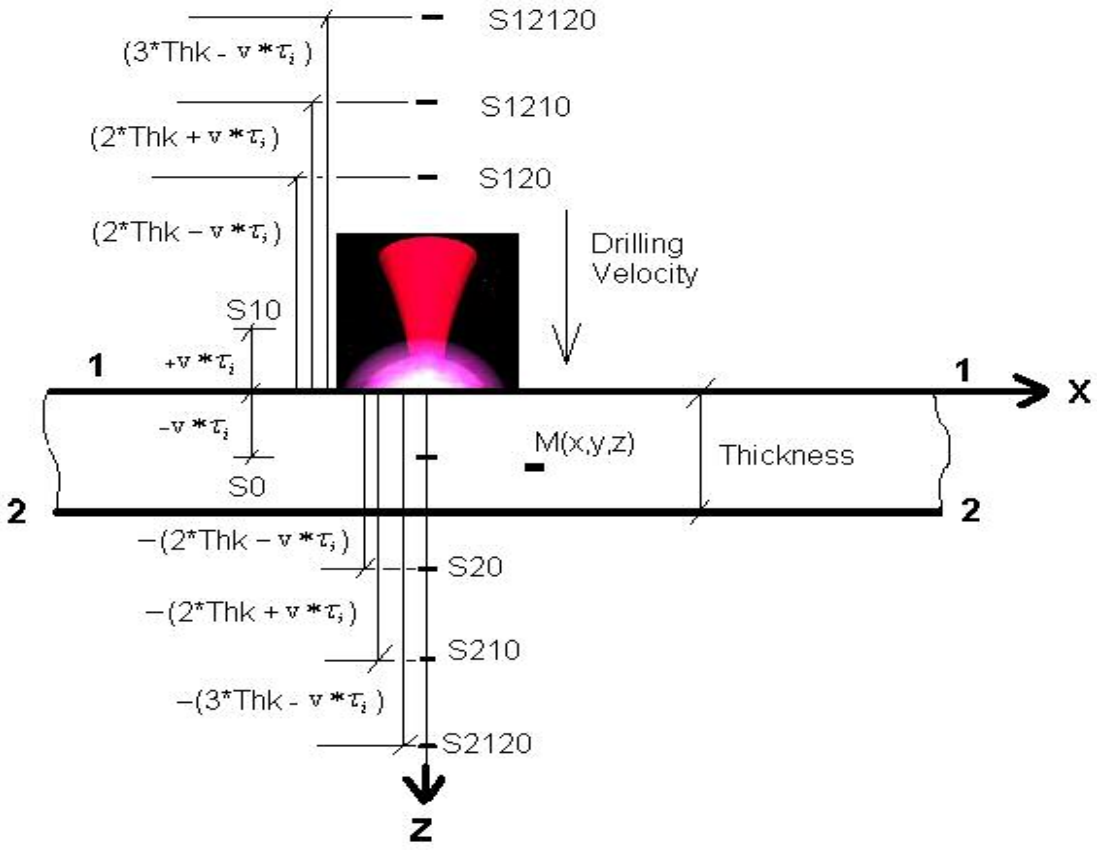

1-1, 2-2	Boundaries of the workpiece
S0	Primary heat source
S10	Image of primary heat source w.r.t 1-1 boundary
S120	Image of S20 heat source w.r.t 1-1 boundary
S1210	Image of S210 heat source w.r.t 1-1 boundary
S12120	Image of S2120 heat source w.r.t 1-1 boundary
S20	Image of primary heat source w.r.t 2-2 boundary
S210	Image of S10 heat source w.r.t 2-2 boundary
S2120	Image of S120 heat source w.r.t 2-2 boundary

Fig. 5.2 Laser drilling -Thin workpiece

At the beginning of laser pulse, the laser beam is at the surface of the workpiece. After time τ_i, the laser beam passes a distance of $v\tau_i$ in the Z-direction inside the workpiece with a velocity, v. The images of the primary heat sources also move in the Z-direction away from the corresponding boundaries of the workpiece as shown in Figure 5.2.

The total temperature rise at point M(x,y,z) at time t caused by this moving circular disc heat source using the image heat source technique (see Chapter 4) is given by,

$$\theta_m = \theta_0 + gg\cdot\theta_{20} + gg^2.\theta_{210} + gg^3.\theta_{2120} + gg.\theta_{10} + gg^2.\theta_{120} + gg^3.\theta_{1210} + gg^4.\theta_{12120} \qquad (5.3)$$

$$\theta_m = A\left(\frac{2P*a}{\lambda(4\pi a)^{3/2}r_o{}^2}\right)\int_{r_i=0}^{r_i=r_o} B*r_i \left\{\int_{\tau=0}^{\tau=t}\left(\frac{1}{\tau^{3/2}}\right)*I_0\left(\frac{r*r_i}{2a\tau}\right)\left\{\begin{array}{l} e^{\left(-\frac{r_i^2+r^2+(z-vt+v\tau)^2}{4a\tau}\right)} + \\ gg*e^{\left(-\frac{r_i^2+r^2+(z-2*THK*+vt-v\tau)^2}{4a\tau}\right)} + \\ gg^2*e^{\left(-\frac{r_i^2+r^2+(z-2*THK*-vt+v\tau)^2}{4a\tau}\right)} + \\ gg^3*e^{\left(-\frac{r_i^2+r^2+(z-3*THK*+vt-v\tau)^2}{4a\tau}\right)} + \\ gg*e^{\left(-\frac{r_i^2+r^2+(z+vt-v\tau)^2}{4a\tau}\right)} + \\ gg^2*e^{\left(-\frac{r_i^2+r^2+(z+2*THK*-vt+v\tau)^2}{4a\tau}\right)} + \\ gg^3*e^{\left(-\frac{r_i^2+r^2+(z+2*THK*+vt-v\tau)^2}{4a\tau}\right)} + \\ gg^4*e^{\left(-\frac{r_i^2+r^2+(z+3*THK*-vt+v\tau)^2}{4a\tau}\right)} \end{array}\right\} d\tau \right\} dr_i \qquad .. (5.4)$$

Therefore, the temperature rise in a thin workpiece is a combination of temperature rise due to primary moving circular disc heat source and its image heat sources with respect to two boundaries with the corresponding values of the coefficient gg.

5.1.3 Assumptions in the thermal drilling model

1. The incident beam is normal to the original surface of the irradiated surface and the analysis is made as an axi-symmetric 2D problem.
2. Fluctuations in the laser beam power are neglected.
3. The substrate remains stationary relative to the laser beam. Laser beam is incident at the center and at right angles to the substrate. The laser beam moves relative to the substrate.
4. For thick workpiece drilling model, the workpiece is infinite in length, width, and thickness; however, it has a finite thickness in the case of thin workpiece drilling model.
5. The thermal conductivity, density, and specific heat are independent of temperature and assumed constant through out the laser drilling process.
6. The radiation losses from the upper and lower surfaces of the workpiece are neglected.
7. Reflectivity of the workpiece surface is assumed constant.
8. The laser power absorbed by the workpiece is dependent on the laser beam intensity distribution, absorptivity, and coefficient for convective boundary.
9. When any location in the workpiece exceeds the boiling temperature, it is considered to have evaporated.
10. Rate of molten evaporation is equal to the rate of ejected material. All the molten material is ejected.
11. Assist gas energy is utilized to remove the molten material from the drilled hole.
12. SI units are used in all the calculations.

5.1.4 Laser drilling parameters

Laser beam radius (r):

The data for laser beam radius is taken from an experimental study [32]. Laser beam radius is generally in the range of 0.05 mm to 2 mm. Laser beam radius is taken as the radius of a moving circular disc heat source.

Laser beam power (P):

Laser beam power is the output from the laser machine. Before reaching to the workpiece surface, this laser power is reduced due to the following factors:

1. Because of the reflectivity of the workpiece surface, some of the incident laser energy is reflected back to the environment.
2. Because of the convective boundary of the workpiece surface, some of the incident laser energy is carried away by the flowing fluid, such as air.
3. Because of plasma formation above the workpiece surface during laser drilling, some of incident laser energy is absorbed by the plasma.

Penetration velocity (v):

In laser drilling operation, the data for the drilling velocity is taken from the experimental study [32]. The assumed velocity in the model and the actual velocity have to be the same. In actual practice, laser beam focal point does not change with time; but remains stationary. Only the erosion front propagates deeper and deeper inside the workpiece as material is removed by melting and evaporation. The drilling velocity is determined experimentally as the slope of the depth of laser drilled hole with time. Depth of cylindrical portion of the laser drilled hole is considered for determining the penetration velocity in the model.

Laser pulse:

Pulsed laser beam is used for drilling the workpiece. In percussion drilling, with the help of pulsed laser pulse, pulsed laser beam removes material through melting and localized detonation or explosions. On-time of the laser pulse ranges from 1ms to 3ms.

Workpiece dimensions:

As discussed earlier, the workpiece width and length are assumed infinite. However, in the thick workpiece model, the thickness is considered infinite and in the thin workpiece model, the thickness of the workpiece is considered finite. In these models, temperature profile of 2 mm x 2 mm x 2 mm workpiece region is determined and used for further calculations.

Boundary coefficient (gg):

This coefficient takes care of the convective boundary; some of the heat is carried away by the cooling fluid such as air. For gg = 1, the boundary is considered perfectly adiabatic. However, in actual case, some of the heat is carried away by the cooling fluid, such as air. So, gg is taken as 0.75 in the model for determining the effect of boundary conditions using the image heat source as explained in Chapter 4.

Absorptivity of the workpiece:

Absorptivity depends on the surface quality rather than the core material property. Material surface should have high absorptivity. [Absorptivity = (1-reflectivity)]. Reflectivity can be defined as the ratio of light reflected from a surface to total incident light. Absorptivity of the steel surface is taken as 75%, i.e. 25 % of the incident laser beam energy is lost to the environment. Absorptivity depends on wavelength of the laser beam and temperature of the workpiece surface.

Plasma absorption of the laser beam energy:

During the laser drilling operation, very high temperatures generate plasma at the surface of the workpiece. It is found in the literature [6] that this plasma absorbs some of the incident laser beam energy and 13% reduction occurs in the incident laser output power at the plane at 2.6 mm above the workpiece.

In this investigation the following laser beam parameters are taken for modeling the laser drilling process.

Table 5.2 Laser beam parameters [32]

Total power, KJ/s	30
Radius of the laser beam, mm	0.1
On- time of pulse, ms	3
Off- time of pulse, ms	40

Table 5.3 Thermal properties of AISI -1036 steel and CP-titanium [76]

Properties	AISI 1036 steel	CP-titanium
Thermal conductivity, J/mm s ^{0}C	0.0339	0.0219789
Thermal diffusivity, mm^2 /s	6.1	8.9584
Density, kg/m^3	7860	4510
Melting point, ^{0}C	1470	1668
Evaporation point, ^{0}C	3000	3287
Latent heat of fusion, KJ/kg	247	440
Latent heat of vaporization, KJ/kg	1.26*10^3	9.83*10^3

5.1.5 Computational analysis of the thermal drilling process

Equations 5.1 and 5.2 for thick and thin workpiece laser drilling, respectively are solved using Simpson 1/3rd numerical integration method. Three-dimensional temperature rise array is determined using VisualBasic.NET programming tool.

Flow-chart for solving the temperature rise equations is given in Appendix-A. The interface for thermal laser drilling model is shown in Figure 5.3. As shown in the Figure 5.3, by selecting the material type, drilling method, laser beam distribution, and other parameters, such as absorptivity, coefficient for the boundary, and plasma absorption coefficient; 3D temperature rise array of the workpiece is determined. Temperature rise is symmetrical around the axis of the laser beam. After calculating the temperature array, the hole profile (diameter and depth), material removal rate, penetration velocity, and thickness of the heat affected zone are determined. Using the temperature rise in the workpiece, energy consumed for melting and evaporation, and energy consumed for temperature rise and conduction losses in the workpiece are determined.

5.1.5.1 Material removal mechanism

Localized heating of the workpiece increases the temperature to melting point. With time, the temperature increases to the evaporation point and the material is removed by evaporation forming drilled hole. Along with the flow of evaporating material, molten material is also carried away and forms the drilled hole. At the end of on-time of laser pulse molten and evaporating material is removed and there is no conduction between the removed material and the parent material. After on-time of laser pulse, temperature of the drilled hole starts to reduce and re-solidification occurs and the remaining molten material deposits in the drilled hole forms a recast layer.

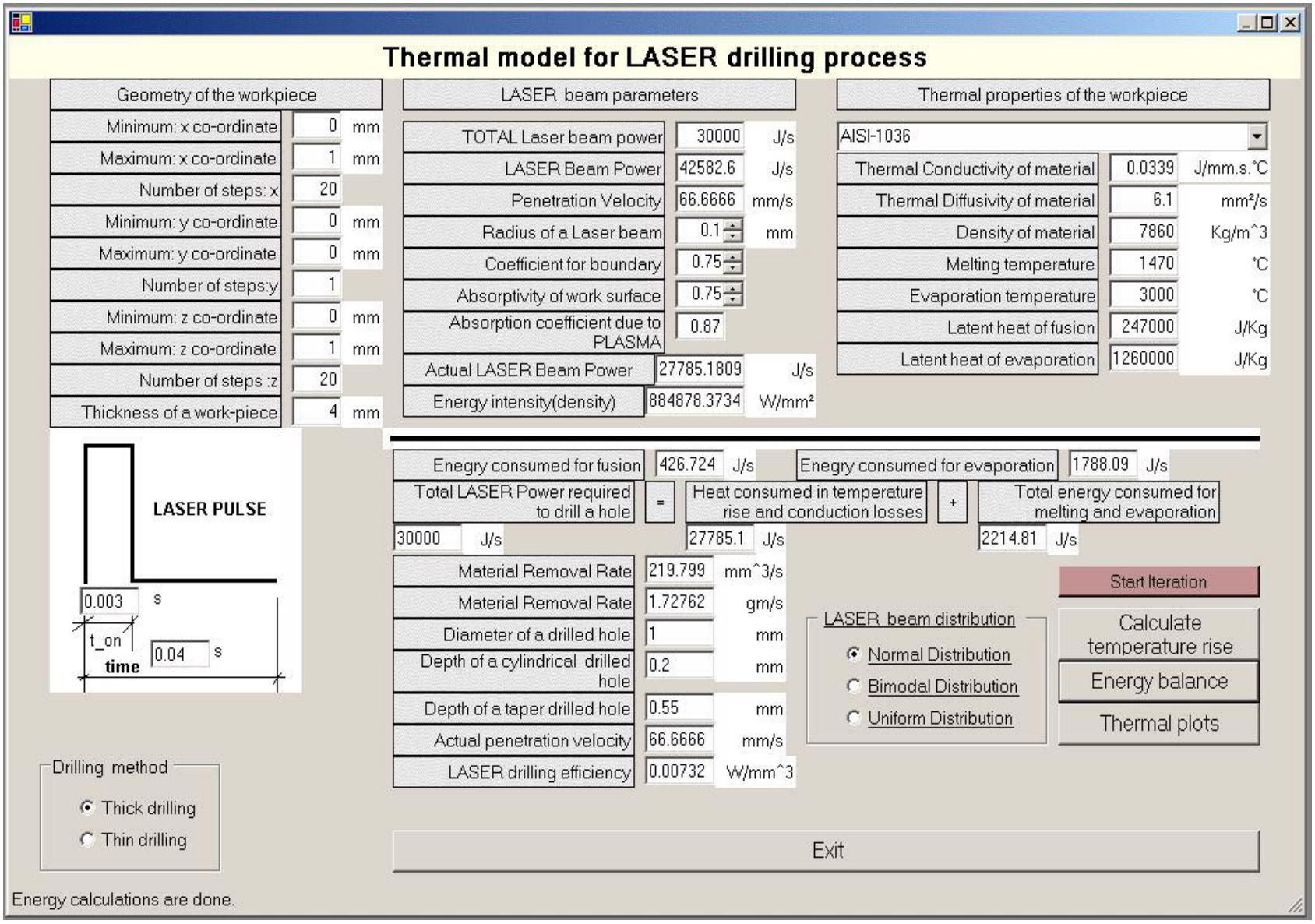

Fig. 5.3 Computer interface for the computation of temperature profile at the end of the laser pulse

Table 5.4 Determination of laser drilled hole profile and energy balance of an axi-symmetric laser drilling model

Assumption_1	Normal distribution		
Peff, J/s	**28942**	**Solution**	
velocity, mm/s	**66.66**		
Density of AISI-steel, kg/m^3	**7860**	**Melting point, ^{0}C**	**1470**
Pulse time, s	**0.003**	**Evaporation point, ^{0}C**	**3000**
Latent heat of fusion, J/kg	**247000**		
Latent heat of vaporization, J/kg	**1.26E+06**		
total_Actual_Power, J/s	**30000**		

Z\X, mm	0	0.05	0.1	0.15	0.2	0.25	0.3	0.35	0.4	0.45	0.5	0.55	0.6
0	494515	455261	362131.7	254942	163089	96801.17	53887.305	28307.457	14065.235	6609.2	2936.915	1232.7651	488.68536
0.05	567383	515525	397205.9	269368	167132	97166.25	53389.54	27818.3613	13751.115	6440.05	2855.4214	1196.7506	473.90857
0.1	725805	638754	455260.4	283758	165053	92095.02	49410.48	25399.2617	12459.838	5810.45	2570.247	1075.9137	425.8112
0.15	887223	756341	490801.1	277275	150419	80434.22	42138.363	21383.3379	10418.615	4842.22	2138.8752	895.0287	354.30792
0.2	732908	664648	426645.1	229718	120369	63025.7578	32637.926	16466.0977	8003.001	3717.64	1643.0765	688.36066	272.8862
0.25	501125	426126	274371.5	153254	82214	43607.5469	22750.805	11536.0605	5629.7437	2624.78	1163.986	489.18588	194.49103
0.3	224521	196577	138179.6	84540	48354	26693.38	14267.832	7347.557	3624.4019	1703.5	760.269	321.2098	128.27919
0.35	89225	80687.9	61458.54	41114	25276	14671.39	8106.214	4269.068	2139.371	1017.38	458.16968	194.98059	78.33175
0.4	34863	32216.8	25891.57	18527	12108	7367.92432	4214.012	2275.83057	1161.8622	560.371	255.13301	109.53081	44.318367
0.45	13578	12722.1	10577.17	7918.8	5415.9	3427.61621	2023.3355	1120.14539	582.9629	285.454	131.53354	57.020977	23.25677
0.5	5219.5	4932.76	4189.548	3231	2283.1	1490.24939	903.79913	511.7968	271.31302	134.871	62.915085	27.55315	11.33327
0.55	1953.6	1856.58	1599.274	1258.4	910.35	608.5914	377.4254	217.982635	117.51724	59.26	27.977259	12.377496	5.1349874
0.6	705.09	672.615	585.1261	466.95	343.67	234.02681	147.78966	86.79947	47.49643	24.2671	11.586946	5.1767216	2.165798
0.65	243.78	233.166	204.2863	164.71	122.79	84.81784	54.353443	32.37494	17.945866	9.27743	4.476064	2.0183318	0.8512548
0.7	80.35	77.0003	67.82128	55.107	41.483	28.9754143	18.78952	11.3238068	6.346979	3.31546	1.6147348	0.7343574	0.3120829
0.75	25.157	24.1431	21.35091	17.451	13.236	9.327037	6.1067905	3.716507	2.1029387	1.10856	0.5444729	0.2495581	0.1068049
0.8	7.4615	7.16865	6.359466	5.222	3.9841	2.82742882	1.8658859	1.14485753	0.6530635	0.34701	0.1717157	0.0792638	0.034143
0.85	2.092	2.01159	1.788948	1.4744	1.1302	0.806686461	0.5358253	0.3310248	0.1901361	0.10173	0.0506766	0.0235416	0.0102006
0.9	0.5535	0.53259	0.474585	0.3923	0.3019	0.216478214	0.1445718	0.08983039	0.0519036	0.02794	0.0139994	0.0065407	0.0028493
0.95	0.138	0.13287	0.11859	0.0983	0.0759	0.054608956	0.0366359	0.022875255	0.0132847	0.00719	0.0036208	0.0017004	0.0007443
1	0.0324	0.0312	0.027886	0.0232	0.0179	0.012942608	0.0087164	0.005465134	0.0031879	0.00173	0.0008769	0.0004137	0.0001819

Volume of melting zone			Volume of evaporation zone			
radius	depth	vol, mm^3	radius	depth	vol, mm^3	
0.5	0.05	0.03925	0.45	0.05	0.0317925	mass melting zone, kg
0.5	0.05	0.03925	0.45	0.05	0.0317925	mass evapor zone, kg
0.5	0.05	0.03925	0.45	0.05	0.0317925	fusion heat , J/s
0.5	0.05	0.03925	0.45	0.05	0.0317925	vaporization heat, J/s
0.5	0.05	0.03925	0.45	0.05	0.0317925	total heat, J
0.5	0.05	0.03925	0.45	0.05	0.0317925	total heat, J/s
0.45	0.05	0.031793	0.4	0.05	0.02512	Power_eff
0.45	0.05	0.031793	0.4	0.05	0.02512	total, J/s
0.4	0.05	0.02512	0.35	0.05	0.0192325	difference
0.35	0.05	0.019233	0.3	0.05	0.01413	% of total power goes
0.3	0.05	0.01413	0.25	0.05	0.0098125	away in to material
0.25	0.05	0.009813	0.15	0.05	0.0035325	removed
0.1	0.05	0.00157				
		0.3297			0.25591	

2.591E-06	
2.011E-06	
213.36206	
8.45E+02	
3.17E+00	
1.06E+03	
28942	
30000.172	
0.17215	
3.53	

Melting line

Evaporating line

Since laser drilling is an axi-symmetric problem, temperature rise in X-Z plane only is determined to reduce the computational time. So, the X dimension varies from 0 to 1 mm, the Z dimension varies from 0 to -1 mm, and Y = 0 mm.

Jaeger's heat source equations are based on conduction of heat in solids. Therefore, it is assumed that there is no melting and evaporation and no material is removed. Equations (5.1) and (5.2) give only the temperature rise and do not include the effect of melting and evaporation of the material. Latent heat of fusion and evaporation are consumed while melting and evaporation during laser machining process. However, during fusion and evaporation there is no temperature rise, only heat is consumed during phase change. Therefore, this energy utilized in melting and evaporation of metal has to be added to the laser power, P used in the equation to obtain the total actual laser beam power used for drilling material with the required profile. For this purpose, trial and error method is used. In this, for a give laser power, P the temperature rise in the workpiece region is determined. From this, fusion and evaporation volumes are determined. Thus, the latent heat of fusion and evaporation is determined. This energy has to be added to the laser power, P used in the temperature rise equation to obtain total laser beam power to drill a hole of required profile. For example, for a laser power used in heat source equation, P = 27.785 KJ/s and for the laser drilled hole profile, latent heat of fusion and evaporation is 2.215 KJ/s. Then the total actual laser beam power is 30 KJ/s to drill a hole of required profile.

5.1.5.2 Profile of the laser drilled hole

From the temperature rise array, the location where the temperature has reached the melting point of the workmaterial is marked and this area is assumed to be removed

by laser beam pulse. In this way, the diameter, depth, and taper of the laser drilled hole are determined. Also, the material removal rate is determined by calculating the volume of this region divided by the laser pulse on-time.

5.1.5.3 Penetration velocity

In the model, the circular disc heat source moves inside the workpiece with a certain velocity called the penetration velocity. It is the ratio of cylindrical depth of the drilled hole to the on-time of laser pulse.

5.1.5.4 Mass balance of the laser drilling process

All the melted and evaporated material is rejected away from the workpiece. Recoil pressure is built due to evaporation and thus helps to remove the molten material along with the evaporating material.

5.1.5.5 Energy balance of laser drilling process

The volume of the material which has reached the melting temperature is determined. Also, the volume of material which has reached evaporation temperature is determined. Fusion mass and evaporated mass of the material are calculated by multiplying the volumes of these zones by density of the workmaterial. Thus, the energy consumed in fusion and evaporation is determined by multiplying respective masses by latent heat of fusion and evaporation of the workpiece. Total power output from the laser machine is consumed as shown in Figure 5.4.

As shown in Figure 5.4, the incident laser beam energy is reduced by reflection, convective boundary cooling, and plasma absorption before being absorbed by the workpiece surface. Part of this energy reaching the workpiece surface is consumed for

temperature rise, melting, and evaporation of the workpiece material. Rest of the energy is lost due to conduction in the workpiece.

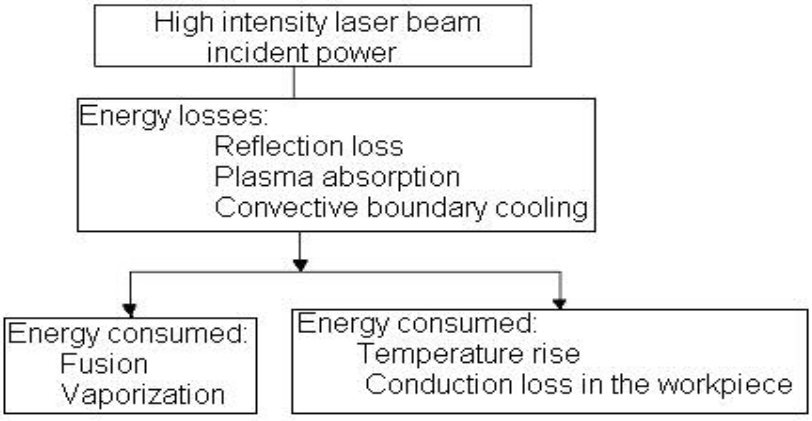

Fig. 5.4 Power balance diagram illustrating the effects of a laser beam impinging on the surface of a material

Energy required to eject the droplet of molten material is provided by the kinetic energy of high pressure vapor and assist gas.

5.1.5.6 Laser drilling efficiency

Laser drilling efficiency is the ratio of laser beam power consumed to form a hole to input laser energy.

5.1.6 Heat affected zone determination of laser drilling process

Heat affected zone (HAZ) is the region near the melting zone where the temperature has reached the phase transformation temperature of the material being drilled with the laser. It is calculated graphically as shown in Figure 5.5 by determining the width of the melting point isotherm and phase transformation isotherm in the X-Z plane.

For AISI-1036 steel, HAZ of 0.05 mm thickness is observed for the given laser drilling parameters. HAZ is of uniform thickness for the low velocities of laser beam

penetration. However, for the higher penetration velocities of laser drilling, the HAZ thickness is not uniform and HAZ thickness reduces as the depth increases. At higher laser intensities, the recast layer thickness decreases as the beam radius decreases.

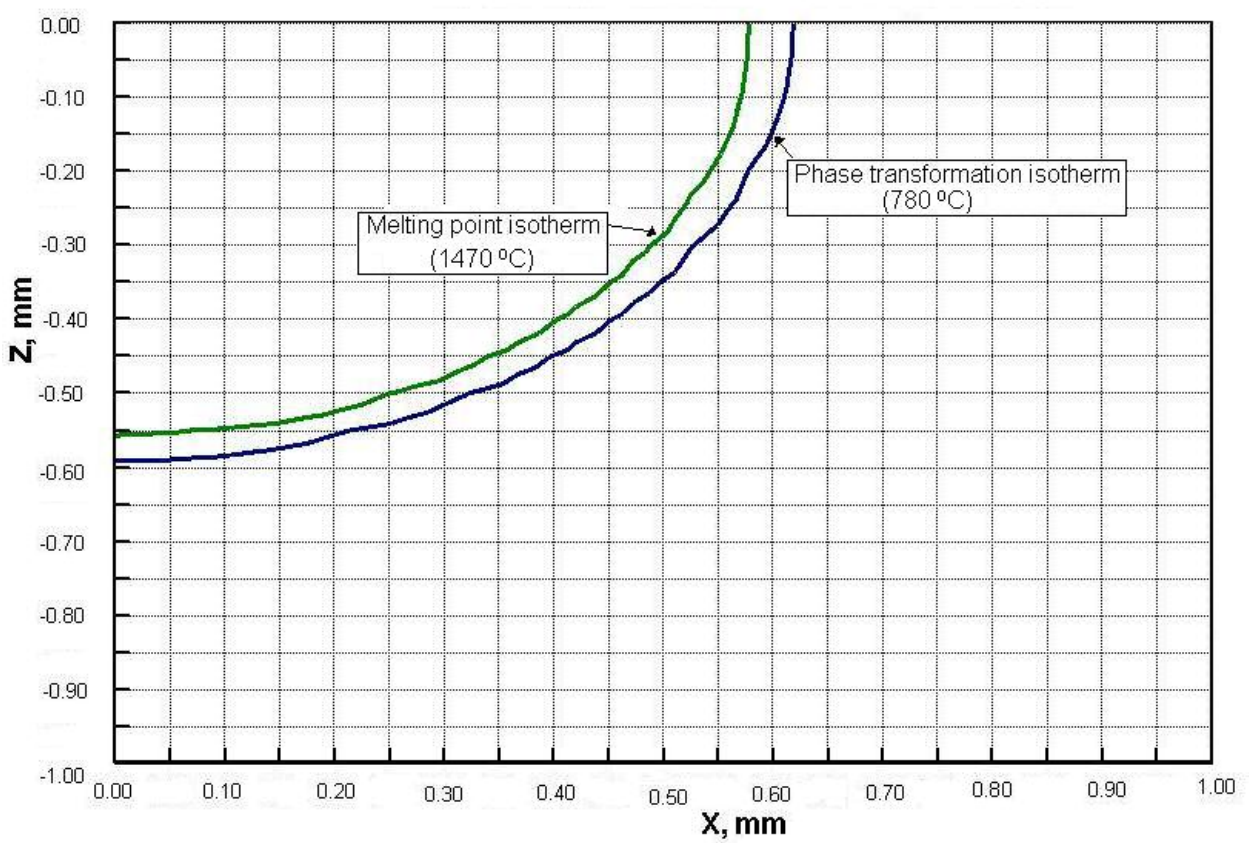

Fig. 5.5 Heat affected zone in AISI-1036 steel by laser drilling process

5.2 Thermal modeling of laser cutting and grooving process

Thick workpiece cutting and thin workpiece cutting models are developed using the concept of image heat source. These models can be used for laser cutting, grooving from the side as well as from the central region of the workpiece.

5.2.1 Laser central cutting model for thick workpiece

In thick workpiece central laser cutting, the workpiece thickness is assumed infinite. Therefore, we need to consider the effect of the top boundary condition only. In

thick workpiece side laser cutting model as shown in Figure 5.6, S_0 and S_{10} are the primary and its image heat source with respect to boundary 1-1.

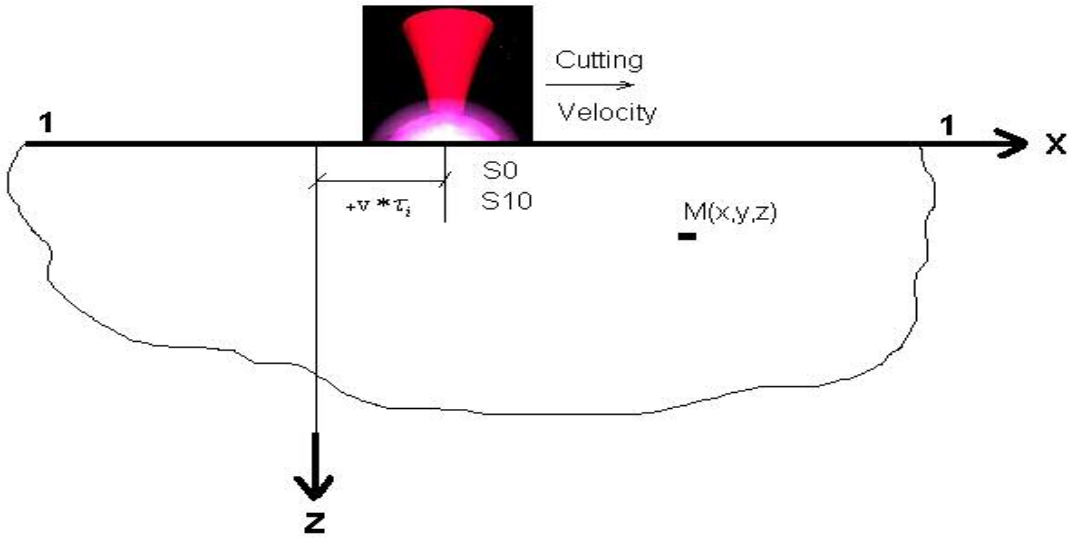

Fig. 5.6 Laser central cutting- Thick workpiece

At the beginning, the laser beam is at the surface of the workpiece. After some time, the laser beam traverses a distance $v\tau_i$ in the X-direction along the OX - axis with a velocity, v. The image of the primary heat source also moves in the X-direction along with the primary heat source as shown in Figure 5.6.

The total temperature rise at point M at time t caused by this moving circular disc heat source and its image heat source (using image heat source technique as explained in Chapter 4) is given as,

$$\theta_m = \theta_0 + gg \cdot \theta_{10} \tag{5.5}$$

$$\theta_m = A\left(\frac{2P*a}{\lambda(4\pi a)^{3/2} r_o^{\,2}}\right)\int_{r_i=0}^{r_i=r_o} B*r_i \left[\int_{\tau=0}^{\tau=t}\left(\frac{1}{\tau^{3/2}}\right)\left[\frac{(1+gg).I_o\left(\frac{r_i\sqrt{(x-vt+v\tau)^2+y^2}}{2a\tau}\right)}{e^{\left(-\frac{r_i^2+(x-vt+v\tau)^2+y^2+z^2}{4a\tau}\right)}}\right]d\tau\right]dr_i$$

……..….(5.6)

5.2.2 Laser side cutting model for thick workpiece

In thick workpiece side laser cutting, the workpiece thickness is assumed infinite. However, the laser beam cutting starts from the left side of the workpiece. Therefore, we need to consider the effect of the top boundary and left side boundary conditions.

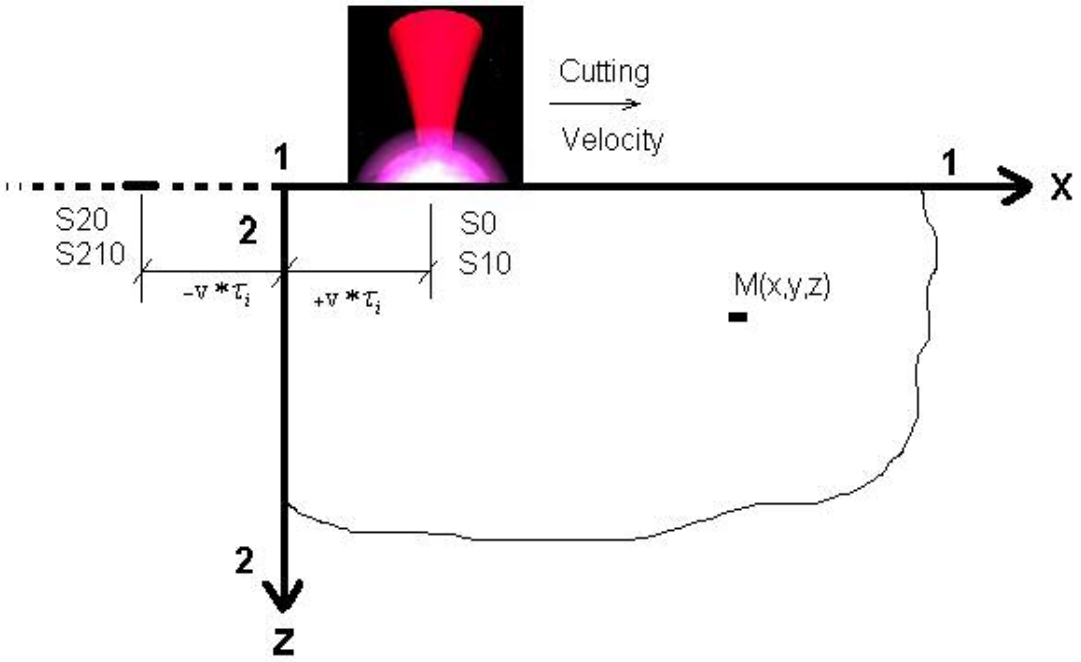

1-1	Top boundary of the workpiece
2-2	Side boundary of the workpiece
S0	Primary heat source
S10	Image of primary heat source w.r.t 1-1 boundary
S20	Image of primary heat source w.r.t 2-2 boundary
S210	Image of S10 heat source w.r.t 2-2 boundary

Fig. 5.7 Laser side cutting- Thick workpiece

In thick workpiece side laser cutting model as shown in Figure 5.7, S_0 and S_{10} are primary and its image heat source with respect to boundary 1-1. Also S_{20} and S_{210}

are image heat sources of S_0 and S_{10} with respect to boundary 2-2. At the beginning, the laser beam is at the top left edge of the workpiece. After some time, the laser beam traverses a distance $v\tau_i$ in the X-direction along the OX - axis with a velocity, v.

The total temperature rise at point M at time t caused by this moving circular disc heat source and its image heat source is given as,

$$\theta_m = \theta_0 + gg \cdot \theta_{10} + gg \cdot \theta_{20} + gg^2 \cdot \theta_{210} \tag{5.7}$$

$$\theta_m = A\left(\frac{2P*a}{\lambda(4\pi a)^{3/2} r_o^{\,2}}\right)\int_{r_i=0}^{r_i=r_o} B*r_i \left\{ \int_{\tau=0}^{\tau=t} \left(\frac{1}{\tau^{3/2}}\right) \left\{ \begin{bmatrix} (1+gg).I_o\left(\dfrac{r_i\sqrt{(x-vt+v\tau)^2+y^2}}{2a\tau}\right) \\ \exp\left(-\dfrac{r_i^2+(x-vt+v\tau)^2+y^2+z^2}{4a\tau}\right) \end{bmatrix} + \begin{bmatrix} (gg+gg^2).I_o\left(\dfrac{r_i\sqrt{(x+vt-v\tau)^2+y^2}}{2a\tau}\right) \\ \exp\left(-\dfrac{r_i^2+(x+vt-v\tau)^2+y^2+z^2}{4a\tau}\right) \end{bmatrix} \right\} d\tau_i \right\} dr_i \tag{5.8}$$

5.2.3 Laser central cutting model for thin workpiece

In thin workpiece central laser cutting, the workpiece thickness is finite. Therefore, we need to consider the effect of top as well as bottom boundary conditions. In thin workpiece central laser cutting model as shown in Figure 5.8, S_0 is the primary heat source and S_{10}, $S_{120,}$ and S_{1210} are image heat sources with respect to boundary 1-1. Also S_{20} and $S_{210,}$ are image heat sources with respect to the side boundary 2-2. At the beginning, the laser beam is at some location on the workpiece surface. After some time, the laser beam traverses a distance $v\tau_i$ in the X-direction along the OX-axis with a velocity, v.

The images of primary heat source with respect to two boundaries also move in the X- direction along the OX-axis as shown in Figure 5.8.

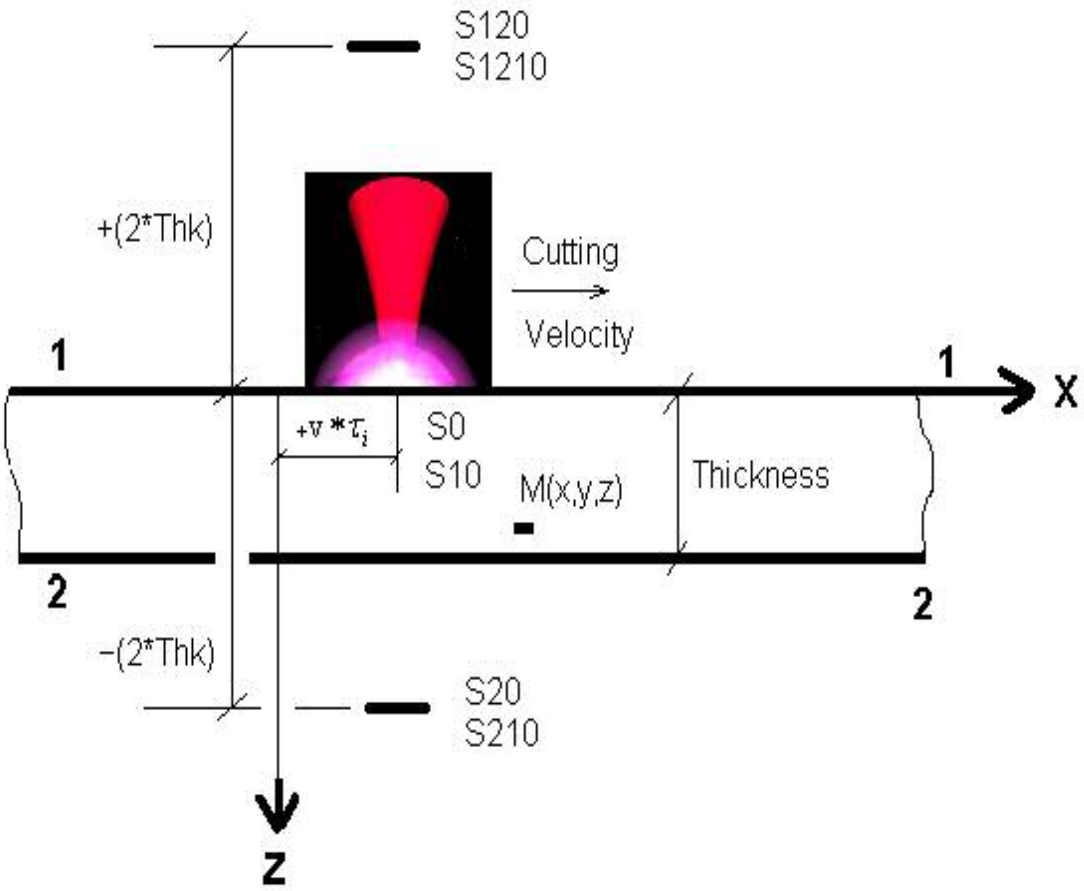

1-1	Top boundary of the workpiece
2-2	Bottom boundary of the workpiece
S0	Primary heat source
S10	Image of primary heat source w.r.t. 1-1 boundary
S20	Image of primary heat source w.r.t. 2-2 boundary
S210	Image of S10 heat source w.r.t. 2-2 boundary
S120	Image of S20 heat source w.r.t. 1-1 boundary
S1210	Image of S210 heat source w.r.t. 1-1 boundary

Fig. 5.8 Laser central cutting- Thin workpiece

The total temperature rise at point M at time t caused by this moving circular disc heat source and its image heat sources is given as,

$$\theta_m = \theta_0 + gg \cdot \theta_{10} + gg \cdot \theta_{20} + gg^2 \cdot \theta_{210} + gg^2 . \theta_{120} + gg^3 . \theta_{1210} \tag{5.9}$$

$$\theta_m = A\left(\frac{2P * a}{\lambda(4\pi a)^{3/2} r_o{}^2}\right)\int_{r_i=0}^{r_i=r_o} B * r_i \left\{ \int_{\tau=0}^{\tau=t} \left(\frac{1}{\tau^{3/2}}\right) \left\{ \begin{bmatrix} (1+gg).I_o\left(\frac{r_i\sqrt{(x-vt+v\tau)^2+y^2}}{2a\tau}\right) \\ e^{\left(-\frac{r_i^2+(x-vt+v\tau)^2+y^2+z^2}{4a\tau}\right)} \end{bmatrix} + \begin{bmatrix} (gg+gg^2).I_o\left(\frac{r_i\sqrt{(x-vt+v\tau)^2+y^2}}{2a\tau}\right) \\ e^{\left(-\frac{r_i^2+(x-vt+v\tau)^2+y^2+(-2*THK+z)^2}{4a\tau}\right)} \end{bmatrix} + \begin{bmatrix} (gg^2+gg^3).I_o\left(\frac{r_i\sqrt{(x-vt+v\tau)^2+y^2}}{2a\tau}\right) \\ e^{\left(-\frac{r_i^2+(x-vt+v\tau)^2+y^2+(2*THK+z)^2}{4a\tau}\right)} \end{bmatrix} \right\} d\tau_i \right\} dr_i$$

……...(5.10)

5.2.4 Laser side cutting model for thin workpiece

In thin workpiece side laser cutting, the workpiece thickness is finite. However, the laser beam cutting starts from the left side of the workpiece. Therefore, we need to consider the effect of the top, bottom, and left side boundary conditions. In thin workpiece side laser cutting model as shown in Figure 5.9, S_0 is the primary heat source; $S_{10,}$ S_{120}, S_{1210} are image heat sources with respect to boundary 1-1; $S_{20,}$ S_{210} are image heat sources with respect to boundary 2-2; and $S_{3120,}$ S_{31210}, $S_{30,}$ $S_{310,}$ S_{320}, S_{3210} are image heat sources with respect to boundary 3-3. At the beginning, the laser beam is at the top left edge of the workpiece. After some time, the laser beam passes a distance of $v\tau_i$ in the X-direction along the OX-axis with a velocity, v. The images of primary heat source also move with respect to the X-direction away from the boundary 3-3 of the workpiece as shown in Figure 5.9.

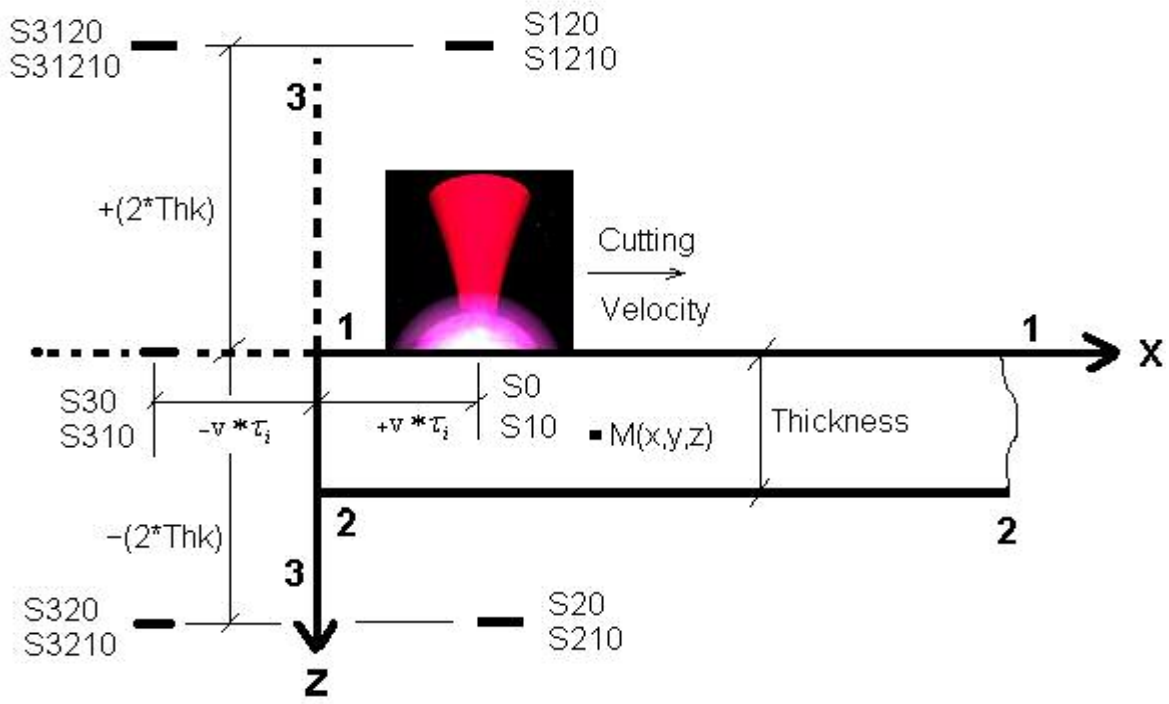

1-1	Top boundary of the workpiece
2-2	Bottom boundary of the workpiece
3-3	Side boundary of the workpiece
S0	Primary heat source
S10	Image of primary heat source w.r.t. 1-1 boundary
S30	Image of primary heat source w.r.t. 3-3 boundary
S310	Image of S10 heat source w.r.t. 3-3 boundary
S20	Image of primary heat source w.r.t. 2-2 boundary
S210	Image of S10 heat source w.r.t. 2-2 boundary
S320	Image of S20 heat source w.r.t. 3-3 boundary
S3210	Image of S210 heat source w.r.t. 3-3 boundary
S120	Image of S20 heat source w.r.t. 1-1 boundary
S1210	Image of S210 heat source w.r.t. 1-1 boundary
S3120	Image of S120 heat source w.r.t. 3-3 boundary
S31210	Image of S1210 heat source w.r.t. 3-3 boundary

Fig. 5.9 Laser side cutting- Thin workpiece

The total temperature rise at point M at time t caused by this moving circular disc heat source and its image heat sources is given by,

$$\theta_m = \theta_0 + gg \cdot \theta_{10} + gg \cdot \theta_{30} + gg^2 \cdot \theta_{310} + gg.\theta_{20} + gg^2.\theta_{120} + gg^2.\theta_{320} + gg^3.\theta_{3210} + gg^2.\theta_{120} + gg^3.\theta_{1210} + gg^3.\theta_{3120} + gg^4.\theta_{31210}$$

……..(5.11)

$$\theta_m = A\left(\frac{2P*a}{\lambda(4\pi a)^{3/2} r_o{}^2}\right)\int_{r_i=0}^{r_i=r_o} B*r_i \left\{\int_{\tau=0}^{\tau=t}\left(\frac{1}{\tau^{3/2}}\right)\left\{\begin{array}{l}
\left[(1+gg).I_o\left(\frac{r_i\sqrt{(x-vt+v\tau)^2+y^2}}{2a\tau}\right)\right]_{e^{\left(-\frac{r_i^2+(x-vt+v\tau)^2+y^2+z^2}{4a\tau}\right)}} + \\
\left[(gg+gg^2).I_o\left(\frac{r_i\sqrt{(x+vt-v\tau)^2+y^2}}{2a\tau}\right)\right]_{e^{\left(-\frac{r_i^2+(x+vt-v\tau)^2+y^2+z^2}{4a\tau}\right)}} + \\
\left[(gg+gg^2).I_o\left(\frac{r_i\sqrt{(x-vt+v\tau)^2+y^2}}{2a\tau}\right)\right]_{e^{\left(-\frac{r_i^2+(x-vt+v\tau)^2+y^2+(-2*THK+z)^2}{4a\tau}\right)}} + \\
\left[(gg^2+gg^3).I_o\left(\frac{r_i\sqrt{(x+vt-v\tau)^2+y^2}}{2a\tau}\right)\right]_{e^{\left(-\frac{r_i^2+(x+vt-v\tau)^2+y^2+(-2*THK+z)^2}{4a\tau}\right)}} + \\
\left[(gg^2+gg^3).I_o\left(\frac{r_i\sqrt{(x-vt+v\tau)^2+y^2}}{2a\tau}\right)\right]_{e^{\left(-\frac{r_i^2+(x-vt+v\tau)^2+y^2+(2*THK+z)^2}{4a\tau}\right)}} + \\
\left[(gg^3+gg^4).I_o\left(\frac{r_i\sqrt{(x+vt-v\tau)^2+y^2}}{2a\tau}\right)\right]_{e^{\left(-\frac{r_i^2+(x+vt-v\tau)^2+y^2+(2*THK+z)^2}{4a\tau}\right)}}
\end{array}\right\} d\tau_i \right\} dr_i$$

……(5.12)

5.2.5 Assumptions of thermal cutting/grooving model

1. The incident beam is normal to the original surface of the irradiated surface and the analysis is performed as an axi-symmetric, 2D problem.
2. The substrate remains stationary relative to the laser beam. Laser beam is incident at the center at right angles to the substrate. The laser beam moves relative to the substrate.

3. Fluctuations in the laser beam power are neglected.
4. For thick workpiece cutting and grooving, the workpiece is infinite in length, width, and thickness; but has finite thickness in the case of thin workpiece cutting and grooving processes.
5. The thermal conductivity, density, and specific heat are independent of temperature.
6. The radiation losses from the upper and lower surfaces of the workpiece are neglected.
7. When any location in the workpiece exceeds the boiling point temperature, it is considered to have evaporated.
8. Rate of molten evaporation is equal to the rate of ejected material.

5.2.6 Laser cutting and grooving parameters

Laser beam power, laser beam radius, laser pulse, absorptivity of the workpiece, boundary coefficient of cooling (gg), and absorption coefficient due to plasma absorption are the same as for laser drilling model.

Cutting/grooving velocity (v):

Laser beam travels in the X-direction along the surface of the workpiece with a certain cutting velocity. The cutting velocity determines the kerf width of the workpiece. Therefore, to obtain a minimum kerf width, cutting velocity has to be optimized using laser cutting model.

Workpiece dimension:

As discussed earlier, the workpiece width and length are assumed infinite. However, in thick workpiece model, thickness is infinite and in thin workpiece model

thickness of the workpiece is finite. In this model, temperature profile of 20 mm x 2 mm x 5 mm workpiece region is determined and used for further calculations.

The same laser beam parameters are used for laser cutting and grooving. Laser cutting and grooving model is developed for AISI-1036 and CP-titanium.

5.2.7 Computational analysis of thermal cutting and grooving

Equations (5.3) to (5.6) for thick and thin workpiece laser cutting, respectively are solved using Simpson 1/3rd numerical integration method. Temperature rise array is determined using VisualBasic.NET programming tool. Flow-chart for solving these equations are given in Appendix-B. The interface for thermal laser drilling model is shown in Figure 5.10. By selecting the material type, cutting/grooving method, laser beam distribution, and other parameters, such as absorptivity, coefficient for the boundary condition, and plasma absorption coefficient; 3D temperature rise array of the workpiece are determined.

After calculating the temperature array, the profile of the kerf width, material removal rate, cutting velocity, and HAZ thickness are determined. Using temperature rise of the workpiece, energy consumed for melting and evaporation and energy consumed for temperature rise and conduction losses in the workpiece are determined.

5.2.7.1 Material removal mechanism

Localized heating of the workpiece increases the temperature to the melting point with time and further increase in temperature leads to evaporation. Thus, material is removed by evaporation forming a cut/ groove in the workpiece. Along with the flow of evaporating material, molten material is also carried away.

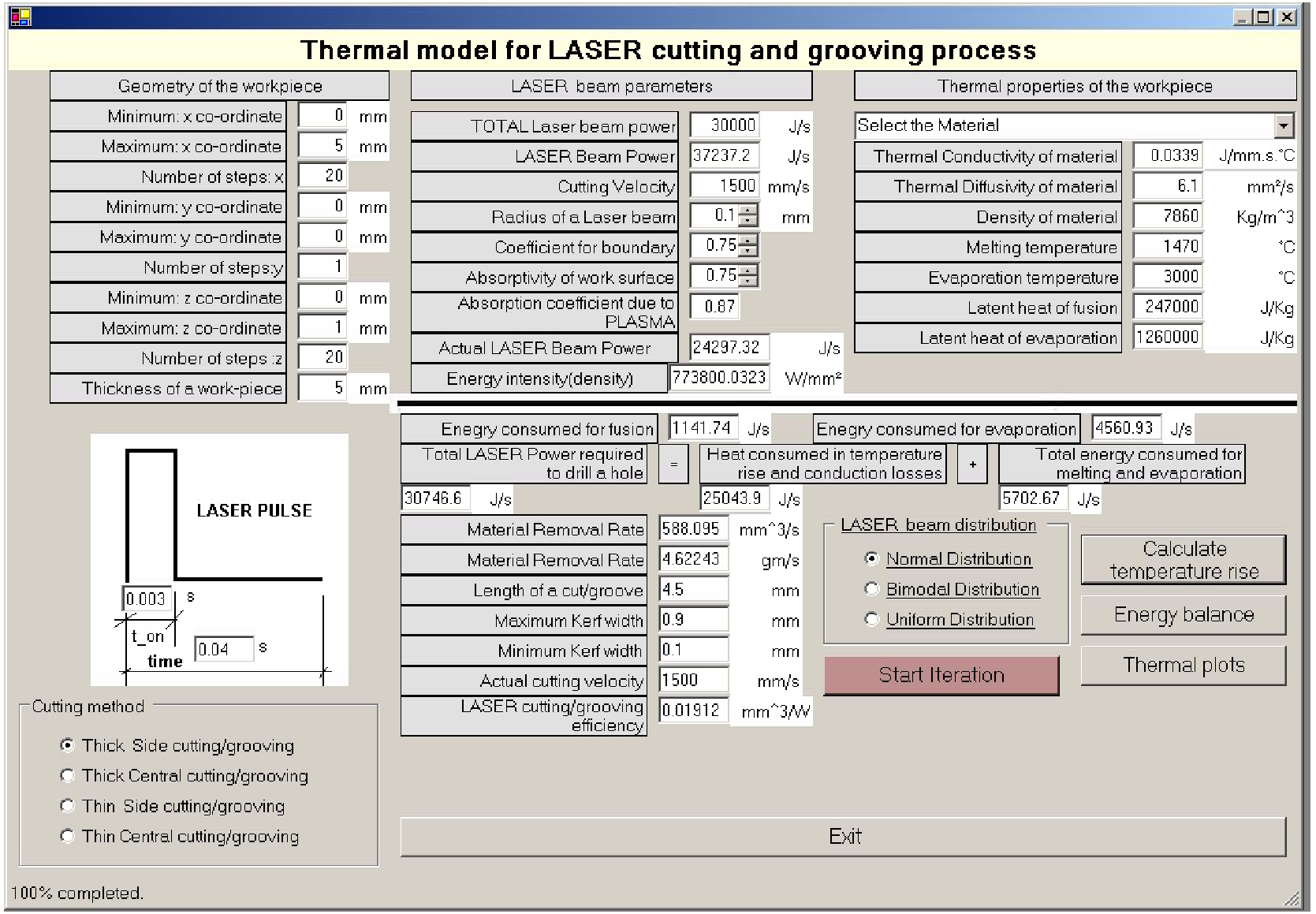

Fig. 5.10 Computer interface for the computation of temperature profile at the end of the laser pulse

For laser cutting, molten material is removed from the bottom of the workpiece in the case of thin workpiece laser cutting model. At the end of on-time of laser pulse, molten and evaporated materials are removed. There is no conduction between the removed material and the parent material. The kerf width is assumed to reduce gradually along the depth of the cut. At the end of laser pulse, temperature of the cut workpiece starts to reduce and re-solidification occurs. The remaining molten material deposits on the cut portion forming a recast layer.

Since laser cutting/grooving is an axi-symmetric problem with respect to the X-axis, temperature rise in X-Y plane as well as Y-Z plane are determined. So, X dimension varies from 0 to 10 mm, Z dimension varies from 0 to -5 mm (depending on type of laser cutting/grooving model), and Y = 0 mm.

5.2.7.2 Profile of the kerf width

From the temperature rise array, the location where the temperature has reached the melting point of the workmaterial is marked and this volume is considered to have been removed by laser beam pulse. In this way, the profile of the kerf of the laser cut/groove is determined. Also, the material removal rate is determined by calculating the volume of this region divided by the laser pulse on-time.

5.2.7.3 Cutting velocity

In the model, the circular disc heat source moves along the OX- axis of the workpiece at the cutting velocity. Penetration velocity is the ratio of length of required cut/groove (with minimum kerf width) to on-time of the laser pulse.

Table 5.5 Determination of laser cut profile and energy balance of an axi-symmetric laser cutting/grooving model

Energy_balance	AISI-1036	
Total_Actual_Power	30000	J/s
Cutting velocity	500	mm/s
Density of AISI steel	7860	kg/m^3
Pulse time	0.003	s
Latent heat of fusion	247000	J/kg
Latent heat of vaporization	1.26E+06	J/kg
Melting point	1470	C
Evaporation point	3000	C

Z\X,mm	0	0.1	0.2	0.3	0.4	0.5	0.6	0.7	0.8	0.9	1	1.1	1.2	1.3	1.4	1.5	1.6	
0	73545.21	79911.26	88447.74	97960.625	108066.16	119411.1	132795.3	149273.4	170507.3	198148.4	238296.7	294885.2	398658.7	477137.75	418532.25	441352.8	189.388153	
-0.1	63156.7969	68392.84	75091.49	82192.05	89296.766	96806.88	105134.2	114702.7	126045.2	139087	155434.4	172325.5	193164.9	178539.141	88291.45	9821.587	39.2529755	
-0.2	40032.9258	42933.1836	46053.08	48708.99	50618.6	51915.21	52641.27	52714.19	51905.21	49602.89	45433.26	38121.9	27267.13	14199.4092	3381.1936	191.467178	1.42582667	
-0.3	18779.6855	19841.84	20530.3	20582.4043	19948.639	18757.12	17095.92	15013.23	12542.15	9731.836	6778.706	3978.162	1752.668	485.6605	63.9557838	2.667429	0.025081271	
-0.4	6545.70361	6788.795	6714.33	6289.56934	5576.3193	4692.46	3737.192	2787.532	1909.521	1162.848	601.0424	244.2749	70.15823	12.04702	1.00475991	0.033233106	0.000367251	
-0.5	1703.3302	1730.87744	1628.337	1413.21753	1132.3309	839.6843	574.187	357.2315	197.584	93.61156	36.08453	10.49769	2.086078	0.249214575	0.015656749	0.000451938	5.45722E-06	
-0.6	332.586243	331.051422	295.9865	237.436264	171.16087	111.1374	64.78442	33.42114	14.90543	5.534473	1.624223	0.352021	0.051802	0.004693978	0.000239779	6.30065E-06	8.06166E-08	
-0.7	48.9622269	47.788208	40.70742	30.2730865	19.687143	11.21813	5.586906	2.399524	0.870241	0.257188	0.059055	0.009928	0.001142	8.37815E-05	3.67507E-06	9.03761E-08	1.2062E-09	
-0.8	5.457663	5.23286772	4.267138	2.96254659	1.7528923	0.884966	0.380446	0.137677	0.041217	0.009894	0.001828	0.000248	2.33E-05	1.44691E-06	5.63972E-08	1.31955E-09	1.81601E-11	
-0.9	0.462229878	0.4363615	0.342664	0.224174932	0.1221704	0.05546	0.020923	0.006498	0.001638	0.000327	5E-05	5.64E-06	4.5E-07	2.44526E-08	8.68543E-10	1.95469E-11	2.7491E-13	
-1	0.029826576	0.0277882	0.021145	0.013166548	0.0067007	0.002783	0.00094	0.000256	5.58E-05	9.5E-06	1.24E-06	1.2E-07	8.35E-09	4.06464E-10	1.3407E-11	2.92376E-13	4.18304E-15	
-1.1	0.001469444	0.00135402	0.001004	0.000600891	0.0002894	0.000112	3.46E-05	8.48E-06	1.64E-06	2.45E-07	2.8E-08	2.39E-09	1.49E-10	6.63321E-12	2.06217E-13	4.38387E-15	6.36268E-17	
-1.2	5.53617E-05	5.055E-05	3.67E-05	2.12965E-05	9.824E-06	3.59E-06	1.04E-06	2.34E-07	4.1E-08	5.55E-09	5.72E-10	4.42E-11	2.53E-12	1.04946E-13	3.11353E-15	6.48817E-17	9.52354E-19	
-1.3	1.59716E-06	1.4474E-06	1.03E-06	5.85358E-07	2.612E-07	9.15E-08	2.5E-08	5.3E-09	8.67E-10	1.09E-10	1.04E-11	7.44E-13	3.98E-14	1.56837E-15	4.49003E-17	9.219E-19	1.36417E-20	
-1.4	3.53237E-08	3.1812E-08	2.24E-08	1.2459E-08	5.418E-09	1.84E-09	4.82E-10	9.77E-11	1.52E-11	1.8E-12	1.62E-13	1.1E-14	5.63E-16	2.13414E-17	5.95384E-19	1.20972E-20	1.80012E-22	
-1.5	5.99568E-10	5.3711E-10	3.75E-10	2.0509E-10	8.743E-11	2.89E-11	7.37E-12	1.44E-12	2.16E-13	2.46E-14	2.13E-15	1.4E-16	6.89E-18	2.54141E-19	6.96398E-21	1.40496E-22	2.099E-24	
-1.6	7.81808E-12	6.972E-12	4.82E-12	2.6086E-12	1.095E-12	3.55E-13	8.85E-14	1.69E-14	2.46E-15	2.73E-16	2.3E-17	1.47E-18	7.07E-20	2.55655E-21	6.92084E-23	1.38976E-24	2.08255E-26	
-1.7	7.83836E-14	6.9628E-14	4.78E-14	2.56226E-14	1.062E-14	3.39E-15	8.31E-16	1.56E-16	2.22E-17	2.41E-18	1.99E-19	1.25E-20	5.92E-22	2.11325E-23	5.67389E-25	1.13597E-26	1.70631E-28	
-1.8	6.04624E-16	5.3527E-16	3.66E-16	1.94281E-16	7.971E-17	2.52E-17	6.08E-18	1.12E-18	1.58E-19	1.69E-20	1.37E-21	8.48E-23	3.98E-24	1.407E-25	3.75633E-27	7.50649E-29	1.12977E-30	
-1.9	3.58916E-18	3.1681E-18	2.15E-18	1.13676E-18	4.625E-19	1.45E-19	3.45E-20	6.3E-21	8.74E-22	9.25E-23	7.44E-24	4.55E-25	2.12E-26	7.44279E-28	1.97907E-29	3.95032E-31	5.95553E-33	
-2	1.63942E-20	1.4435E-20	9.77E-21	5.12983E-21	2.072E-21	6.43E-22	1.52E-22	2.75E-23	3.78E-24	3.96E-25	3.16E-26	1.92E-27	8.86E-29	3.09979E-30	8.2181E-32	1.63921E-33	2.47495E-35	
																		total_volume
volume_fusion	0.03925	0.03925	0.03925	0.02512	0.02512	0.02512	0.02512	0.02512	0.02512	0.01413	0.01413	0.01413	0.01413	0.00628	0.00628	0.00157		0.33912
volume_evaporation	0.03925	0.03925	0.03925	0.02512	0.02512	0.02512	0.02512	0.01413	0.01413	0.01413	0.01413	0.01413	0.00628	0.00628	0.00628	0.00157		0.30929

mass of melting zone,kg	2.66548E-06
mass of evaporation zone,kg	2.43102E-06
heat for fusion,J/s	219.46
heat for vaporization,J/s	1021.03
total heat,J/s	1240.49

5.2.7.4 Mass balance of the laser cutting/grooving process

All the material which is melted and evaporated is rejected away from the workpiece. Recoil pressure is generated due to the evaporation of the workmaterial and facilitates in the removal of the molten material along with the evaporated material.

5.2.7.5 Energy balance of laser cutting/grooving process

Volume of the material which has reached the melting temperature is determined. Also, the volume of material which has reached evaporation temperature is determined. Fusion mass and evaporated mass of the material are calculated by multiplying the volumes of these zones by the density of the workmaterial. Thus, the energy consumed in fusion and evaporation is determined by multiplying respective masses by the latent heat of fusion and evaporation of the workpiece. Energy balance is conducted in the same manner as for laser drilling operation.

5.2.7.6 Laser cutting/grooving efficiency

Laser cutting/grooving efficiency is the ratio of laser beam power consumed to form a cut/groove to the laser input power.

5.2.8 Heat affected zone determination of laser cutting process

Heat affected zone (HAZ) is the region near the melt zone where the temperature has reached the phase transformation temperature of the material being cut/grooved with the laser. It is calculated graphically as shown in Figure 5.11 by determining the width of the melting point isotherm and phase transformation isotherm in the X-Z plane.

For AISI-1036 steel, HAZ of 0.05 mm thickness is observed for the given laser cutting/grooving parameters. For the higher laser cutting velocities, the HAZ thickness is not uniform. HAZ has higher thickness at the start of the cut and slowly get reduced as

the laser beam passes through the workpiece as shown in Figure 5.11. At higher laser intensities, the recast layer thickness decreases as the beam radius decreases.

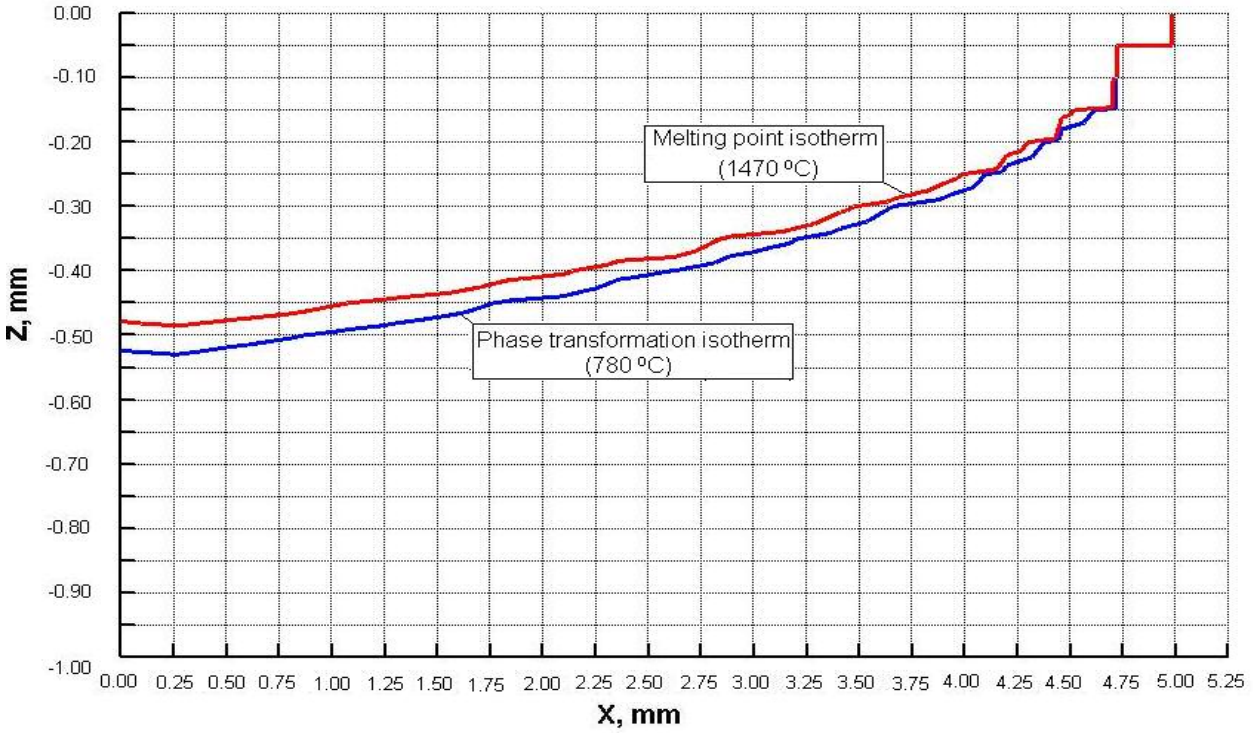

Fig. 5.11 Heat affected zone in AISI-1036 steel by laser cutting/grooving process

5.3 Trepanning laser drilling using laser cutting model.

For drilling bigger holes into the workpiece, one can optimize the laser trepanning parameters with the help of laser cutting model.

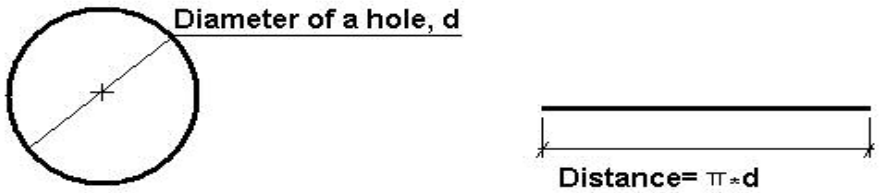

Fig. 5.12 Transformation of laser trepanning drilling to equivalent laser cutting

In trepanning laser drilling, laser beam basically moves circumferentially a distance equal to the circumference of the hole. This is equivalent to laser cutting/grooving in a straight line for a distance equal to circumference of the hole as shown in Figure 5.12.

5.4 Limitations of the thermal model

1) Effect of assist gas on laser drilling and cutting is not included in the model.
2) Effect of multiple reflection of the laser beam inside the cavity of the drilled hole and cut are not considered.

CHAPTER 6

RESULTS AND DISCUSSION

The thermal laser drilling model developed in this investigation using Jaeger's heat source technique facilitates in the optimization of the laser beam parameters. Using this model, for any material, laser beam parameters can be optimized for maximum productivity for laser drilling, cutting, and grooving processes.

In this model, thermal analysis is performed only for a single laser pulse. Therefore, from the analysis of the process for a single laser pulse, characteristics of laser drilling process can be determined. Efforts are made to model the process such that it represents the actual laser machining process e.g. effect of surface reflectivity, convective boundary cooling, and absorption of laser beam energy due to plasma are considered in the model. With the help of this model, profiles of laser drilled hole and laser cut/ groove can be determined. Drilling velocity which is an important factor for obtaining the required diameter and depth of the laser drilled hole can be optimized using this model. In the case of cutting/grooving operation, it is important to have higher depth and minimum kerf width of the cut/groove. Laser cutting/grooving velocity which affects the width and depth of kerf can be optimized using this model. Heat and mass balance are performed to give the physical insight of laser machining processes.

Different cases of laser drilling, cutting, and grooving are considered. In thin workpiece laser machining model, the thickness of the workpiece is finite. However, in

the case of thick workpiece laser machining model, the thickness of the workpiece is infinite. Depending on the thickness of the workpiece, the effect of boundary conditions is incorporated into the thermal model. Also, in the case of laser cutting/grooving, laser can start from the side of the workpiece so the effect of the side boundary condition is also included in the thermal model.

One of the limitations of the laser machining process is the formation of heat affected zone (HAZ). HAZ can be minimized by controlling the laser beam parameters using thermal model. Laser beam energy density can be controlled to get a minimum HAZ.

6.1 Determination of optimum laser parameters for the drilling process

In laser drilling, the type of laser pulse plays an important role in obtaining the required laser drilled hole profile. Generally, to get a deeper hole, percussion drilling with multiple laser pulses is practiced. Bigger diameter holes are produced with the help of CW laser. To achieve high aspect ratio of the laser drilled hole, high energy density is required in which very high laser beam energy incident on a very small area causes localized heating of the workpiece. Penetration velocity/propagation front velocity depends on thermal conductivity and diffusivity of the workmaterials. Effect of all the laser beam and workpiece parameters is studied in detail.

Initially, one value of penetration velocity is assumed for the moving circular disc heat source. For the given laser beam power, energy balance is done to determine the latent heat of fusion and evaporation. Since, Jaeger's heat source equation does not take into account the latent heat of fusion and evaporation, this energy has to be added to the energy (for temperature rise and conduction loss) that is used in the heat source

equation. Also, simulations are run several times so that the assumed velocity and actual velocity (which is calculated as ratio of depth of cylindrical hole to duration of laser pulse) is equal for a given energy balance of the process.

6.1.1 Effect of energy density on the profile of the laser drilled hole

Energy density is the ratio of the laser beam energy to the area of the laser beam. Normal distribution of the laser beam with 0.1 mm radius and 3 ms laser pulse is used to investigate the effect of energy density on the dimensions of the laser drilled hole.

Table 6.1 Effect of laser beam energy on the profile of laser drilled hole

Laser beam energy, KJ/s	Energy density, $W/mm^2 \times 10^{12}$	Diameter, mm	Depth, mm	Material removal rate, mm^3/s	Energy for fusion and evaporation, J/s	Energy for temperature rise and conduction loss, J/s
1	0.03	0.5	0.30	43.96	355	645
5	0.16	0.8	0.40	116.18	1050	3950
10	0.32	0.9	0.45	178.39	1501	8499
15	0.48	0.9	0.50	167.79	1711	13289
20	0.64	1	0.50	221.76	2128	17872
25	0.80	1	0.45	235.50	2074	22926
30	0.96	1	0.50	238.12	2385	27615

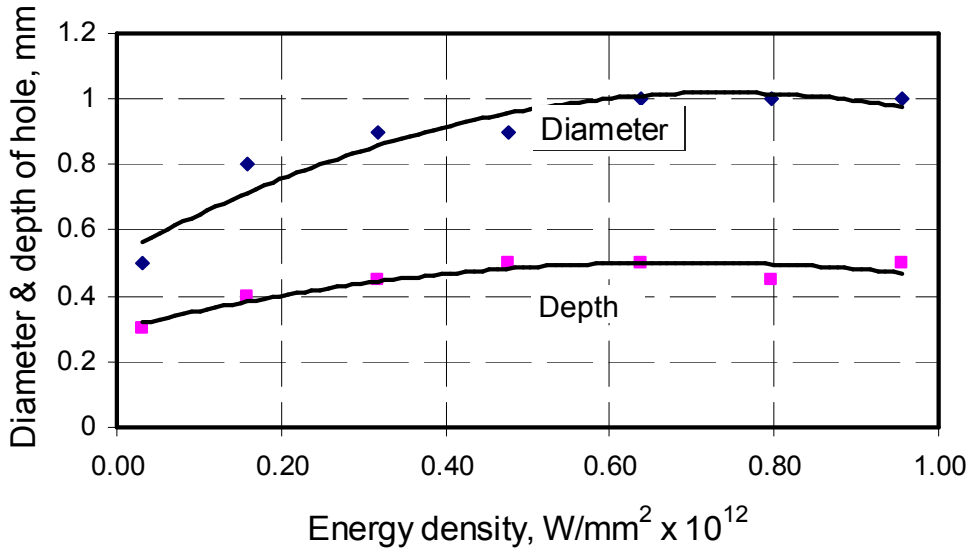

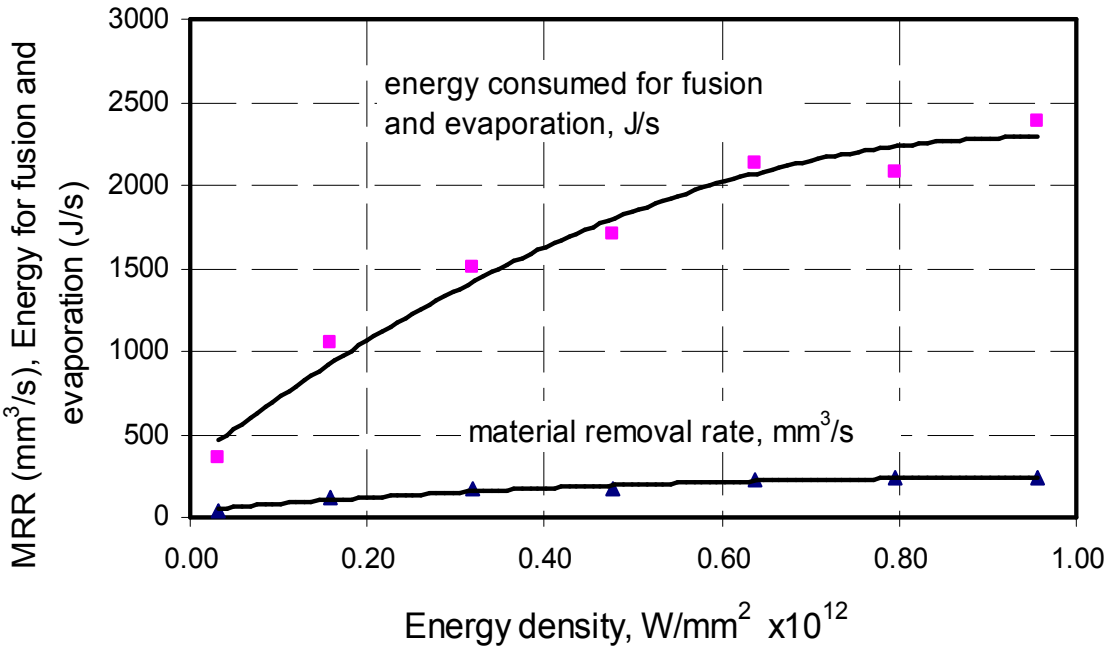

Figs. 6.1 (a) & (b) Effect of laser beam energy density on the profile of drilled hole, material removal rate, and energy consumption for fusion and evaporation for AISI-1036 steel

It is observed that with increase in laser beam energy density, there is an increase in depth and diameter of the laser drilled hole keeping the remaining parameters same. Also, there is an increase in the material removal rate thus increasing the energy consumption of fusion and evaporation as shown in Figures 6.1 (a) and (b).

6.1.2 Effect of pulse duration on the profile of the laser drilled hole

Normal laser beam distribution with 30 KJ/s laser power and 0.1 mm beam radius laser pulse is used to check the effect of pulse duration on the dimensions of the laser drilled hole and energy balance.

Table 6.2 Effect of laser pulse duration on the profile of laser drilled hole

Laser pulse duration, ms	Energy density, $W/mm^2 \times 10^{12}$	Diameter, mm	Depth, mm	Material removal rate, mm^3/s	Energy for fusion and evaporation, J/s	Energy for temperature rise and conduction loss, J/s
0.5	0.96	0.4	0.2	157.00	1424	28576
1	0.96	0.6	0.3	166.42	1754	28246
1.5	0.96	0.7	0.4	205.15	2057	27943
2	0.96	0.8	0.4	222.15	2212	27788
3	0.96	1	0.5	238.12	2385	27615
4	0.96	1.2	0.6	254.34	2484	27516
5	0.96	1.2	0.7	245.86	2548	27452
6	0.96	1.2	0.7	276.32	2547	27453
7	0.96	1.5	0.8	299.87	3003	26997
8	0.96	1.6	0.8	303.80	2938	27062
9	0.96	1.6	0.9	314.00	3166	26834
10	0.96	1.8	0.9	329.70	3103	26897

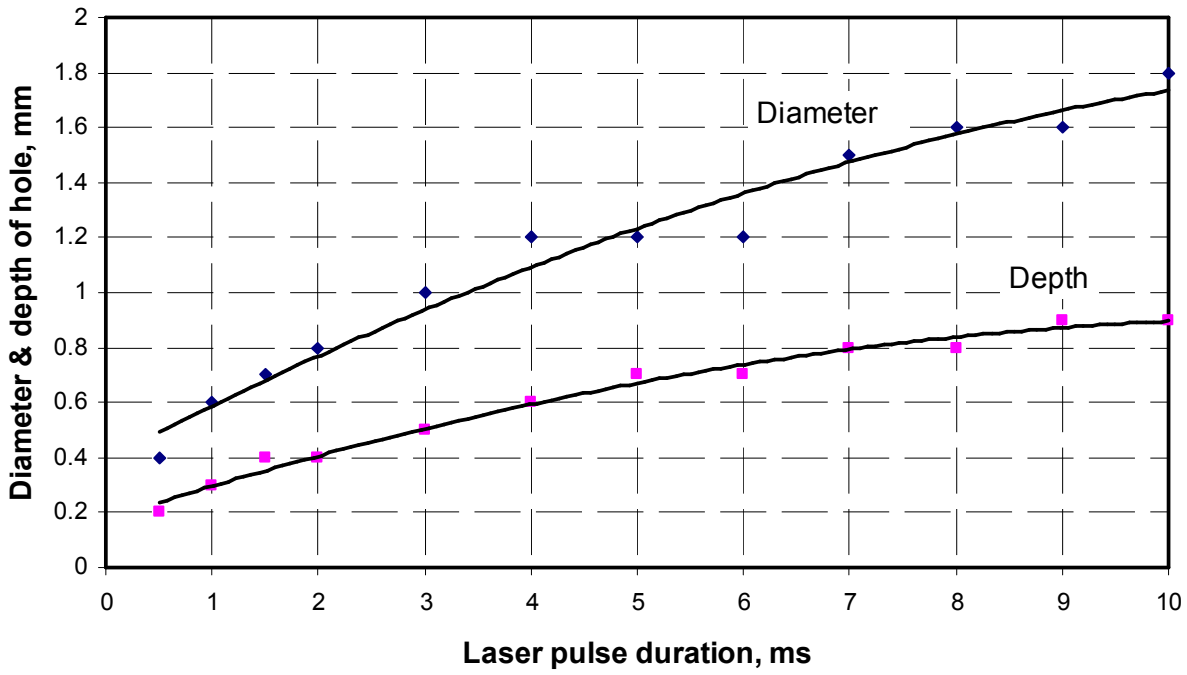

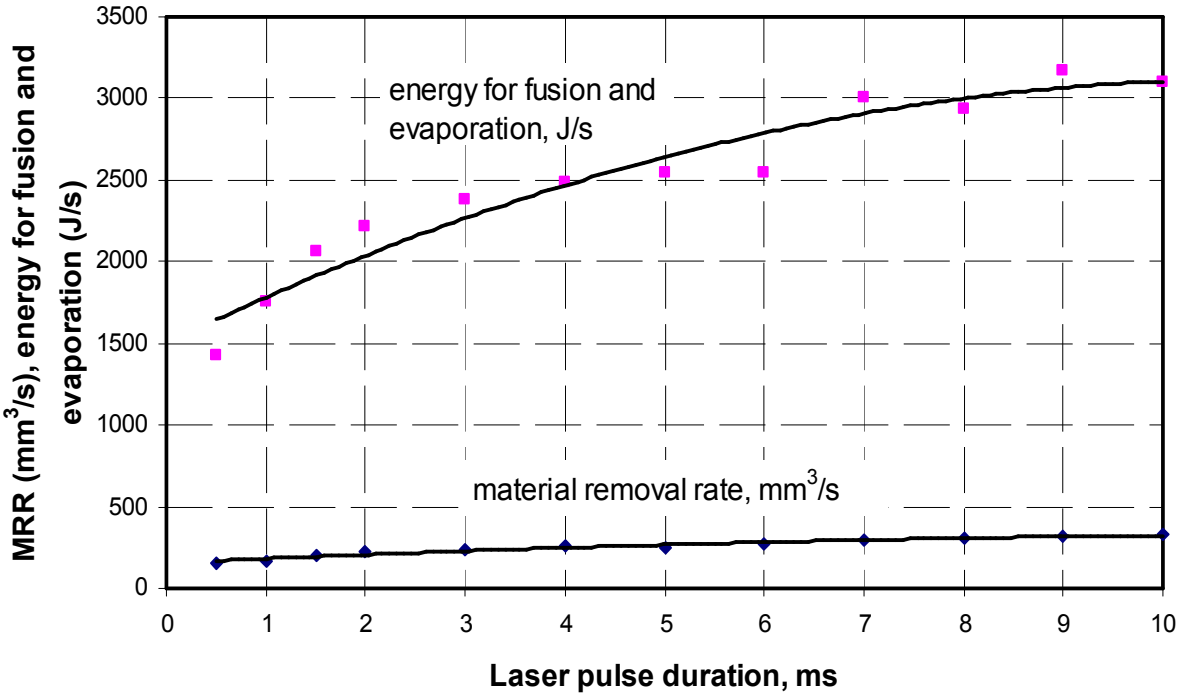

Figs. 6.2 (a) & (b) Effect of laser pulse duration on the profile of a drilled hole, material removal rate, and energy consumption for fusion and evaporation for AISI-1036 steel

It is observed that with increase in laser pulse duration, diameter and depth of the drilled hole increase. Also, there is an increase in material removal rate and energy consumption for fusion and evaporation of the material with the increase in laser pulse duration as shown in Figures 6.2 (a) and (b).

6.1.3 Effect of laser beam radius on profile of the laser drilled hole

Normal laser beam distribution with 30 KJ/s power and 3 ms laser pulse is used to check the effect of laser beam radius on the dimensions of the laser drilled hole. With increase in the laser beam radius, the diameter of the laser drilled hole is found to increase as shown in Figures 6.3 (a) and (b).

Table 6.3 Effect of laser beam radius on the profile of laser drilled hole

Laser beam radius, mm	Energy density, $W/mm^2 \times 10^{12}$	Diameter, mm	Depth, mm	Material removal rate, mm^3/s	Energy for fusion and evaporation, J/s	Energy for temperature rise and conduction loss, J/s
0.025	15.287	1	0.5	238.12	2287	27713
0.05	3.822	1	0.5	238.12	2287	27713
0.1	0.955	1	0.5	238.12	2385	27615
0.2	0.239	1	0.5	249.11	2505	27495
0.3	0.106	1.1	0.5	255.39	2470	27530
0.4	0.060	1.1	0.5	288.88	2945	27055
0.5	0.038	1.2	0.5	308.24	2977	27023
0.6	0.027	1.3	0.5	342.78	3392	26608
0.7	0.019	1.4	0.5	392.50	3835	26165
0.8	0.015	1.4	0.4	426.52	4171	25829
0.9	0.012	1.5	0.4	472.05	4529	25471
1	0.010	1.6	0.4	533.80	5198	24802
1.25	0.006	1.8	0.45	692.37	5962	24038
1.5	0.004	2	0.3	828.96	6709	23291
1.75	0.003	2	0.3	828.96	8948	21052
2	0.002	2.4	0.3	1105.28	9485	20515

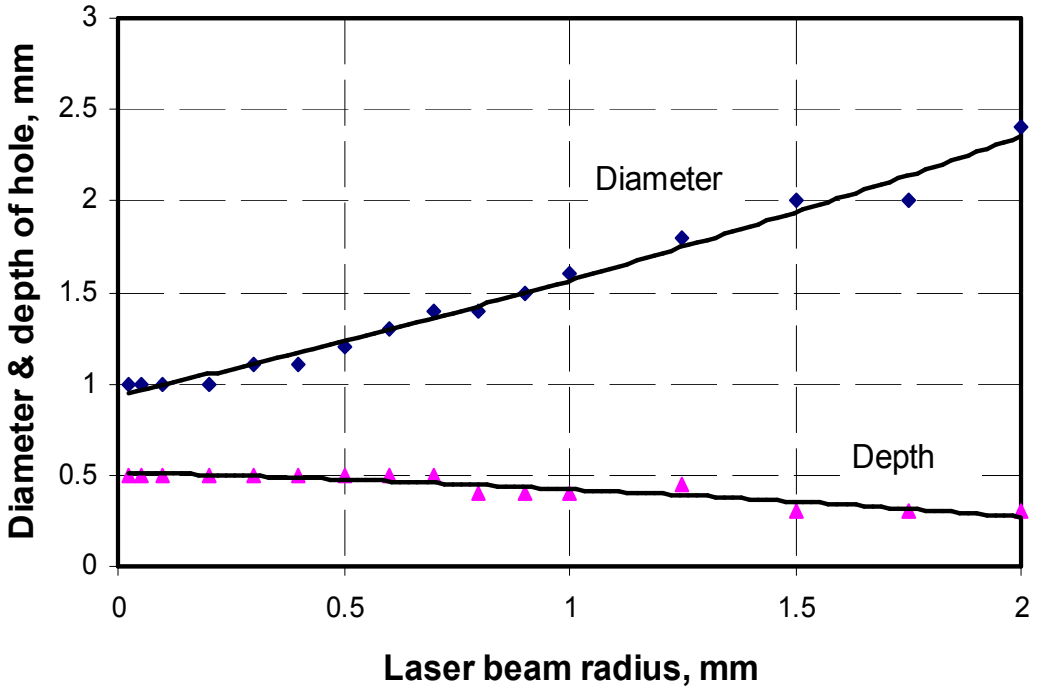

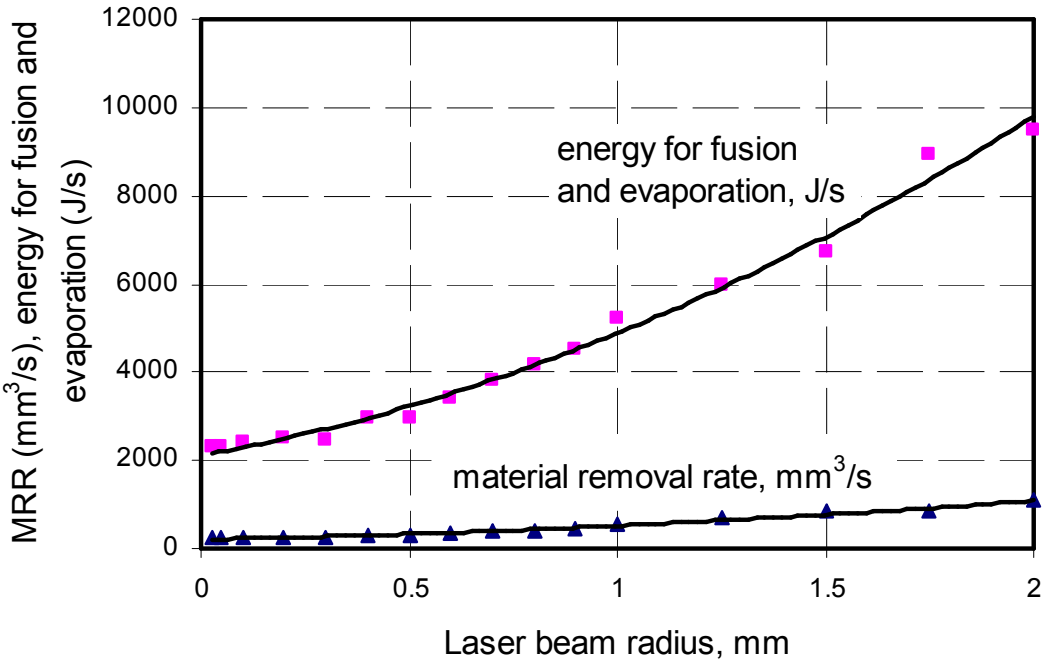

Figs. 6.3 (a) & (b) Effect of laser beam radius on laser drilled hole profile, material removal rate, and energy consumption for fusion and evaporation for AISI-1036 steel

There is no significant change in the depth of laser drilled hole due to change in the laser beam radius. With increase in the laser beam radius, the material removal rate, thus the energy consumption for fusion and evaporation also increases as shown in Figures 6.3 (a) and (b).

6.1.4 Effect of laser beam distribution on profile of the laser drilled hole

By keeping all the laser beam parameters, such as laser beam radius, laser pulse duration, and laser power the same; effect of type of laser beam distribution on the profile of the laser drilled hole is studied. From Table 6.4, there is no significance difference on the profile of the laser drilled hole due to change in laser beam distribution.

Table 6.4 Effect of laser beam distribution the profile of laser drilled hole

Laser pulse distribution	Energy density, $W/mm^2 \times 10^{12}$	Diameter, mm	Depth, mm	Material removal rate, mm^3/s	Energy for fusion and evaporation, J/s	Energy for temperature rise and conduction loss, J/s
Normal	0.96	1	0.5	238.12	2385	27615
Bimodal	0.96	1	0.5	217.71	2143	27857
Uniform	0.96	1	0.5	232.36	2358	27642

However, material removal rate is highest for normal distribution and lowest for bimodal distribution. Generally, normal distribution is used. To obtain uniform distribution, an expensive special arrangement of lenses is required.

6.1.5 Effect of thermal properties of the workmaterial on the laser drilled hole

Results are obtained for stainless steel-304, AISI-1036 steel, CP-titanium, mild steel, and aluminum workmaterial. Table 6.5 gives the thermal properties of these materials.

Table 6.5 Thermal properties of some engineering materials

Type of Material	Thermal diffusivity, mm^2/s	Thermal conductivity, J/mm s ^0C	Melting point, ^0C	Evaporation point, ^0C	Density, Kg/m^3
Stainless steel-304	3.52	0.01398	1420	3000	7916
AISI-1036 steel	6.1	0.0339	1470	3000	7860
CP-titanium	6.35	0.0156	1668	3287	4510
Mild steel	16.43	0.08	1535	2750	7850
Aluminum	99.31	0.237	1083	2467	2643

Table 6.6 Effect of thermal properties of materials on laser drilled hole profile and material removal rate

Type of material	Thermal diffusivity, mm^2/s	Thermal conductivity, J/mm s °C	Energy density, $W/mm^2 \times 10^{12}$	Diameter, mm	Depth, mm	Material removal rate, mm^3/s
Stainless steel-304	3.52	0.01398	0.96	0.8	0.4	127.69
AISI-1036 steel	6.10	0.0339	0.96	1	0.5	217.71
CP-titanium	6.35	0.0156	0.96	1	0.6	263.76
Mild steel	16.43	0.08	0.96	1.4	0.7	590.32
Aluminum	99.31	0.237	0.96	2.8	1.4	4180.39

It is observed that material removal rate is dependent on the thermal diffusivity of the material, more the thermal diffusivity; more is the material removal rate for the given laser beam parameters.

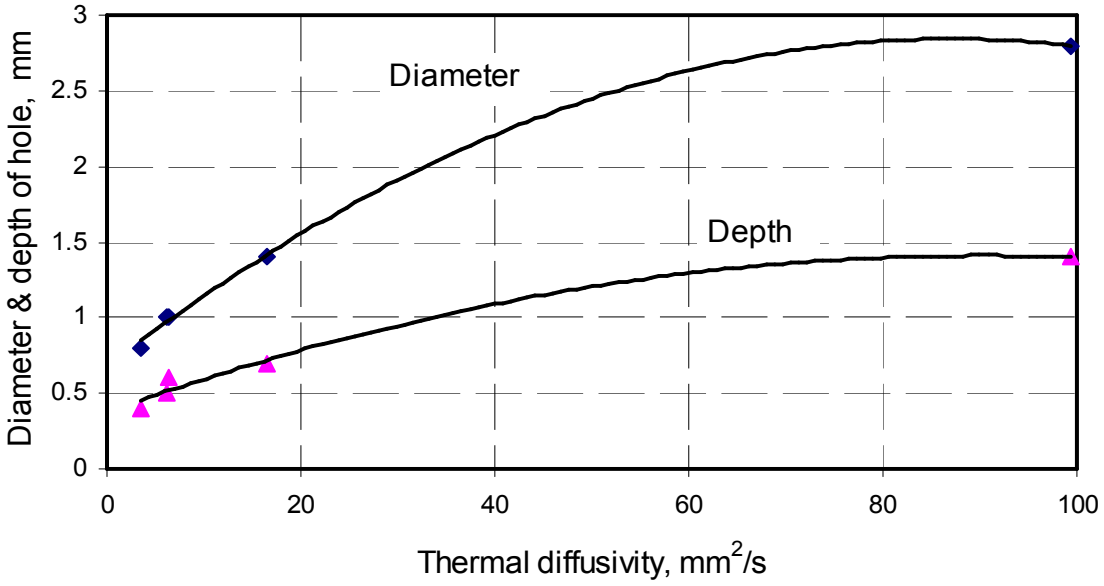

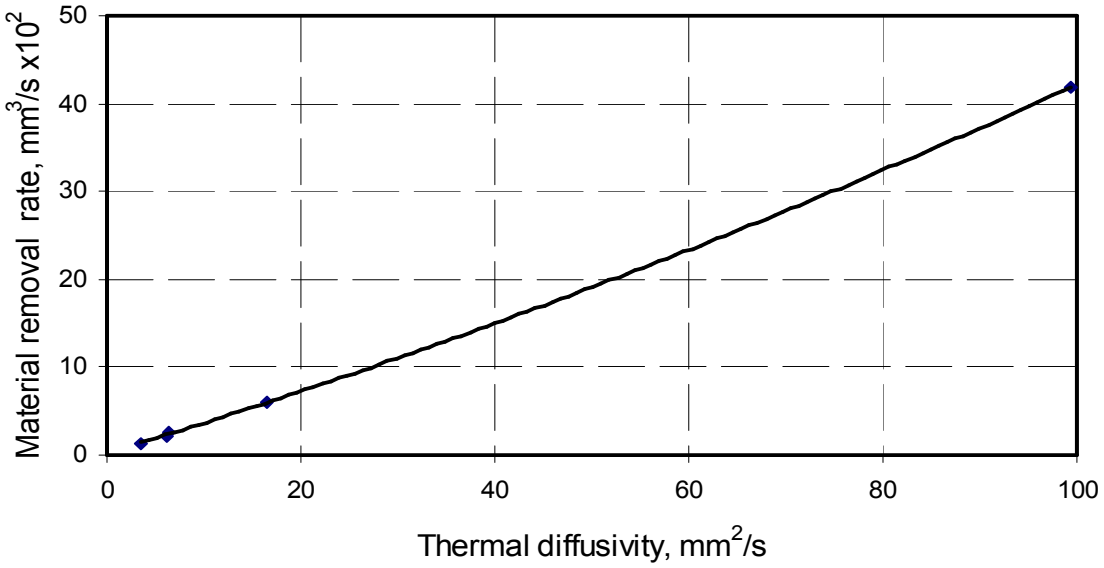

Figs. 6.4 (a) & (b) Effect of thermal properties of material on laser drilled hole profile and material removal rate

As shown in Figures 6.4 (a) and (b), maximum material removal rate is obtained for aluminum and minimum material removal rate is obtained for stainless steel-304 for the given laser beam parameters.

6.1.6 Effect of laser beam energy density on thickness of the heat affected zone

Keeping all the laser beam parameters same, effect of laser beam power on the heat affected zone is studied.

Table 6.7 Effect of energy density on thickness of heat affected zone for AISI-1036 steel

Laser beam energy, KJ/s	Energy density, $W/mm^2 \times 10^{12}$	Thickness of heat affected zone, mm
1	0.03	0.040
5	0.16	0.035
10	0.32	0.032
15	0.48	0.030
20	0.64	0.030
25	0.80	0.030
30	0.96	0.030

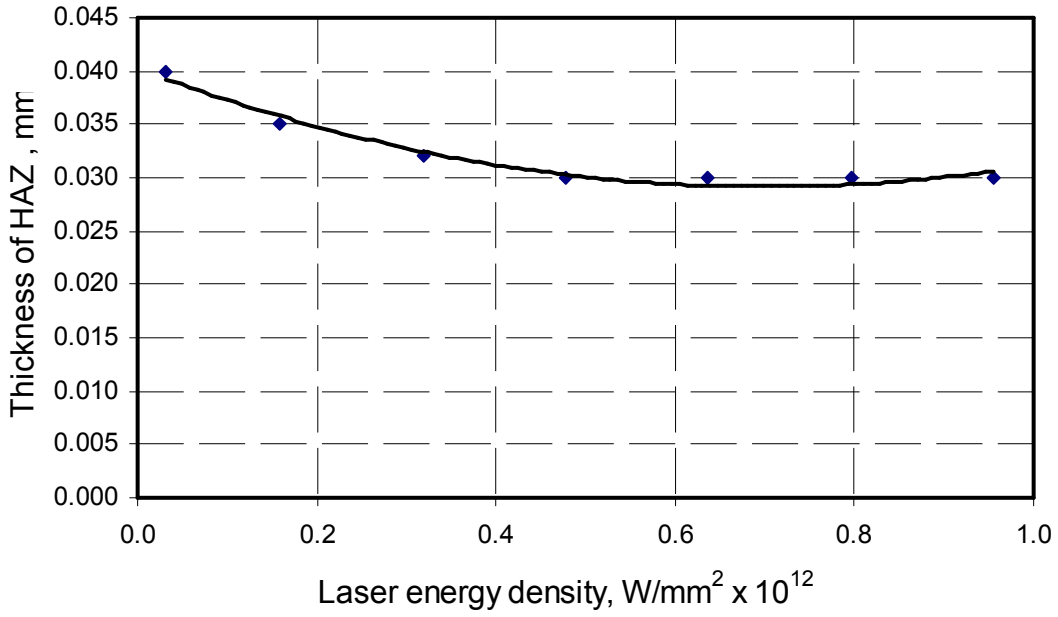

Fig 6.5 Effect of energy density on the thickness of HAZ for AISI-1036 steel

It is observed that with increase in laser energy density, there is a decrease in width of the heat affected zone in the AISI-1036 steel material as shown in Figure 6.5. However, due to increase in material removal rate with increase in laser power, there is an increase in the overall heat affected region around the drilled hole profile.

6.2 Determination of optimum laser beam parameters for the cutting/grooving process

In laser cutting/grooving processes, laser cutting velocity can be determined from laser cutting/grooving model. Generally, cutting is done for thin workpiece. Therefore, for this purpose a thin workpiece cutting model is developed, which takes care of the effect of boundary conditions of the top and bottom boundaries of thin workpiece.

Grooving operation is generally performed on thick workpieces. For this purpose, a thick workpiece cutting/grooving model is developed. Grooving can be started from the side or from anywhere in the workpiece. So, the effect of side and top boundary conditions is considered in the thick workpiece side and central model using image heat sources method.

In laser cutting operation of thin workpieces, lower energy density is used so that material is only melted and removed from the bottom of the cut. However, in the case of grooving operation, we need to have higher energy density, so that material is evaporated and removed from the groove of the workpiece as a vapor.

Cutting/grooving velocity should be such that minimum kerf width is obtained with required depth of cut. In grooving operation, the width of kerf should be uniform. This optimization of kerf width can be determined using laser cutting/grooving model. It is observed from the analysis of laser cutting/grooving model, using Jaeger's heat source

method, the kerf width is equal to twice of the depth of cut. In cutting operation, the kerf width is not critical. So, laser beam parameters are chosen such that maximum cut length and depth are obtained. In the case of grooving operation, width and depth of groove are critical and needs to be uniform. Effect of laser beam parameters on the kerf width and depth of cut/groove is investigated using laser cutting /grooving model.

Keeping all other laser beam parameters same, the cutting velocity is varied for thin workpiece side cutting model. Table 6.8 shows the effect of cutting velocity on the length, depth, and kerf width of laser cut. Maximum kerf width is obtained at the beginning of cut and minimum kerf width is observed at the end of a laser pulse.

Table 6.8 Effect of cutting velocity on the profile of laser cut

Cutting Velocity, mm/s	Length of cut , mm	Depth of cut , mm	Maximum kerf width, mm	Minimum kerf width, mm	Material removal rate, mm^3/s
50	0.5	0.55	1.1	0.6	168.12
100	0.65	0.58	1.16	0.7	176.63
150	0.77	0.58	1.16	0.7	176.63
200	0.96	0.58	1.16	0.3	192.33
250	1.05	0.58	1.16	0.5	213.91
500	1.73	0.58	1	0.3	287.18
750	2.5	0.58	1	0.1	387.27
1000	3.28	0.58	1	0.1	474.92
1250	4.05	0.58	0.9	0.1	534.45
1500	4.75	0.58	0.9	0.1	616.22

As shown in Figures 6.6 (a) and (b), with increase in cutting velocity, the length of cut increases. Consequently, the material removal rate also increases. Also, by controlling the laser beam radius one can control the width of the groove in laser grooving operation. Depth of the cut does not change significantly with the increase in laser cutting velocity.

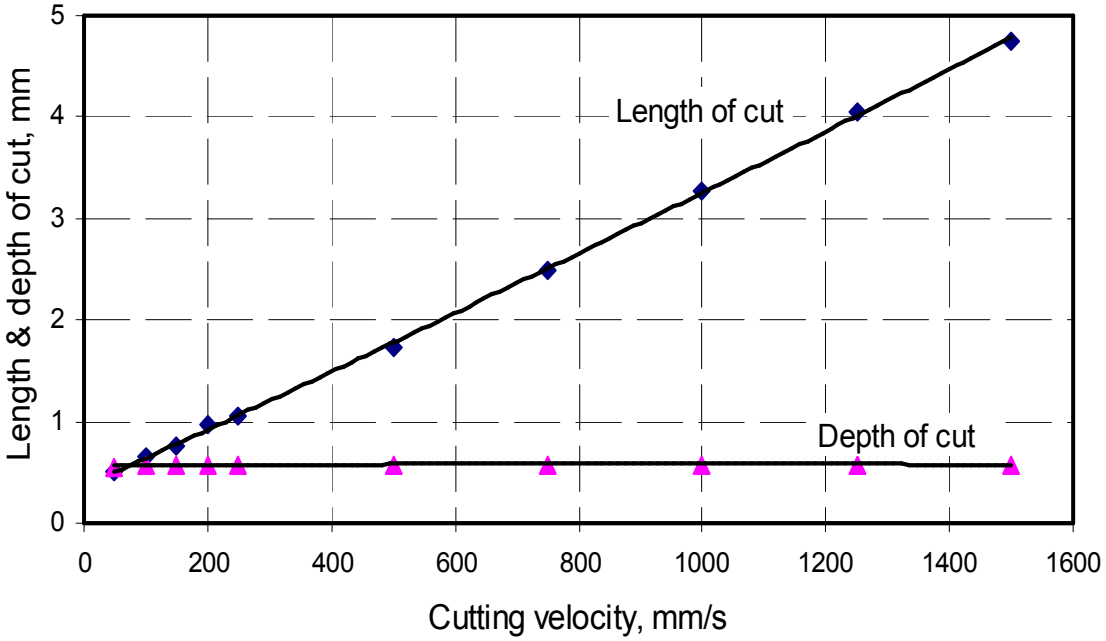

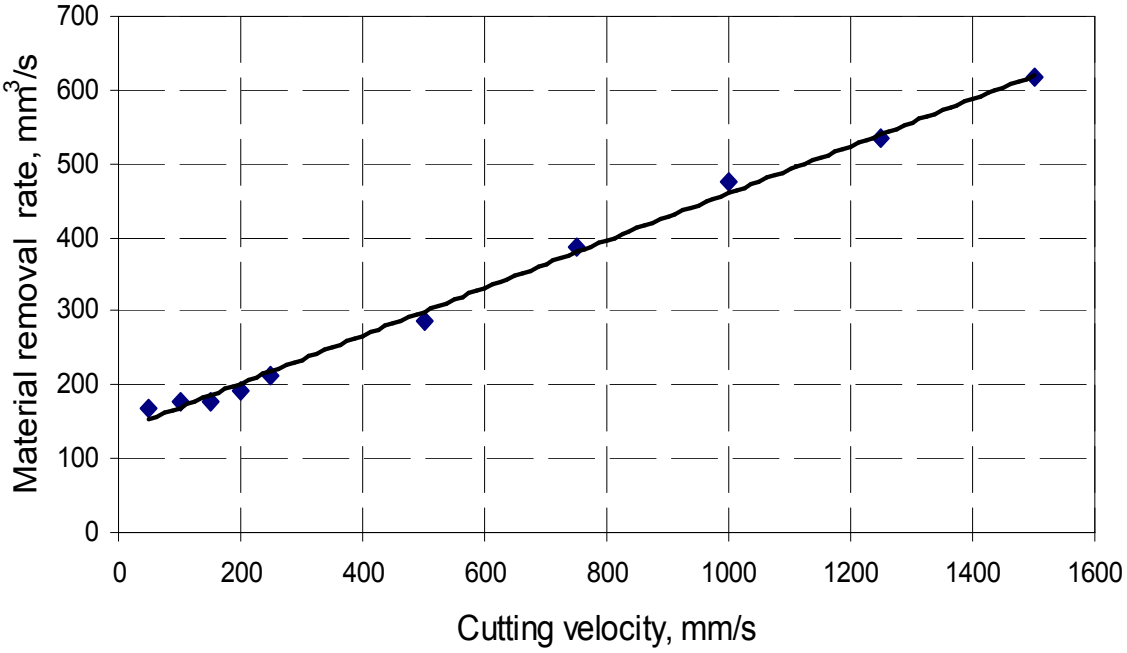

Figs. 6.6 (a) & (b) Effect of cutting velocity on the profile of laser cut and material removal rate

6.3 Sensitivity analysis of laser beam parameters

Sensitive analysis of laser beam parameters, such as laser beam energy, pulse duration, and laser beam radius on the profile of laser drilled hole and material removal rate is conducted.

Table 6.9 Sensitivity analysis for laser beam energy

Laser beam energy, J/s	% Change in beam energy	Energy density, $W/mm^2 \times 10^{12}$	Diameter, mm	% Change in diameter	Depth, mm	% Change in depth	Material removal rate, mm^3/s	Energy for fusion and evaporation, J/s
1000		0.03	0.5		0.3		43.96	355
5000	400	0.16	0.8	60.00	0.4	33.33	116.18	1050
10000	100	0.32	0.9	12.50	0.45	12.50	178.391	1501
15000	50	0.48	0.9	0.00	0.5	11.11	167.793	1711
20000	33	0.64	1	11.11	0.5	0.00	221.762	2128
25000	25	0.80	1	0.00	0.5	0.00	235.5	2074
30000	20	0.96	1	0.00	0.5	0.00	238.116	2385

Table 6.10 Sensitivity analysis for laser pulse duration

Laser pulse duration, ms	% Change in pulse duration	Energy density, $W/mm^2 \times 10^{12}$	Diameter, mm	% Change in diameter	Depth, mm	% Change in depth	Material removal rate, mm^3/s	Energy for fusion and evaporation, J/s
0.5		0.96	0.4		0.2		157.00	1424
1	100.00	0.96	0.6	50.00	0.3	50.00	166.42	1754
1.5	50.00	0.96	0.7	16.67	0.4	33.33	205.15	2057
2	33.33	0.96	0.8	14.29	0.4	0.00	222.15	2212
3	50.00	0.96	1	25.00	0.5	25.00	238.12	2385
4	33.33	0.96	1.2	20.00	0.6	20.00	254.34	2484
5	25.00	0.96	1.2	0.00	0.7	16.67	245.86	2548
6	20.00	0.96	1.2	0.00	0.7	0.00	276.32	2547
7	16.67	0.96	1.5	25.00	0.8	14.29	299.87	3003
8	14.29	0.96	1.6	6.67	0.8	0.00	303.80	2938
9	12.50	0.96	1.6	0.00	0.9	12.50	314.00	3166
10	11.11	0.96	1.8	12.50	0.9	0.00	329.70	3103

Table 6.11 Sensitivity analysis for laser beam radius

Laser beam radius, mm	% change in beam radius	Energy density, $W/mm^2 \times 10^{12}$	Diameter, mm	% change in diameter	Depth, mm	% change in depth	Material removal rate, mm^3/s	Energy for fusion and evaporation, J/s
0.025		15.287	1		0.5		238.12	2287
0.05	100.00	3.822	1	0.00	0.5	0.00	238.12	2287
0.1	100.00	0.955	1	0.00	0.5	0.00	238.12	2385
0.2	100.00	0.239	1	0.00	0.5	0.00	249.11	2505
0.3	50.00	0.106	1.1	10.00	0.5	0.00	255.39	2470
0.4	33.33	0.060	1.1	0.00	0.5	0.00	288.88	2945
0.5	25.00	0.038	1.2	9.09	0.5	0.00	308.24	2977
0.6	20.00	0.027	1.3	8.33	0.5	0.00	342.78	3392
0.7	16.67	0.019	1.4	7.69	0.5	0.00	392.50	3835
0.8	14.29	0.015	1.4	0.00	0.4	-20.00	426.52	4171
0.9	12.50	0.012	1.5	7.14	0.4	0.00	472.05	4529
1	11.11	0.010	1.6	6.67	0.4	0.00	533.80	5198
1.25	25.00	0.006	1.8	12.50	0.45	12.50	692.37	5962
1.5	20.00	0.004	2	11.11	0.3	-33.33	828.96	6709
1.75	16.67	0.003	2	0.00	0.3	0.00	828.96	8948
2	14.29	0.002	2.4	20.00	0.3	0.00	1105.28	9485

At a time one laser beam parameter is changed, and its effect on the laser dilled hole profile is determined. It is observed that for the change of 100%, 50%, and 33.33 % in laser pulse duration as shown in Table 6.10, diameter and depth of the laser drilled hole changes marginally as compared to the same percentage change in laser energy and laser beam radius. Therefore, from Tables 6.12 to 6.14; it is concluded that for the same percentage change in laser beam parameters, the laser drilled hole profile is more sensitive to laser pulse duration and less sensitive to laser beam radius. The effect of 100%, 50%, and 33.33 % change in laser beam parameters on the diameter and depth of laser drilled hole is analyzed.

6.4 Benchmarking of thermal drilling model

Laser drilled hole profile obtained from the Jaeger's heat source method are compared with the experimental and finite difference method solutions for mild steel and aluminum material reported by Cheng *et al.* [27]. Thermal properties of mild steel and aluminum workmaterial as well as laser beam parameters are taken from this study.

Since, the thickness of the workpiece is 2 mm; thin workpiece laser drilling model is used to compare the results.

Table 6.12 Laser beam parameters from literature [27]

Laser beam radius, mm	0.125
Pulse energy, J	4
Pulse duration, ms	1.5
Number of laser pulses	1

Penetration velocity, as the ratio of the depth of the hole to laser pulse duration for the moving circular disc heat source is determined from the experimental results published in the literature [27]. Table 6.12 shows the laser beam parameters used in the literature, these laser beam parameters are used in Jaeger's heat source model and the results of laser drilled hole profile are tabulated and compared with those given in literature as shown in Figures 6.7,6.8 and Tables 6.13, 6.14.

Depth, inlet and bottom radius of the laser drilled hole by using Jaeger's heat source method are compared with the experimental and finite difference method results published in the literature [27]. Mild steel and aluminum workmaterial are considered.

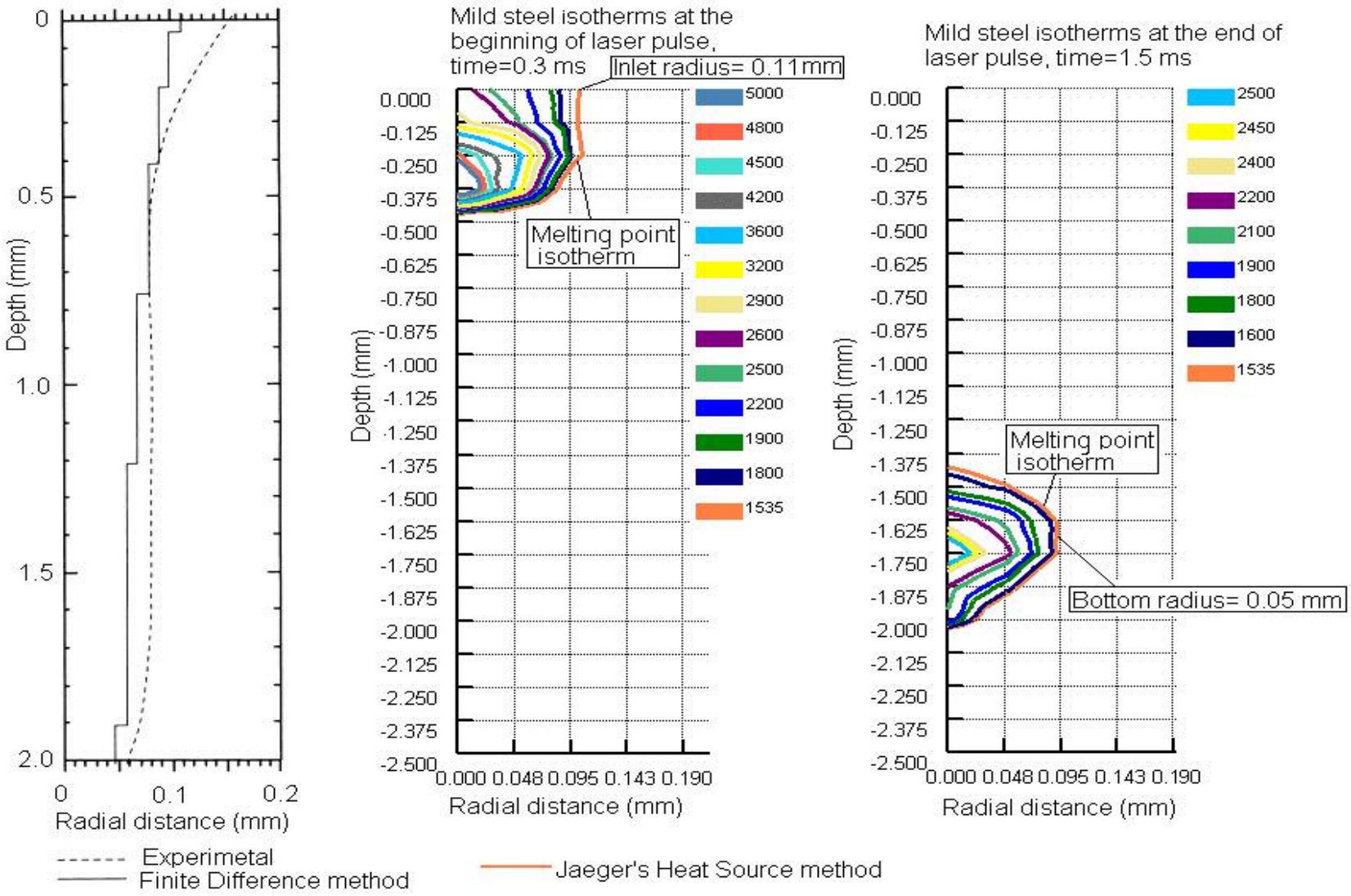

Fig.6.7 Comparison of results of Jaeger's heat source method with finite difference method and experimental results for mild steel [27]

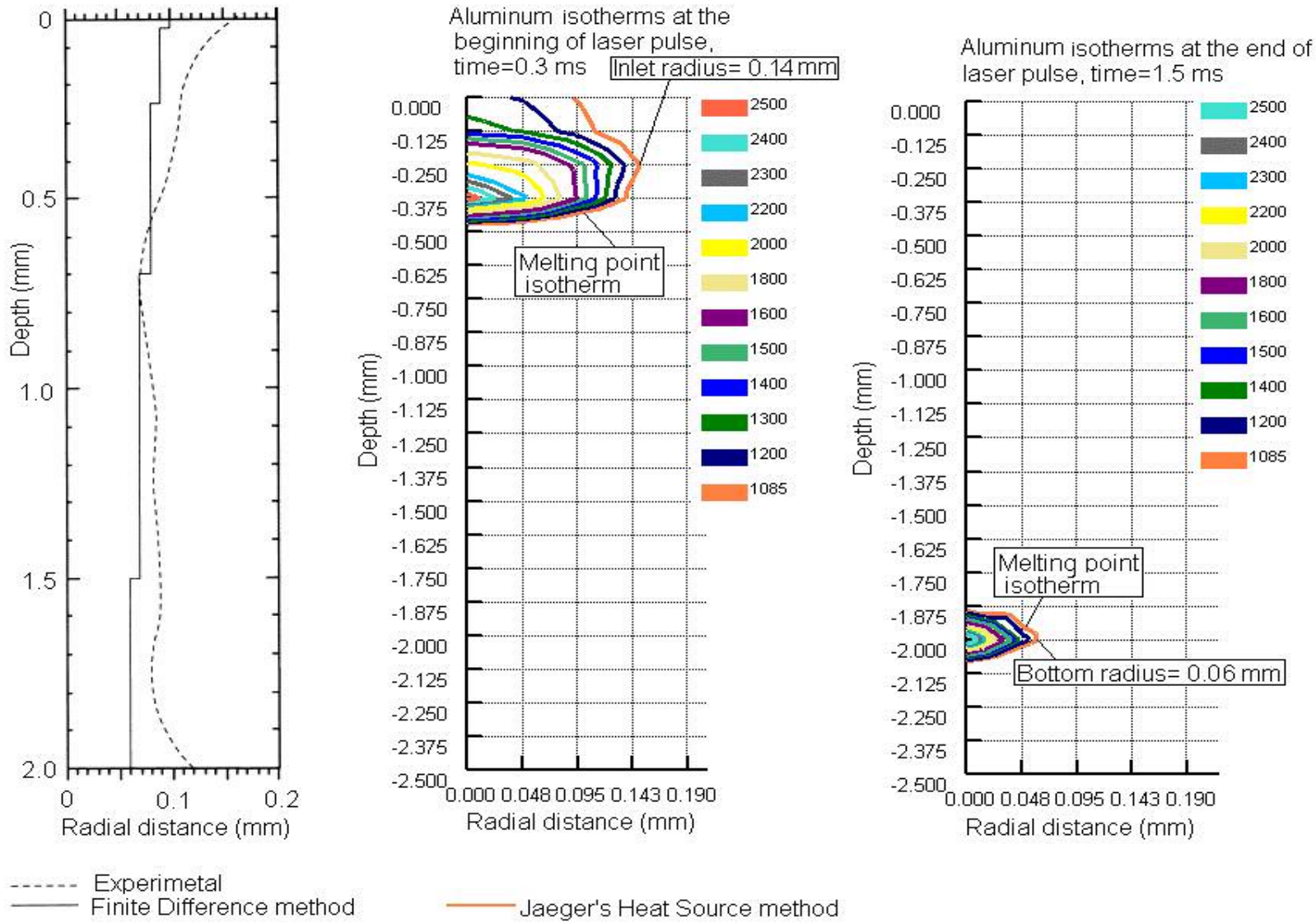

Fig. 6.8 Comparison of results of Jaeger's heat source method with finite difference method and experimental results for aluminum [27]

Table 6.13 Comparison for laser drilled hole profile for mild steel workmaterial

Profile of laser drilled hole	Experimental [27]	Finite difference method [27]	Jaeger's heat source method
Inlet radius, mm	0.15	0.11	0.11
Bottom radius, mm	0.05	0.048	0.05
Depth, mm	2	2	1.9

Table 6.14 Comparison for laser drilled hole profile for aluminum workmaterial

Profile of laser drilled hole	Experimental [27]	Finite difference method [27]	Jaeger's heat source method
Inlet radius, mm	0.16	0.1	0.14
Bottom radius, mm	0.12	0.06	0.06
Depth, mm	2	2	2

In Jaeger's heat source method, the laser drilled hole profile is obtained by determining the melting point isotherms of the respective workmaterial as shown in the Figures 6.7 and 6.8. To obtain the inlet radius of the dilled hole, model is run at 0.3 ms and from the melting point isotherm, profile of the laser drilled hole is determined. Similarly, model is run at the end of laser pulse (1.5 ms) to obtain the bottom radius of the drilled hole.

It is observed that Jaeger's heat source method's results are close to the finite difference method results. However, values of laser dilled hole parameters are less than the experimental values. Therefore, the Jaeger's heat source model has been found to give good general agreement with finite difference model as given in the literature [27]. Major source of error between the Jaeger's heat source model and experimental study may be more because of assumption of constant thermal properties of the workmaterial in Jaeger's heat source model. Also, the optical properties of the workpiece are assumed constant during laser drilling. However, the reflectivity and thermal properties of the workpiece change with temperature of the surface.

CHAPTER 7

CONCLUSIONS AND FUTURE WORK

7.1 CONCLUSIONS

1. Using Jaeger's heat source method laser drilling, laser cutting, and laser grooving models are developed. These models are very convenient and can be used rapidly using a computer.
2. The models are validated by comparing the results with the experimental and finite difference method results given in the literature [27].
3. Different aspects of laser machining, such as thin and thick workpieces are considered. Also, situations such as cutting/grooving from side or central of the workpiece are considered.
4. The model can be applied for practical situations.
5. Laser drilled hole profile, material removal rate, mass balance, and energy balance for laser drilling, cutting, and grooving process can be determined using the thermal model developed in the present investigation.
6. The effect of laser beam parameters on the profile of laser drilled hole and laser cut width are investigated. Based on this model, we can predict the profile of the hole, cut, and groove. The number and duration of a laser pulses required to drill a hole of required diameter, and cut of required length and depth can be determined.

7. Penetration and cutting/grooving velocity can be optimized for laser machining process.
8. Based on this model, to obtain a deeper hole with smaller diameter, we need to use more number of short laser pulses. To get a larger diameter hole, we need to use only a few pulses but of longer duration.
9. It is observed that normal laser beam distribution gives more material removal rate compared to bimodal and uniform laser beam distributions.
10. In the case of cutting/grooving process, continuous laser is found to be useful and in case of drilling, pulsed laser found to be effective.
11. Thickness of the Heat affected zone for laser machining process is determined and can be controlled by controlling laser beam parameters, such as laser energy and drilling/cutting velocity.
12. Laser machining process conditions can be developed for any engineering material with the help of these models.

7.2 FUTURE WORK

Present thermal model can be extended to laser welding process using moving circular disc heat source. In laser welding, low energy density is required since only fusion and no evaporation of the joining material is required.

Thermal residual stresses are developed because of large thermal gradients during laser machining process in the workpiece. These stresses can affect the fatigue life of the laser drilled hole. Thermal gradient can be determined from the present thermal model and then thermal stress analysis can be done with the help of finite element analysis tool to determine residual stresses.

REFERENCES

1. Chryssolouris, G., ”Laser machining-theory and practice,” Mechanical Engineering Series Springer- Verlag (1991).
2. Bellows, G., and J. Kohls, ”Drilling without drills,” American Machinist (1982) 173-188.
3. Adams, Jr., C.M., and G. Hardway, “Fundamental of Laser Beam Machining and drilling,” IEE Transactions on Industry and General Applications (1965) 90-96.
4. Paek, U., and F. Gagliano, “Thermal Analysis of Laser Drilling Processes,” IEEE Journal of Quantum Electronics 8 (1972)112-119.
5. Allmen, M.V., “Laser drilling velocity in metals,” Journal of Applied Physics 47 (1976) 5460-5463.
6. Yilbas, B.S., “The absorption of incident beams during laser drilling of metals,” Optics and Laser Technology (1986) 27-32.
7. Yilbas, B.S., Yilbas, Z., and N. Akcakoyun, ”Investigation into absorption of the incident laser beam during Nd:YAG laser processing of metals,” Optics and Laser Technology 28 (1996) 503-511.
8. Allmen, M.V., Blaser, P., Affolter, K., and E. Sturmer, “Absorption phenomena in metal drilling with Nd-Lasers,” IEEE Journal of Quantum Electronics 2 (1972)85-88.

9. Sankaranarayanan, S., Emminger, H., and A. Kar, “Energy losses in the metal plasma during laser drilling,” Journal of Physics D: Applied Physics 32 (1999) 1605-1611.

10. Duley, W.W., and W.A. Young, “Kinetic effects in drilling with the CO_2 laser,” Journal of Applied Physics 44 (1973).

11. Dabby, F.W., and U. Paek, “High-Intensity Laser-Induced Vaporization and Explosion of Solid Material,” IEEE Journal of Quantum Electronics 2 (1972) 106-111.

12. Hamilton, D.C., and I.R. Pashby, “Hole drilling studies with a variable pulse length CO_2 laser,” Optics and Laser Technology 11 (1979) 183-188.

13. Yoshioka, S., and T. Miyazaki, “Numerical prediction of hole shape in energy beam drilling of metals,” Precision Engineering 6 (1984) 181-186.

14. Yilbas, B.S., “A study of affecting parameters in the laser hole- drilling of sheet metals,” Journal of Mechanical Working Technology 13 (1986) 303-315.

15. Han, W., “Computational and experimental investigations of laser drilling and welding for microelectronic packaging,” Dissertation, Mechanical Engineering Department, Worcester Polytechnic Institute (2004) 50-51.

16. Chan, C. L., and J. Mazumder, “One dimensional steady-state model for damage by vaporization and liquid expulsion due to laser-material interaction,” Journal of Applied Physics 11 (1987) 4579-4586.

17. Yilbas, B.S., “Investigation into drilling speed during laser drilling of metals,” Optics and Laser Technology 20 (1988) 29-32.

18. Kar, A., Rockstroh, T., and J. Mazumder, “Two dimensional model for laser-induced materials damage: Effects of assist gas and multiple reflections inside the cavity,” Journal of Applied Physics 6 (1992) 2560-2569.
19. Yilbas, B.S., Sami, M., Kar, A.K., and A.Z. Sahin, “First and second law efficiencies for laser drilling of stainless steel,” Energy 21 (1995) 197-203.
20. Modest, M. F., “Three-dimensional, transient model for laser machining of ablating/decomposing materials,” International Journal of Heat Transfer 39 (1996) 221-234.
21. Ganesh, R. K., Bowley, W. W., Bellantone, R. R., and Y. Hahn, ”A model for laser hole drilling in metals,” Journal of Computational Physics 125 (1996) 161-176.
22. Semak, V., and A. Matsunawa, “The role of recoil pressure in energy balance during laser materials processing,” Journal of Physics D: Applied Physics 30 (1997) 2541-2552.
23. Kaplan, A.F.H., “An analytical model of metal cutting with a laser beam,” Journal of Applied Physics 79 (1996) 2198-2208.
24. Duan, J., Man, H.C., and T.M. Yue, “Modeling the laser fusion cutting process: I. Mathematical modeling of the cut kerf geometry for laser fusion cutting of thick metal,” Journal of Physics D: Applied Physics 34 (2001) 2127-2134.
25. Prusa, J.M., Venkitachalam, G., and P.A. Molian, “Estimation of heat conduction losses in laser cutting,” Int. Journal of Machine Tools and Manufacture 39 (1999) 431-458.

26. Luft, A., Franz, U., Emsermann, J., and J. Kaspar, “A Study of thermal and mechanical effects on materials induced by pulsed laser drilling,” Applied Physics A- Materials Science and Processing 63 (1996) 93-101.

27. Cheng, C. F., Tsui, Y.C., and T.W. Clyne, “Application of a three dimensional heat flow model to treat laser drilling of carbon fibre composites,” Acta Materiala 46 (1998) 4273-4285.

28. Ganesh, R.K.., and A. Faghri, “A Generalized thermal modeling for laser drilling process-I. Mathematical modeling and numerical methodology,” Int. Journal of Heat Transfer 40 (1997) 3351-3360.

29. Komanduri, R., and Z.B. Hou, “Thermal analysis of manufacturing processes,” for publication by Oxford University Press (2006).

30. Iyer, R., “Material processing using a CO_2 laser,” MS -Thesis, School of Mechanical and Aerospace Engineering, Oklahoma State University, Stillwater, OK (1997).

31. Hixson, J. L., “Installation of a ND: YAG laser facility and initial single pulse laser drilling of some advanced materials,” MS -Thesis, School of Mechanical and Aerospace Engineering, Oklahoma State University, Stillwater, OK (1998).

32. Aphale R.R., “Experimental and thermal modeling of multipulse laser drilling process,” MS -Thesis, School of Mechanical and Aerospace Engineering, Oklahoma State University, Stillwater, OK (2000).

33. http://www.thefabricator.com/Articles/Fabricating_Article.cfm?ID=172

34. http://www.alu-info.dk/Html/alulib/modul/A00601.htm

35. Hou, Z.B., “Mathematical heat transfer modeling of laser cutting process,” Modeling, Measurement and Control, C, ASME 46 (1994) 57-64.

36. Komanduri, R. and Z.B. Hou, “Generalized solutions for stationary /moving plane heat source problems in manufacturing and tribology,” International Journal of Heat and Mass Transfer 43 (2000) 1679-1698.

37. Komanduri, R. and Z.B. Hou, “Thermal analysis of the laser surface transformation hardening process,” International Journal of Heat and Mass Transfer 44 (2001) 2845-2862.

38. Komanduri, R. and Z.B. Hou, “Thermal analysis of laser surface transformation hardening—optimization of process parameters,” International Journal of Machine Tools and Manufacture 44 (2004) 991-1008.

39. Jaeger, J.C., “Moving sources of heat and the temperature at sliding contacts,” Proceedings Royal Society of New South Wales 76 (1942) 203-224.

40. Yilbas, B.S., “Parametric study to improve laser hole drilling process,” Journal of Material processing Technology 70 (1997) 264-273.

41. Yilbas, B.S., Sahin, A.Z., and R. Davies, “Laser heating mechanism including evaporation process initiating laser drilling,” Int. Journal of Machine Tools Manufacturing 35 (1995) 1047-1062.

42. Qiu, W., Watson, J., Thompson, D.S., and W.F. Deans, “Modeling the interaction between laser and target material in laser micro spectral analysis,” Optics and Laser Technology 26 (1994) 157-166.

43. Ho, C.Y., and J.K. Lu, “A closed form solution for laser drilling of silicon nitride and alumina ceramics,” Journal of Material Processing Technology 140 (2003) 260-263.

44. Solana, P., Kapadia, P., Dowden, J.M., and P.J. Marsden, “An analytical model for the laser drilling of metals with absorption within the vapor,” Journal of Physics D: Applied Physics 32 (1999) 942-952.

45. Balderas-Lopez, J.A., “Self-normalized photoacoustic techniques for thermal diffusivity measurement in metals,” Revista Mexicana De Fisica 50 (2004) 120-126.

46. Islam, D., ”Laser processes-cutting,” Central Michigan University (2000) (http://chem.lapeer.org/physicsdocs/Goals2000/Laser1.html)

47. Ng, G.K.L., and L. Li, “The effect of laser peak power and pulse width in the hole geometry repeatability in laser percussion drilling,” Optics and Laser Technology 23 (2001) 393-402.

48. Voisey, K.T., Kudesia, S.S., Rodden, W.S.O., Hand, D.P., Jones, J.D.C., and T.W. Clyne, “Melt ejection during laser drilling of metals,” Material Science and Engineering (2002).

49. Zhang, L., and P. Michaleris, “Investigation of Lagrangian and Eulerian finite elements methods for modeling the laser forming process,” Finite Elements in Analysis and Design 40 (2004) 383-405.

50. Zhang, W., and Y.L. Yao, “Microscale laser shock processing of metallic components,” Journal of Manufacturing Science and Engineering 124 (2002) 369-378.

51. Li, Q., Zheng, Y., Wang, Z., and T. Zou, “A novel high-peak power double AO Q-switches pulse Nd: YAG laser for drilling,” Optics and Laser Technology 37 (2005) 357-362.

52. Solana, P., Kapadia, P., Dowden, J., Rodden, W.S.O., Kudesia, S. S., Hand, D.P., and J. D. C. Jones, “Time dependent ablation and liquid ejection processes during the laser drilling of metals,” Optics Communications 191 (2001) 97-112.

53. Low, D.K.Y., and P.J. Byrd, “Hydrodynamic Physical modeling of laser drilling,” Journal of Manufacturing Science and Engineering 124 (2002) 852-862.

54. Jezersek, M., Gruden, V., and J. Mozina, “High-speed measurement of steel-plate deformation during laser surface processing,” Optics Express 12 (2004) 4905-4911.

55. Araújo, D., Carpio, F. J., Méndez, D., García, A. J., Villar, M. P., García, R., Jiménez, D., and L. Rubio, “Microstructural study of CO_2 laser machined heat affected zone of 2024 aluminum alloy,” Applied Surface Science 208-209 (2003) 210-217.

56. Gadag, S.P., Srinivasan, M.N., and B.L. Mordike, “Effect of processing parameters on the structure of ductile iron,” Material Science and Engineering A 196 (1995)145-151.

57. Ruf, A., Berger, P., and H. Hugel, “Analytical investigation on geometrical influences on laser drilling,” Journal of Physics D: Applied Physics 34 (2001) 2918-2925.

58. Corcoran, A., Sexton, L., Seaman, B., Ryan, P., and G. Byrne, “The laser drilling of multi-layer aerospace material systems,” Journal of Materials Processing Technology 123 (2002) 100 -106.

59. Veiko, V. P., “Laser microshaping: Fundamentals, practical applications, and future prospects,” RIKEN Review 32 (2001) 11-18.

60. Low, D.K.Y., Li, L., and P.J. Byrd, “The effects of process parameters on spatter deposition in laser percussion drilling,” Optics and Lasers Engineering 32 (2000) 347-354.

61. Low, D.K.Y., Li, L., and P.J. Byrd, “The influence of temporal pulse train modulation during laser percussion drilling,” Optics and Lasers Engineering 35 (2001) 149 -164.

62. Atanasov, P.A., Eugenieva, E.D., and N.N. Nedialkov, “Laser drilling of silicon nitride and alumina ceramics: A numerical and experimental study,” Journal of Applied Physics 89 (2001) 2013-2016.

63. Semak, V.V., Damkroger, B., and S. Kemka, “Temporal evolution of the temperature field in the beam interaction zone during laser material processing,” Journal of Physics D: Applied Physics 32 (1999) 1819-1825.

64. Ruf, A., Berger, P., and H. Hugel, “Analytical investigation on geometrical influences on laser drilling,” Journal of Physics D: Applied Physics 34 (2001) 2918-2925.

65. Yilbas, B.S., and M. Sami, “Liquid ejection and possible nucleate boiling mechanism in relation to the laser drilling process,” Journal of Physics D: Applied Physics 30 (1997) 1996-2005.

66. Zhang, Y., and A. Faghri, “Vaporization, melting and heat conduction in the laser drilling process,” Int. Journal of Heat and Mass Transfer 42 (1998) 1775-1790.

67. Bandyopadhyay, S., Sarin Sunder, J.K., Sundarajan, G., and S.V. Joshi, “Geometrical features and metallurgical characteristics of Nd:YAG laser drilled holes in thick IN718 and Ti-6Al-4V sheets,” Journal of Material Processing Technology 127 (2002) 83-95.

68. Rajaram, N., Sheikh-Ahmad, J., and S.H. Cheraghi, “CO_2 laser cut quality of 4130 steel,” Int. Journal of Machine Tools and Manufacture 43 (2003) 351-358.

69. Ho, C.Y., and J.K. Lu, “A closed form solution of laser drilling of silicon nitride and alumina ceramics,” Journal of Material Processing Technology 140 (2003) 260-263.

70. Steen, W.M., “Laser material processing- an overview,” Journal of Optics A: Pure and Applied Optics 5 (2003) S3-S7.

71. Chung, H., and S. Das, “ Numerical modeling of scanning laser –induced melting, vaporization and resolidification in metals subjected to time-dependent heat flux inputs,” Int. Journal of Heat and Mass Transfer 47 (2004) 4165-4175.

72. Tunna, L., O’Neill, W., Khan, A., and C. Sutcliffe, “Analysis of laser micro drilled holes through aluminum for micro-manufacturing applications,” Optics and Lasers in Engineering (2004) Article in Press.

73. Choo, K.L., Ogawa, Y., Kanbargi, G., Otra, V., Raff, L.M., and R. Komanduri, “Micromachining of silicon by short-pulse laser ablation in air and under water,” Materials Science and Engineering A 372 (2004) 145-162.

74. http://alexandria.tue.nl/extra2/200412856.pdf

75. Beyer, W.H., “Standard Mathematical Tables,” (1976) 391.

76. http://www.engineersedge.com/Design_Data.shtml

77. Rosenthal, D., “The theory of moving sources of heat and its application to metal treatments,” Trans. AMSE 80 (1946) 849-866.

APPENDIX-A

Flow Chart for Laser Drilling Process

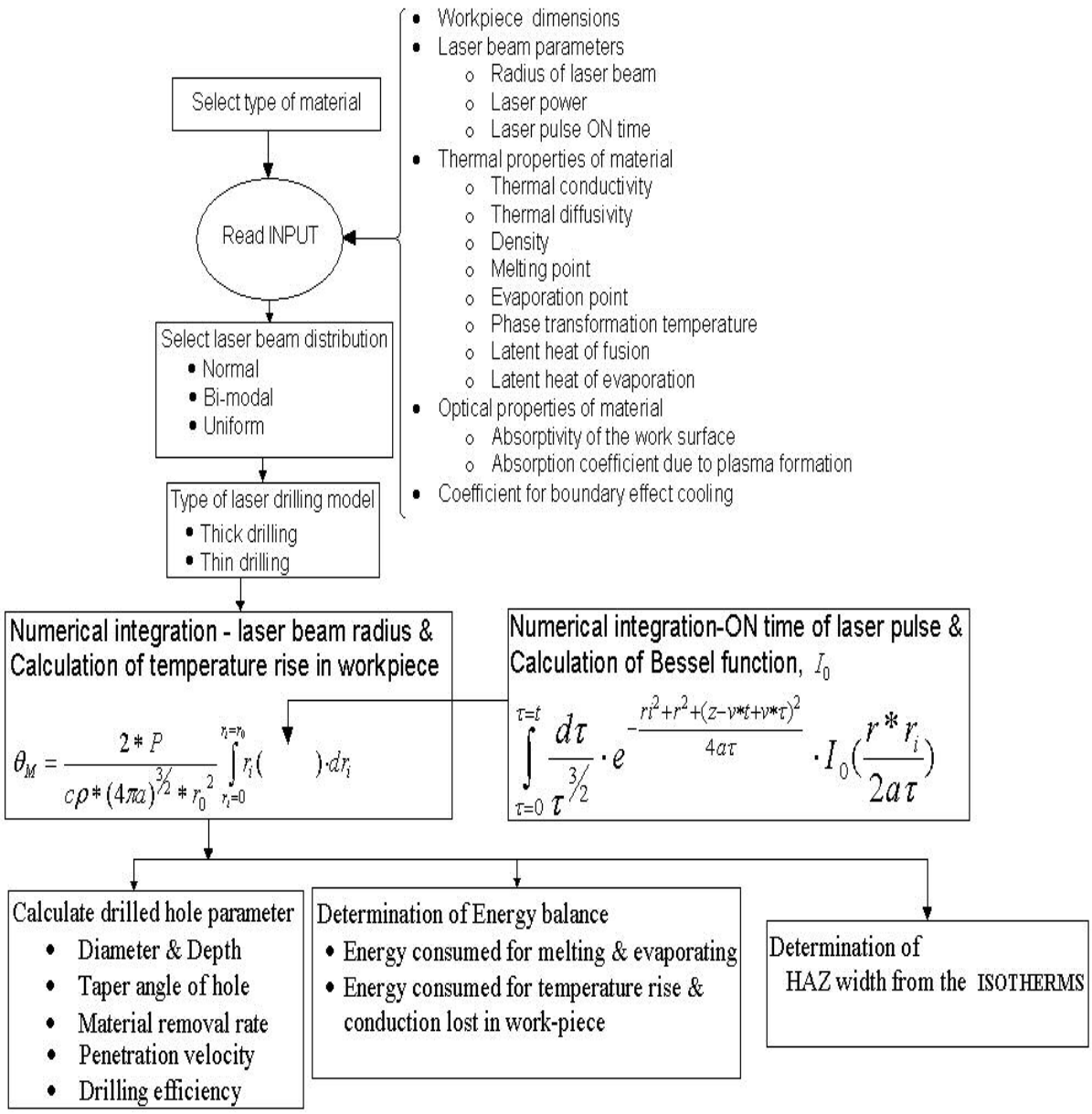

APPENDIX-B

Flow Chart for Laser Cutting/Grooving Process

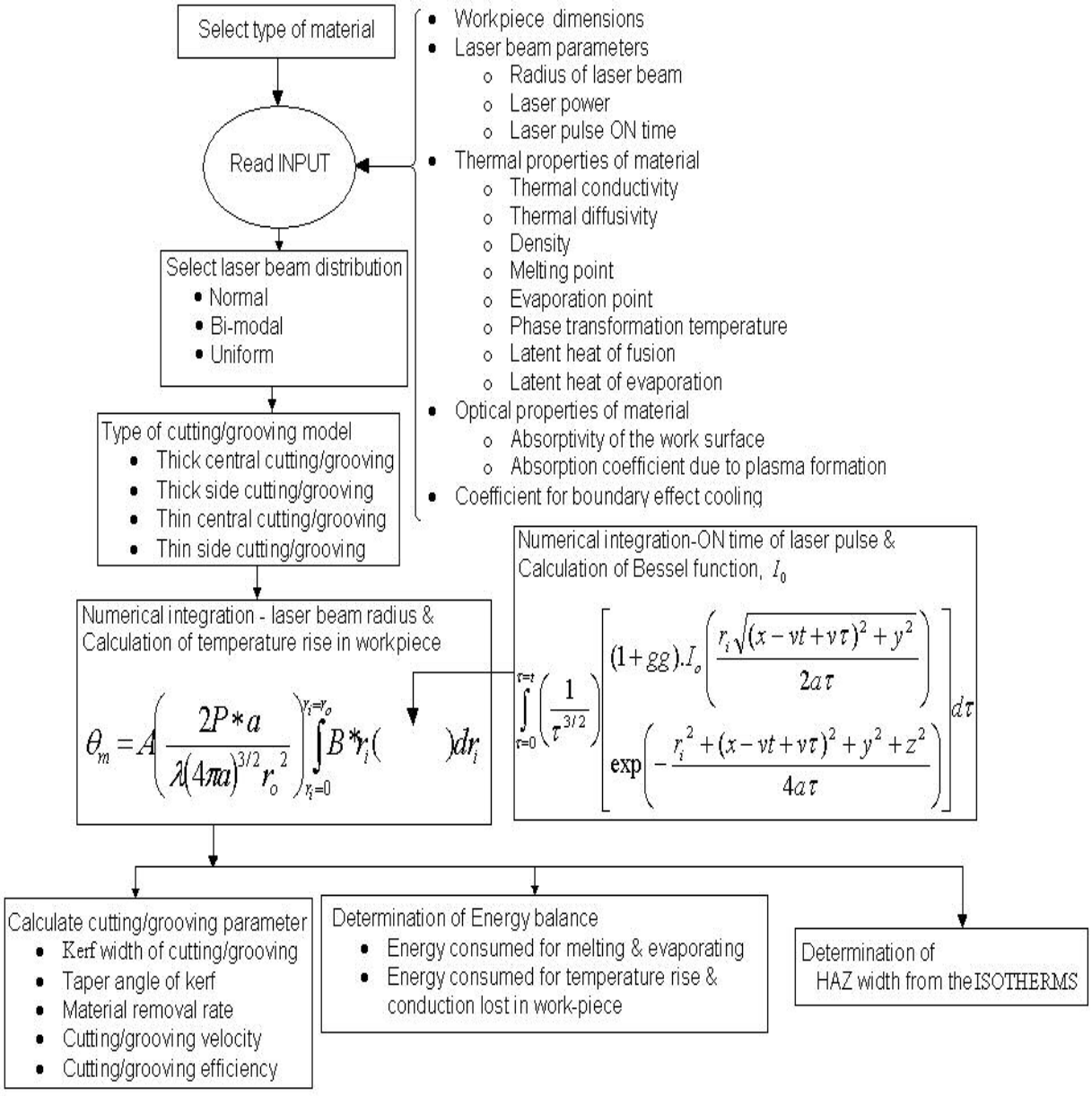

VITA

Ravindra H Patil

Candidate for the Degree of

Master of Science

Thesis: THERMAL MODELING OF LASER DRILLING AND CUTTING OF ENGINEERING MATERIALS

Major Field: Mechanical Engineering

Biographical:

Personal Data: Born at Amalgaon, Maharashtra, India, on April 1, 1976, the son of Mr. Hiraman B. Patil and Mrs. Vatsalabai H. Patil.

Education: Received Bachelor of Engineering degree in Mechanical Engineering from Government College of engineering (University of Pune), Pune, India, in July 1997. Completed the requirements for the Master of Science degree with a major in Mechanical Engineering at Oklahoma State University, Stillwater, Oklahoma in July, 2005

Experience:

- Graduate Research Assistant, Oklahoma State University, Stillwater, Oklahoma, January 2003 - May 2005.
- Piping Engineer in Uhde India Limited, Mumbai, India, September 1997 - July 2002